An-Najah National University

Faculty of Graduate Studies

MAGNETIC AND ELECTRONIC PROPERTIES OF InAs ANISOTROPIC DOPED QUANTUM DOT WITH SPIN-ORBIT COUPLING: COMPUTATIONAL STUDY

By

Ayham Anwar Ahmad Shaer

Supervisor

Prof. Mohammad Elsaid

This Dissertation is Submitted in Partial Fulfillment of the Requirements for the Degree of PhD of Physics, Faculty of Graduate Studies, An-Najah National University, Nablus - Palestine.

2023

MAGNETIC AND ELECTRONIC PROPERTIES OF InAs ANISOTROPIC DOPED QUANTUM DOT WITH SPIN-ORBIT COUPLING: COMPUTATIONAL STUDY

By

Ayham Anwar Ahmad Shaer

This Dissertation was Defended Successfully on 15 /5 /2023 and approved by

Prof. Mohammad Elsaid Supervisor	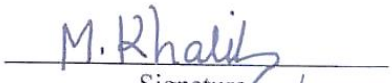 Signature
Dr. Muayad Abu Saa External Examiner	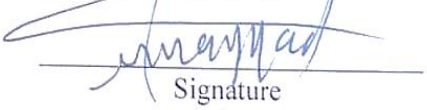 Signature
Prof. Mohammed S. Abu-Jafar Internal Examiner	 Signature
Dr. Khalid Ilawi Internal Examiner	 Signature

An-Najah National University

Faculty of Graduate Studies

MAGNETIC AND ELECTRONIC PROPERTIES OF InAs ANISOTROPIC DOPED QUANTUM DOT WITH SPIN-ORBIT COUPLING: COMPUTATIONAL STUDY

By
Ayham Anwar Ahmad Shaer
Supervisor
Mohammad Elsaid

In accordance with An-Najah National University Deans Council regulations for the award of Doctor of Philosophy, the following papers have been published after their extraction from the dissertation:

Shaer, A., & Elsaid, M. K. (2022). The Gaussian Impurity Effect on The Electronic and Magnetic Properties of an Electron Confined in a Lateral Quantum Dot. Nanosystems: Physics, Chemistry, Mathematics, 13(3), 265-273.

Dedication

This work is dedicated to my parents, who always loved me unconditionally.

My dear wife makes it possible for me to finish my task.

My tiny family (Huda & Qasam) makes the task really challenging.

Acknowledgments

First and foremost, I would like to express my gratitude to Allah for helping me to complete this task. Then I'd like to thank my supervisor, Prof. Mohammad Elsaid, for granting me to undertake such a challenging task. Throughout this endeavor, I am grateful for his valuable guidance, encouragement, understanding, and insightful support.

Declaration

I, the undersigned, declare that I submitted the thesis entitled:

MAGNETIC AND ELECTRONIC PROPERTIES OF InAs ANISOTROPIC DOPED QUANTUM DOT WITH SPIN-ORBIT COUPLING: COMPUTATIONAL STUDY

I declare that the work provided in this thesis, unless otherwise referenced, is the researcher's own work and has not been submitted elsewhere for any other degree or qualification.

Student's Name: **Ayham Anwar Ahmad Shaer**

Signature: _____

Date: **15 / 5 / 2023**

List of Contents

List of Tables

List of Figures

List of Appendices

MAGNETIC AND ELECTRONIC PROPERTIES OF InAs ANISOTROPIC DOPED QUANTUM DOT WITH SPIN-ORBIT COUPLING: COMPUTATIONAL STUDY

By

Ayham Anwar Ahmad Shaer

Supervisor

Prof. Mohammad Elsaid

Abstract

The anisotropic quantum dot (QD) Hamiltonian has been solved using the diagonalization method in the presence of a perpendicular magnetic field and Gaussian impurity, considering both types of spin-orbit interaction (SOI): Rashba and Dresselhaus. The diagonalization process has been carried out using the one-dimensional harmonic oscillator basis.

The acceptor impurity's presence significantly affects the system's eigensolution, specifically causing an interesting level crossing between the states and changing the ground state order. Furthermore, the impurity's strength, position, and spatial stretch have been investigated, and the result shows that the impurity plays an important role in manipulating the QD properties.

The magnetization and magnetic susceptibility as important quantities of the QD system made from InAs are studied. The results show a diamagnetic-paramagnetic phase transition at low temperatures due to the impurity presence. This magnetic transition strongly correlates with the impurity profiles (strength, position, and influence domain), magnetic field, and temperature. As the strength of the impurity increases, the diamagnetic-paramagnetic transition occurs at a lower value of the magnetic field.

In addition, the effective Lande factor g of the system has been studied. The result shows that, as the electric field increases, the Rashba SOI increases |g|, while the Dresselhaus SOI reduced |g| of the QD. Furthermore, in the presence of both types of SOI, increasing the electric field enhances the |g| since in the InAs material, the Rashba SOI dominates the Dresselhaus SOI. The result emphasizes the role of Rashba SOI in spintronics devices.

The confinement strength effect on the g has been investigated, the g shows a peak value at particular confinement strength. In addition, the anisotropy of the QD shows a significant role in controlling g.

The density of states of the system has also been computed to physically describe the impact of each system parameter on the energy spectrum. As the magnetic field turns on, the figures demonstrate how the anisotropy of the confinement potential also causes the harmonic oscillator symmetry to be broken.

Keywords: Quantum dot; Magnetic properties; Rashba spin-orbit interaction; Dresselhaus spin orbit interaction; Lande g factor; Computational physics; Density of states;

Chapter One
Introduction

Spin-orbit coupling (SOC), one of the most critical consequences of Dirac's theory for particles in condensed matter physics, is widely believed to play an important role in electronic devices such as spintronic transistors. In addition to heterostructure confinement and external fields, SOC significantly manipulates the density of states of the system to show different physical properties compared to a bulk system. Adding impurities (donor or acceptor impurities) to the low-dimensional system also can manipulate the system properties.

1.1 Quantum confinement

Quantum-confined structures, known as Nanostructures, are classified according to their degree of spatial confinement. In the quantum well, the carrier has the freedom to move in a two-dimensional space where the motion in the third spatial dimension is confined, while in the quantum wire, the carrier is confined to move freely in one dimension only, the ultimate quantum structure being a system that confines carriers in all three dimensions. These quantum structures are termed quantum dots (QDs). A QD is a nanometer-scale structure of narrow-band gap semiconductors (such as GaAs), frequently surrounded by a wider-band gap semiconductor (such as AlGaAs). One of the fundamental properties of QDs which is of considerable importance in dealing with those nanostructures, is their capacity to confine carriers in all three directions, presenting a discrete spectrum of energy spectra similar to that of pure atoms that gave quantum dots the name of "artificial atoms" (Ashoori, 1996).

QDs have a size similar to the electron and hole wave functions, which allows for efficient spatial confinement of these charge carriers. Typically, their size falls in the range of a few to tens of nanometers. The charge carriers' quantum confinement is a semiconductor nanostructure's primary physical property. Spatial confinement occurs in ways that significantly alter material characteristics. First, it moves the bulk semiconductor's conduction and valence bands, allowing its forbidden bandgap to expand. Second, quantum confinement alters the electronic density of states of the nanostructure dramatically. Therefore, a significant change in the system's physical properties will take a place (Reimann & Manninen, 2002).

The discrete energy spectra in the QD strongly depend on the dot size, material type, and QD shape; a smaller size means larger confinement.

The relationship between dot size and confinement can be intuitively understood by considering the spatial constraints imposed on the charge carriers. In a larger quantum dot, electrons have more space to move around, and their energy levels are less discrete. However, when the dot size is reduced, the available space for electrons becomes limited, resulting in a higher degree of localization. Consequently, the energy levels become more discrete, forming distinct energy states that are well-separated from each other.

Moreover, in addition to dot size, other factors such as the material type and QD shape also play crucial roles in determining the discrete energy spectra. The material properties, including the band structure and electronic properties, influence the energy levels that can be occupied within the quantum dot. Different materials exhibit varying energy gaps between their electronic bands, which further impact the discrete energy levels within the QD.

1.2 Spintronics

Spintronics, also known as spin electronics, is an expanding field of nanoscale electronics in which the spin and charge of an electron are utilized to convey information. It is considered one of the most promising area of research, given its diverse applications (Bader & Parkin, 2010).

The common objective of spintronics is to comprehend the interaction of particle spin and its surroundings and find a practical way of controlling electronic properties, such as current, by spin or magnetic field, as well magnetic properties gate voltages or electric currents. In addition, to comprehend the core logic of spin, such as relaxation of spin (how spins vanish and arise) and spin transit (how spins move in semiconductors and metals). It is fundamentally important as basic physics concerns because of their demonstrated value as phenomena in electronic technology (Hu & Xiang, 2020; Wolf et al., 2001; Žutić et al., 2004).

Electronic devices use an electron's elementary charge to move it. The electrical conductivity of a semiconductor may be modified by applying a voltage to it, resulting in the realization of a controlled switch. These switches are the foundation of every

hardware logic system. Electrons carry angular momentum, known as "spin," in addition to charge. The Stern-Gerlach experiment quantifies this inherent feature of electrons, demonstrating that the spin has two possibilities, down or up, depending on the measurement devices; this is equivalent to the digital states "1" and "0," raising the possibility that the spin might be used to represent binary memory states. A spin field-effect transistor (see Fig. A.1), for example, would switch its logic state from off to on by changing the magnetic field orientation (Dieny et al., 2020; Schliemann et al., 2003).

Spintronics is essential in the memory field to meet the demands of high storage capacity, compact size, and fast response. New devices that mix logic, sensor, and storage applications are also available. Furthermore, these "spintronics" technologies may lead to quantum computers and quantum computing based on solid-state electrical devices, altering the future of information technology (Yakout, 2020). Fig. A.1 shows a schematic presentation for a spin transistor where the electron moves from the source to the drain according to its spin orientation; the applied voltage controls the electron transition.

1.3 Spin-orbit interaction

As the name suggests, spin-orbit interaction (SOI) is a link between an electron's spin dynamics and its orbital motion in space.

According to the theory of special relativity, when the inertial frame of reference changes, electric and magnetic fields are Lorentz transformed. Thus, an electron traveling through an electric field "sees" a moving electric field, which is caused by moving charges, in its rest frame. These flowing charges – or electrical current – generate an "internal magnetic field" in the electron's rest frame. This "internal magnetic field" connects back to the electron's spin. The magnitude and direction of this internal magnetic field are determined by the electron's velocity and travel direction in a material, therefore, SOI produces a k-dependent internal magnetic field, where k represents the electron's wave vector.

When comparing the Zeeman effect to the spin-orbit interaction (SOI), it becomes evident that the latter has a distinct influence on the behavior of electronic spins in materials. While the Zeeman effect is responsible for the splitting of energy levels based on the interaction between the spin and an external magnetic field, the spin-orbit

interaction goes beyond the direct influence of an applied magnetic field, as shown in Fig. A.2.

The lack of structural inversion symmetry of the confinement potential of electrons in a quantum heterostructure, also known as Rashba SOI (Rashba, 1960), and lack of crystal inversion symmetry, also known as Dresselhaus SOI (Dresselhaus, 1955), are the two primary "sources" of the electric field that lead to SOI.

1.4 Density of states

The density of states (DOS) of a system in condensed matter and solid-state physics refers to the proportion of states that the system will occupy at each energy. The number of states in a unit of energy is known as the density of states. Which is typically an average over the space and time domains of the many states in which the system exists. The distribution of these states is theoretically represented by a probability density function. The dispersion relations of the system's attributes are directly correlated with the density of states. High DOS for a given energy level indicates that numerous states are open for occupation.

The DOS of the matter is often continuous. Whereas, the density distribution is discrete in isolated systems, such as atoms or molecules in the gas phase. Therefore, the local densities of states are frequently used to show the local variations of DOS.

The DOS is dependent upon the dimensional limits of the structure itself. The units of DOS in a system characterized by three orthogonal parameters (3 Dimensions) are $Volume^{-1}Energy^{-1}$, in a two-dimensional system, the units of DOS are $Area^{-1}Energy^{-1}$, in a one-dimensional system, the units of DOS are $Length^{-1}Energy^{-1}$.

The distribution of electrons varies as dimensionality is decreased, as demonstrated by calculations of the density of states for small structures. For example, compared to bulk semiconductors, quantum wires have a DOS greater at some energy, and QDs have electrons that are quantized at specific energies.

The density of states represents the number of permitted electron (or hole) states per volume at a given energy level and is derived from the principles of quantum mechanics. It is simple to demonstrate that, concerning dimensionality, the dependence

of the density of states on system energy considerably changes. Table 1 and Fig. A.3 illustrate how the DOS changes for bulk (3D), 2D, 1D, and 0D systems.

Table 1

The effect of spatial confinement on DOS as a function of energy

System	Dimensionality	DOS vs. E
Bulk	3D	$DOS \propto \sqrt{E}$
Quantum well	2D	$DOS \propto Constant$
Quantum wire	1D	$DOS \propto \frac{1}{\sqrt{E}}$
Quantum dot	0D	$DOS \propto \delta\,(E - E_n)$

There exist finite energy ranges in a real structure (which is not exactly 2-D) over which the energy independence holds (the derivation holds for each single, well-separated possible value of k_z). A staircase is what a quantum well's density of states looks like. The density of state functions becomes ever more limited when semiconductor dimensionality is more constrained to 1-D (quantum wire) and 0-D (QD).

1.5 Literature survey

Researchers have shown a particular interest in low-dimensional systems, and a considerable number of theoretical research have been carried out to investigate the impact of external fields on thermal, magnetic, and optical properties (Ali et al., 2022; Avetisyan et al., 2016; Baghdasaryan et al., 2018; Boda & Chatterjee, 2016; Bzour et al., 2017; Castano-Yepes et al., 2019; Chakraborty & Pietiläinen, 2005; Datta & Ghosh, 2011; Elsaid, Abu Alia, et al., 2020; Elsaid, Shaer, et al., 2020; Gumber et al., 2015; Gumber et al., 2016; Jha et al., 2014; Khordad, 2017; Stufler et al., 2005). The presence of impurities has been discovered to have a significantly influence on system modification (Boda & Chatterjee, 2016; Datta & Ghosh, 2011; Elsaid et al., 2019; Kandemir & Cetin, 2005; Yahyah et al., 2019).

Numerous theoretical studies have been devoted to solve the Schrodinger equation for the QD system using various approaches, such as the variational approach (Ciftja & Faruk, 2005; Kandemir & Cetin, 2005; Shaer et al., 2016), the 1/N expansion method

(Yahyah et al., 2019; Yaseen et al., 2019), and the exact diagonalization method (Ali et al., 2019; Alia et al., 2019; Sharma et al., 2019).

Shaer et al. have studied the two electrons in a GaAs QD system using the variational method and investigated the thermal and magnetic properties of the system. The magnetic susceptibility shows an oscillatory behavior due to the Coulomb interaction between the two electrons, which caused the ground state changing (Shaer et al., 2016; Shaer et al., 2019).

The exact diagonalization method was used to study the magnetization and magnetic susceptibility of a donor impurity in parabolic GaAs QD by Alia et al. (Alia et al., 2019). The computed results show that the electric field can tune the magnetic properties of the QD GaAs medium by flipping the sign of its magnetic susceptibility from diamagnetic to paramagnetic. In addition, the magnetic susceptibility transition has shown to be strongly correlated to Hamiltonian parameters such as magnetic field, electric field, donor impurity, and Rashba SOI.

The electrical properties of elliptical quantum dot in the presence of the Rashba spin-orbit interaction and a perpendicular external magnetic field have been investigated (S. Avetisyan et al., 2012). The research has shown that when the quantum dots anisotropy increases, the Fock-Darwin spectra strongly depend on the Rashba spin-orbit coupling, even without the magnetic field. It is discussed how the anisotropy contributes to this strong influence. Since the resulting dipole-allowed optical transitions conspicuously display the significant spin-orbit-coupling effect, it can be directly observed experimentally.

The effect of the spin-orbit interaction on the electron magnetization and magnetic susceptibility of parabolic InAs QD has been investigated by Voskoboynikov et al. (Voskoboynikov et al., 2003), where the work gives a theoretical investigation of the influence of spin-orbit interaction on electron magnetic properties of tiny semiconductor QDs at low temperatures, these properties exhibit quite exciting behavior. The sudden variations in magnetization and susceptibility at low magnetic fields are attributable to the alternate crossing of the spin–split electron levels in the energy spectrum, primarily caused by spin-orbit interaction.

Hosseinpour (Hosseinpour, 2020) provided a brief investigation of the influence of Rashba SOI and Gaussian impurity on the thermal properties of an asymmetric QD. The Rashba SOI was considered when the author calculated the doped QD's internal energy, heat capacity, and entropy. It has been shown that Rashba coupling, Gaussian impurity parameters, and applied fields may manipulate thermal properties and that increasing the electric field and Rashba coupling strength lowers the internal energy. Entropy (internal energy) drops due to changes in some factors, such as the magnetic field and intensity of the confinement potential. In different work, Hosseinpour (Hosseinpour & systems, 2020) has studied the nonlinear optical properties of QDs in the presence of the Rashba SOI, and in this work she shown a significant impact of the Rashba SOI on the system's optical properties.

Prabhakar et al. (S. Prabhakar et al., 2011) investigated the change in an electron's Lande' g factor by anisotropic gate potentials and magnetic fields in InAs QDs. For both isotropic and anisotropic QDs, the author tried to offer analytical formulations and numerical simulations of the change in the Lande' g factor in this study. The authors demonstrated that the Rashba spin-orbit coupling significantly affects the fluctuation of Lande' g factor with electric fields using both analytical approaches and numerical simulations. In particular, significant Rashba spin-orbit interaction demonstrates that the electric-field tunability covers an extensive range of g factor values.

The study also uncovers a significant finding that, if the area of the symmetric and asymmetric QD is kept equal, the anisotropic gate potential leads to a quenching effect in the orbital angular momentum that minimizes the variance in the electric field and magnetic field tunability of the Lande' g factor.

In a separate study, Madhav et al. (Madhav & Chakraborty, 1994) have investigated the electronic properties of anisotropic quantum dots in a magnetic field. They authors have calculated the energy spectra and pair-correlation function of a two-electron system to analyze the impact of inter-electron interaction on isotropic and anisotropic QDs.

In Ref (de Sousa & Das Sarma, 2003), the effective Lande g factor have been studied and the spin-flip time of a heterojunction of III-V semiconductor QDs. The results have shown that the Lande g factor is highly sensitive to the Rashba and Dresselhaus spin-orbit interactions. In addition, the study highlights a strong sensitivity of g and T_1 to dot

radius and magnetic field, providing opportunities for the development of a QD spin quantum computer, where external gates may control the spin-orbit coupling to engineer the g factor and spin-flip time.

For a single uncapped InAs self-assembled quantum dot, anisotropy of the spin-orbit interaction (SOI) is investigated in Ref (Takahashi et al., 2010). The SOI energy is calculated from anticrossing or SOI-induced hybridization between the ground and excited states with opposing spins.

1.6 Research gap

The purpose of this section is to demonstrate, in great detail, the main differences between this work and previously published results related to the QD research field. By conducting a comprehensive analysis and comparison, we aim to highlight the unique contributions and advancements offered by our study, shedding new light on the understanding of QDs.

As mentioned earlier, numerous publications seek to investigate the QD magnetic properties, where the authors usually solve the single electron Hamiltonian and study the system properties.

Some studies have focused on the GaAs / AlGaAs QD properties and have included spin-orbit interaction effects in some of these studies. However, the Rashba coupling parameter in GaAs material is small compared to InAs material, which has a relatively small band gap. Another critical point is that the effective Lande g factor for the InAs material is larger than the GaAs Lande g factor ($g_{GaAs} = -0.44$ while $g_{InAs} = -14.1$); as a result, the spin-dependent terms in InAs material are expected to have a more significant effect, therefore, more expected application in the future. Hence, it will be exciting to study the SOC for this material in QD form.

Another important point, in this work, we deal with both Rashba and Dresselhaus spin-orbit interaction, and each of them has a different source, so to have a wide picture of the spin-orbit interaction, the QD. Hamiltonian has included both (Rashba and Dresselhaus) spin-orbit terms jointly.

Rashba and Dresselhaus spin-orbit interactions were not previously studied together for the InAs QD sample. However, as mentioned before, the higher value for the InAs g-

factor gives the SOC a significant contribution to the system properties; therefore, it may be acceptable to be an excellent candidate for spintronics technology.

The parabolic potential is the most common model to describe the QD confinement, and most previous studies deal with the isotropic potential; however, in the present work, we choose the anisotropic model expected to be closer to experimental results.

Additionally, in Ref (Kahraman & Bulutay, 2021) the authors presented atomistic computations within an empirical pseudopotential framework for the electron s-shell ground state g tensor of InGaAs quantum dots (QDs) embedded to host matrices that grant electronic confinement. The results shown that low Indium concentration offers limited g-factor tunability under shape or confinement variations.

Supported by the recent experimental result of Camenzind et al. (Camenzind et al., 2021), we aim to theoretically calculate the effective Lande g- factor for the InAs material.

The study investigates the combined effects of anisotropic parabolic potential, Gaussian impurity, external fields, and spin-orbit interaction on the magnetic and electronic properties of InAs QD.

1.7 Research objectives

The spin-orbit coupling is critical factor in determining a material's applicability to the spintronics technology. The high g-factor for InAs material is a significant point that demonstrates the impact SOI on the properties of the QDs.

The main objectives of this research project can be summarized as follows:

1. To solve a single electron Hamiltonian confined in an asymmetric QD in the presence of SOI, magnetic fields, and Gaussian impurity by using the diagonalization technique and computing the eigenenergies and eigenfunctions.

2. To study the behavior of the electron density as an important quantity that reflects the effects of the applied fields and the spin-orbit interactions on the electron behavior. The Gaussian impurity potential, which is included in the Hamiltonian, has additional important effects on the behavior of the spectroscopic properties of the confined electron.

3. To study the magnetic quantities of the QD material like magnetization M and the magnetic susceptibility χ. We shall investigate, further, the effects of all physical quantities on the magnetic phase transition from paramagnetic to diamagnetic, in particular, the effect of the electric field as it plays an important role in controlling the magnetic behavior of the QD nanomaterial that has significant applications in the field of spintronics.

4. To calculate the electron Lande g-factor of an electron confined in the InAs QD, an important factor in controlling the spin of the electrons in the field of spintronics. The electron g-factor is highly affected by the spin-orbit (SOI) interaction terms (Rashba and Dresselhaus) and the applied electric field terms, which are included explicitly in the QD Hamiltonian.

5. To investigate further the density of states of the anisotropic QD, considering the significant effects of external fields (magnetic and electric fields) and Gaussian impurity.

1.8 Structure of the dissertation

The dissertation contains four chapters divided as follows:

Chapter 1- Introduction: Chapter one includes a general introduction about the quantum confinement of the charge carriers, spintronics, spin orbit interaction, density of states. In addition, it provides the main differences between current research and previous ones in the research gap section, furthermore, a literature review for previous works related to the quantum dot confinement, numerical methods and spin orbit interaction studies.

Chapter 2- Theory: In the second chapter, we explain, in details, how to construct the Hamiltonian based on effective mass theory for an electron in anisotropic quantum dot, including the effect of an external applied magnetic field, taking into consideration the presence of acceptor Gaussian impurity and spin orbit interaction terms. Furthermore, the numerical method for solving Schrodinger equation using exact diagonalization method. And the physical meaning for the calculated properties: energy spectra of the electon, wave functions, probability density, statistical average energy, effective Lande g factor, density of states, magnetization, and magnetic susceptibility. In addition, in the

theory section, we show all the necessary mathematical expression and steps to simplify the Hamiltonian matrix.

Chapter 3- Results and discussion: In this section, the calculated results will be shown in figures and tables with physical and mathematical investigation for the quantum dot physical properties, in addition to physical properties, we will provide some computational output for advantages of using closed analytical expressions.

Chapter 4- Conclusion: Chapter four includes the conclusions from the research with the results from chapters 3.

Chapter Two
Hamiltonian Theory and Computation Method

2.1 QD Hamiltonian

Starting from the Hamiltonian of an electron in the presence of a magnetic field which was discussed by Landau in 1930, following that work, $\widehat{H}$ can be written as,

$$\widehat{H} = \frac{(\mathbf{p} - e\,\mathbf{A})^2}{2m^*} \tag{1}$$

Where

$\mathbf{p} = \frac{\hbar}{i}(\frac{\partial}{\partial x}, \frac{\partial}{\partial y}, 0)$, is the momentum operator

A is the vector potential corresponding to magnetic field along the Z-direction

m^* is the effective mass of the electron in InAs material

e is the electron charge

the quantity $(\mathrm{p} - \mathrm{e}\,\mathrm{A})$ is known as canonical (total) momentum. Using the symmetric gauge and defining $\omega_c = \frac{eB}{m}$, the eigenenergies were found to be,

$$E = (\,2n\, +\, |m_l| +\, 1)\hbar\,\Omega - \frac{1}{2}\hbar\, m_l\, \omega_c \tag{2}$$

Where $\Omega = \frac{\omega_c}{2}$, $n = 0,1,2,..$, and $m_l = 0, \pm 1, \pm 2, ..$ n and m_l represent the radial and azimuthal quantum numbers, respectively.

When a magnetic field is applied perpendicular to a conducting plane, the motion of electrons becomes quantized into discrete energy states known as Landau levels. Each Landau level represents a set of allowed energy eigenstates for the electrons in the system. The energy spacing between adjacent Landau levels is constant and depends solely on the strength of the magnetic field.

As an extension to the previous Hamiltonian, the single electron in a circular QD confined in parabolic potential in the presence of a magnetic field is presented by the following Hamiltonian,

$$\widehat{H} = \frac{(\mathbf{p} - e\,\mathbf{A})^2}{2m^*} + \frac{1}{2}m^*\omega_0^2\,(x^2 + y^2) \tag{3}$$

The above Hamiltonian was solved by Fock and Darwin (Darwin, 1931; Fock, 1928). Similar to Landau's work, the energy spectra were found as follows,

$$E = (\,2n\, +\, |m_l| +\, 1)\hbar\,\Omega_{\text{eff}} - \frac{1}{2}\hbar\, m_l\, \omega_c \qquad (4)$$

where $\Omega_{eff} = \sqrt{\omega_0^2 + \frac{\omega_c^2}{4}}$, as special case, if $\omega_0 \rightarrow 0$, the energy solution given in Eq. (4) will match the landau energy given by Eq. (2).

The Fock-Darwin states arise from the combined effects of the harmonic oscillator potential and the magnetic field on the charged particle's motion. The harmonic oscillator potential, characterized by its quadratic potential energy term, confines the particle in two dimensions, while the magnetic field introduces a quantization of the particle's orbital motion.

The Fock-Darwin states can be thought of as a two-dimensional analogue of the one-dimensional harmonic oscillator states. They are characterized by the following properties:

- Energy quantization: Similar to the one-dimensional harmonic oscillator, the Fock-Darwin states exhibit quantized energy levels. These energy levels depend on the strength of the magnetic field, the frequency of the harmonic oscillator potential, and the particle's effective mass.
- Radial and azimuthal quantum numbers: The Fock-Darwin states are labeled by two quantum numbers: the radial quantum number, which determines the number of radial nodes in the wavefunction, and the azimuthal quantum number, which specifies the angular momentum of the particle.
- Landau level structure: The Fock-Darwin states exhibit a Landau level structure, with each Landau level corresponding to a different energy eigenstate. Each Landau level can accommodate multiple states with different azimuthal quantum numbers but the same energy.
- Oscillation pattern: The Fock-Darwin wavefunctions exhibit characteristic oscillatory behavior both radially and azimuthally, reflecting the confinement and quantization of the particle's motion in the harmonic oscillator potential and magnetic field.

Fig. A.4 and Eq. 4 show that at $B = 0$, the spectrum matches the symmetric harmonic oscillator energies, and the degeneracy becomes larger with a higher energy level, while as $B \to \infty$, the energy levels converge to Landau level.

In the isotropic potential case, the energy levels of the system possess a $(2n + |m_l| + 1)$ fold degeneracy. Here, n represents the principal quantum number and$|m_l|$ denotes the magnetic quantum number. This degeneracy arises due to the rotational symmetry of the potential, which allows for multiple states with the same energy.

To be closer to a real application, we introduce the asymmetric harmonic oscillator confinement potential (heterostructure confinement) representing the restriction of the motion of the charge carrier, such potential given by

$$\mathrm{V_{conf}(x,y)} = \frac{1}{2}m^*\left(\omega_x^2 x^2 + \omega_y^2 y^2\right) \tag{5}$$

Where $\omega_x \neq \omega_y$,

The potential plot given in Fig. 1(a and b) shows the broken potential circular symmetry in the case of $\omega_x \neq \omega_y$. As an expected result, the solution of such a system is quite similar to the isotropic potential case, except that the $(2n + |m_l| + 1)$ fold degeneracy will be lifted due to broken symmetry. This result was previously reported in Ref (Madhav & Chakraborty, 1994).

2.2 Gaussian impurity

In the semiconductor field, impurity is considered a very important factor in manipulating the system properties, and the Gaussian impurity model was considered a successful model to reflect the physical effect of impurity mathematically,

$$V_{imp}(x,y) = \mathrm{V_0 e}^{-\frac{\left((\mathrm{x}-\mathrm{x_0})^2+(\mathrm{y}-\mathrm{y_0})^2\right)}{\mathrm{d}^2}} \tag{6}$$

where (x_0, y_0) denotes impurity position and the positive (negative) value of V_0 corresponds to an acceptor (donor) impurity potential strength where d is a tunable parameter to impact impurity stretch.

The Gaussian impurity model provides a mathematical framework to describe the behavior of impurity atoms within a semiconductor. In this model, the impurity atoms are represented by Gaussian-like potential profiles. These profiles represent the spatial distribution of the impurity charge or potential energy within the QD.

The Gaussian shape of the impurity potential arises due to the distribution of charge or potential energy associated with the impurity atom. The model assumes that the impurity atom is localized, and the charge or potential energy associated with it decreases smoothly and symmetrically away from the impurity site.

One of the key advantages of the Gaussian impurity model is its simplicity, which makes it computationally tractable. The model provides a reasonable approximation for many impurity-related phenomena, especially when the impurity concentration is relatively low.

The presence of the impurity (donor or acceptor) plays an essential role by changing the potential shape, therefore, expected to change the probability distribution of the charge carrier resulting in a significant change of the system properties.

Density plots of the effective potential for different cases of impurity types and positions are demonstrated in Fig. 1, the effective potential for isotropic case (c, d, and e) and anisotropic case (f, g, and h) in the presence of acceptor impurity (c, d, f, and g) and donor impurity (e, and h), the impurity positions are: (0,0), (1,0), (0,1), (0,0), (0,1), (1,1) in c, d, e, f, g and h, respectively.

Up to now, our Hamiltonian describes the spin-independent properties, so we still have to take care of spin contribution, the normal Zeeman effect due to interaction between the electron spin and external magnetic field, expressed by the Hamiltonian,

$$\widehat{H}_{Zeeman} = \frac{1}{2} g_0 \mu_B \sigma_z \qquad (7)$$

where, g_0 , μ_B , $\boldsymbol{\sigma}$ is the material Lande g factor, Bohr magneton, and spin Pauli matrices, respectively.

The inclusion of this term allows us to investigate the influence of the external magnetic field on the spin states and energy levels of the electron. The Zeeman effect leads to the splitting of energy levels based on the orientation of the electron's spin relative to the magnetic field direction.

Figure 1

Density plot for the confinement potential for the isotropic and anisotropic case without impurity (a and b) and in presence of the impurity (c-h)

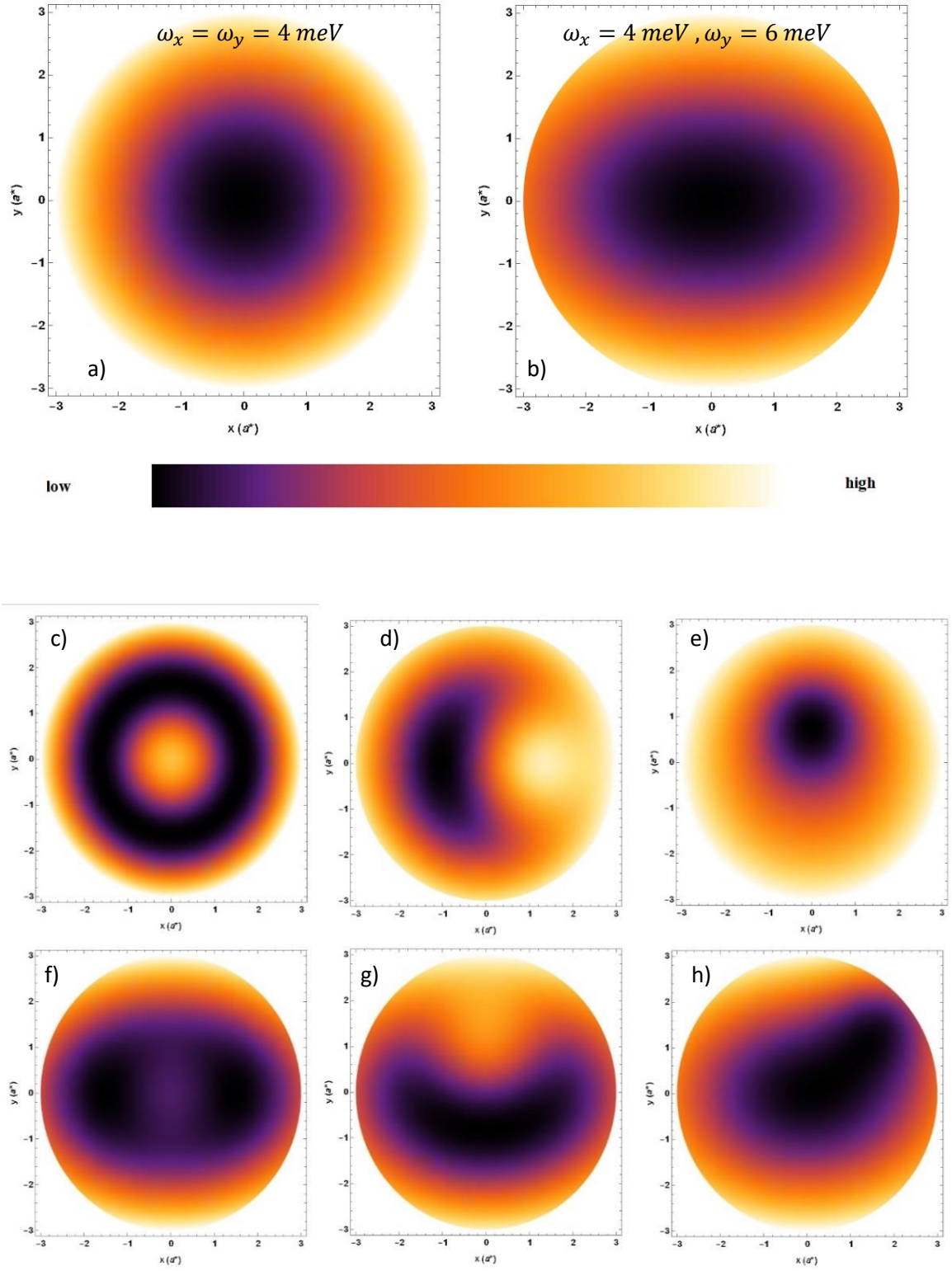

The magnitude of the Zeeman effect depends on the Lande g-factor, which represents the ratio between the magnetic moment of the electron and its spin angular momentum. Different materials and systems can exhibit different g-factors, leading to variations in the strength and behavior of the Zeeman effect.

2.3 Spin-orbit interaction

The spin-orbit interaction (SOI) arises from the coupling between the intrinsic spin angular momentum of electrons and their orbital angular momentum. This interaction plays a crucial role in various physical phenomena, particularly in condensed matter systems. The SOI term incorporates the effects of both Rashba and Dresselhaus spin-orbit interactions, which are two prominent mechanisms responsible for spin-orbit coupling in solid-state materials.

The Rashba spin-orbit interaction arises in systems with structural inversion asymmetry. It can occur at interfaces or surfaces of materials or in heterostructures where the lack of inversion symmetry breaks the degeneracy between spin-up and spin-down states. The Rashba effect is typically characterized by a linear momentum dependence of the spin-orbit coupling strength. In the presence of an electric field gradient, the Rashba interaction leads to a spin-dependent potential that couples the electron's spin and momentum, resulting in spin splitting and influencing electronic transport properties.

On the other hand, the Dresselhaus spin-orbit interaction arises due to the lack of bulk inversion symmetry in materials, such as zinc-blende crystals. It can be present in systems with structural asymmetry, such as quantum wells or nanowires. The Dresselhaus effect is described by a linear and cubic momentum dependence of the spin-orbit coupling strength. Similarly, to the Rashba interaction, the Dresselhaus interaction leads to spin splitting and affects the electronic band structure, transport properties, and spin dynamics in the material.

When considering the SOI term, which encompasses both the Rashba and Dresselhaus contributions, we take into account the combined effect of these two mechanisms. The SOI term quantifies the strength and nature of the spin-orbit coupling in the system, providing a framework to describe the interplay between the electron's spin and its orbital degrees of freedom.

Mathematically, the Hamiltonian term includes the effects of Rashba and Dresselhaus SOI can be written as,

$$\hat{H}_{SO} = \hat{H}_R + \hat{H}_D \tag{8}$$

$$\hat{H}_R = \frac{\alpha_R}{\hbar}[\boldsymbol{\sigma} \times (\mathbf{p} - e\,\mathbf{A})]_z \tag{9}$$

$$\hat{H}_D = \frac{\alpha_D}{\hbar}[\boldsymbol{\sigma}.(\mathbf{p} - e\,\mathbf{A})] \tag{10}$$

$\hat{H}_{SO}$ consists of the Rashba interaction, whose strength is characterized by the parameter α_R and the Dresselhaus interaction with a strength characterized by α_D. The electric field E of the quantum well-confining potential affects these coupling characteristics.(i.e., $E = -\partial V/\partial z$) along the z direction at the interface in a heterojunction as (de Sousa & Das Sarma, 2003)

$$\alpha_R = \gamma_R eE \tag{11}$$

$$\alpha_D = 0.78\gamma_D \left(\frac{2m^* e}{\hbar^2}\right)^{2/3} E^{2/3} \tag{12}$$

where the Dresselhaus coefficient $\gamma_D = 130\ eVA^{\circ 3}$, Rashba coefficient $\gamma_R = 110A^o$, and effective mass $m^* = 0.0239m_0$ is considered for InAs QD, where m_0 is the free electron mass.

2.4 Exact diagonalization method

The total Hamiltonian of an electron which is presented in InAs anisotropic doped quantum dot under the presence of external magnetic and electric fields, is given by:

$$\hat{H} = \frac{(\vec{p} - e\vec{A})^2}{2m^*} + V_{\text{conf}}(x,y) + V_{\text{imp}}(x,y) + \hat{H}_{SO} + \hat{H}_{\text{Zeeman}} \tag{13}$$

The analytical solution of the above full Hamiltonian is unobtainable. So, we will apply the Exact Diagonalization Method (EDM) as an efficient technique to solve the desired QD Hamiltonian. The EDM is extremely useful for obtaining accurate estimates of the quantum system's energies and related quantities. Moreover, contrary to other methods, except the computer power, the obtained results from the EDM are unaffected by approximations or limitations. It involves constructing the Hamiltonian matrix in a chosen basis and diagonalizing it to find the eigenvalues and eigenvectors.

To apply the Exact Diagonalization Method, we start by selecting a suitable basis to represent the quantum states of the system. The choice of basis depends on the specific

problem and the symmetries involved. Typically, a basis set that spans the relevant Hilbert space is chosen, and the Hamiltonian is expressed in terms of this basis.

Once the Hamiltonian matrix is constructed, it is diagonalized using numerical algorithms such as the Lanczos algorithm or the Davidson algorithm. These algorithms iteratively find the eigenvalues and eigenvectors of the Hamiltonian matrix, allowing us to determine the energy spectra and corresponding wavefunctions of the system.

The advantage of the Exact Diagonalization Method is that it can provide accurate results for small to moderate-sized systems. However, as the dimension of the Hilbert space increases, the computational requirements grow exponentially, making it challenging to apply the method to larger systems.

As a first step, we need to construct a Hamiltonian matrix with elements evaluated as follows:

$$\langle H \rangle = \left\langle \Psi_{n_x n_y s} \middle| \widehat{H} \middle| \Psi_{n_x' n_y' s'} \right\rangle \tag{14}$$

In this work, these matrix elements ($H_{n_x n_y s, n_x' n_y' s'}$) will be obtained in the simplest closed-form to reduce significantly the computational time needed for the diagonalization process.

To diagonalize that matrix and compute the eigensolution, we have to solve the eigenvalue equation $\left| \left\langle \Psi_{n_x n_y s} \middle| \widehat{H} \middle| \Psi_{n_x' n_y' s'} \right\rangle - E\, I \right| = 0$, and obtaining the eigenvalues and eigenstates.

The one-dimensional Harmonic oscillator wave functions will be used as bases to construct the total wave function;

$$\psi(x,y) = \sum_{n,m} C_{n,m} \phi_n(\widetilde{\alpha_x}, x) \phi_m(\widetilde{\alpha_y}, y) \tag{15}$$

where

$$\varphi_n(x) = \frac{1}{\sqrt{2^n n!}} \left(\frac{\widetilde{\alpha_x}}{\sqrt{\pi}}\right)^{\frac{1}{2}} e^{-\frac{\widetilde{\alpha_x}^2 x^2}{2}} H_n(\widetilde{\alpha_x} x) \quad , \widetilde{\alpha_x} = \left(\frac{m^* \widetilde{\omega_x}}{\hbar}\right)^{1/2} \tag{16}$$

$$\varphi_n(y) = \frac{1}{\sqrt{2^n n!}} \left(\frac{\widetilde{\alpha_x}}{\sqrt{\pi}}\right)^{\frac{1}{2}} e^{-\frac{\widetilde{\alpha_y}^2 y^2}{2}} H_n(\widetilde{\alpha_y} y) \qquad , \widetilde{\alpha_y} = \left(\frac{m^* \widetilde{\omega_y}}{\hbar}\right)^{\frac{1}{2}} \tag{17}$$

the effective frequencies, $\widetilde{\omega_x}$ and $\widetilde{\omega_y}$ given as

$$\widetilde{\omega_x} = \sqrt{\omega_x^2 + \frac{\omega_c^2}{4}} \tag{18}$$

$$\widetilde{\omega_y} = \sqrt{\omega_y^2 + \frac{\omega_c^2}{4}} \tag{19}$$

The matrix terms of the full Hamiltonian can be obtained in a closed analytical form in two different ways, as explained:

1) we can express the position and momentum operators in terms of ladder operators of a one-dimensional harmonic oscillator, shown as:

$$a_q = \frac{\widetilde{\alpha_q}}{\sqrt{2}} \left(\hat{q} + \frac{i}{m^* \widetilde{\omega_q}} \widehat{p_q}\right) \tag{20}$$

$$a_q^\dagger = \frac{\widetilde{\alpha_q}}{\sqrt{2}} \left(\hat{q} - \frac{i}{m^* \widetilde{\omega_q}} \widehat{p_q}\right) \tag{21}$$

And then simplify the matrix elements with the help of relations:

$$a_q |n_q\rangle = \sqrt{n_q} |n_q - 1\rangle \tag{22}$$

$$a_q^\dagger |n_q\rangle = \sqrt{n_q + 1} |n_q + 1\rangle \tag{23}$$

where q can be either x or y coordinate.

The previous ladder operator's technique is expected to be the most efficient approach when dealing with the terms that have a linear dependence on the coordinate of momentum, i.e., the SOI terms.

2) Evaluating the integrals using Hermite polynomial orthogonality and recurrence relations are given as,

$$\int_{-\infty}^{\infty} H_m(x) H_n(x) e^{-x^2} dx = \sqrt{\pi} 2^n n! \, \delta_{nm} \tag{24}$$

$$H_{n+1}(x) = 2xH_n(x) - 2nH_{n-1}(x) \tag{25}$$

$$H_n'(x) = 2nH_{n-1}(x) \tag{26}$$

The last technique will be efficient when the Gaussian impurity Hamiltonian is evaluated

2.5 Hamiltonian matrix elements

To complete the diagonalization process, the matrix elements for the Hamiltonian

$$\hat{H} = \hat{H}_1 + V_{\text{imp}}(x,y) + \hat{H}_R + \hat{H}_D \tag{27}$$

Where

$$\hat{H}_1 = \frac{(\vec{p} - e\vec{A})^2}{2m^*} + V_{\text{conf}}(x,y) + \hat{H}_{\text{Zeeman}} \tag{28}$$

can be expressed as

$$\begin{aligned}\left\langle \Psi_{n_x n_y s} \middle| \hat{H} \middle| \Psi_{n_x' n_y' s'} \right\rangle \\ &= \left\langle \Psi_{n_x n_y s} \middle| \hat{H}_1 \middle| \Psi_{n_x' n_y' s'} \right\rangle + \left\langle \Psi_{n_x n_y s} \middle| \hat{V}_{imp} \middle| \Psi_{n_x' n_y' s'} \right\rangle \\ &+ \left\langle \Psi_{n_x n_y s} \middle| \hat{H}_R \middle| \Psi_{n_x' n_y' s'} \right\rangle \\ &+ \left\langle \Psi_{n_x n_y s} \middle| \hat{H}_D \middle| \Psi_{n_x' n_y' s'} \right\rangle \end{aligned} \tag{29}$$

Since the well-known quantum numbers n_x, n_y for the one-dimensional harmonic oscillator will not be long as good quantum numbers, we prefer to use a new notation $n, and\ m$ for the x and y dimensions, respectively. The first term on the right-hand side above can be expanded as,

$$\begin{aligned}&\langle \Psi_{nms} | \hat{H}_1 | \Psi_{n'm's'} \rangle \\ &= \left\langle \Psi_{\text{nm}s} \middle| \frac{\text{P}_\text{x}^2 + P_y^2}{2m} + \frac{1}{2}\omega_c(P_x y - P_y x) + \frac{1}{2}m\left(\left(\omega_x^2 + \frac{\omega_c^2}{4}\right)x^2 + \left(\omega_y^2 + \frac{\omega_c^2}{4}\right)y^2\right) \middle| \Psi_{n'm's'} \right\rangle \\ &= \left((n+1/2)\hbar * \widetilde{\omega_x} + (m+1/2)\hbar * \widetilde{\omega_y} + \frac{1}{2}g_0\mu_B s\right)\delta_{n,n'}\delta_{m,m'}\delta_{s,s'} \\ &+ \left\langle \Psi_{\text{nm}s} \middle| \frac{1}{2}\omega_c(P_x y - P_y x) \middle| \Psi_{n'm's'} \right\rangle \end{aligned} \tag{30}$$

To simplify the last term in the above equation, the position and momentum can be expressed in terms of the previously mentioned ladders operators as,

$$\hat{q} = \sqrt{\frac{\hbar}{2m\widetilde{\omega_q}}}\left(a_q + a_q^{\dagger}\right) \tag{31}$$

$$\hat{p}_q = -i\sqrt{\frac{\hbar m\widetilde{\omega_q}}{2}}\left(a_q - a_q^{\dagger}\right) \tag{32}$$

$$\begin{aligned}
&\left\langle \Psi_{n_x n_y s}\left|\frac{1}{2}\omega_c\left(P_x y - P_y x\right)\right|\Psi_{n_x' n_y' s'}\right\rangle \\
&\quad = \frac{1}{4}\hbar i\omega_c\Bigg(\left(\sqrt{\frac{\widetilde{\omega_x}}{\widetilde{\omega_y}}} - \sqrt{\frac{\widetilde{\omega_y}}{\widetilde{\omega_x}}}\right)\left(\sqrt{n'+1}\sqrt{m'+1}\,\delta_{n,n'+1}\delta_{m,m'+1}\right. \\
&\quad \left. - \sqrt{n'}\sqrt{m'}\,\delta_{n,n'-1}\delta_{m,m'-1}\right) \\
&\quad + \left(\sqrt{\frac{\widetilde{\omega_x}}{\widetilde{\omega_y}}} + \sqrt{\frac{\widetilde{\omega_x}}{\widetilde{\omega_y}}}\right)\left(\sqrt{n'}\sqrt{m'+1}\,\delta_{n,n'-1}\delta_{m,m'+1}\right. \\
&\quad \left.\left. - \sqrt{n'+1}\sqrt{m'}\,\delta_{n,n'+1}\delta_{m,m'-1}\right)\right)\delta_{s,s'}
\end{aligned} \tag{33}$$

Now, to find the matrix element of the Gaussian impurity term

$$\begin{aligned}
&\left\langle \Psi_{n_x n_y s}\left|\hat{V}_{imp}\right|\Psi_{n_x' n_y' s'}\right\rangle \\
&\quad = V_0\left\langle \phi_n(\widetilde{\alpha_x}, x)\phi_m(\widetilde{\alpha_y}, y)\right|\mathrm{e}^{-\frac{(x-x_0)^2}{d^2}} \\
&\quad \times \mathrm{e}^{-\frac{(y-y_0)^2}{d^2}}\left|\phi_{n'}(\widetilde{\alpha_x}, x)\phi_{m'}(\widetilde{\alpha_y}, y)\right\rangle
\end{aligned} \tag{34}$$

Which can be evaluated by separating the integral into independent x and y integrals as

$$\left\langle \Psi_{n_x n_y s}\left|\hat{V}_{imp}\right|\Psi_{n_x' n_y' s'}\right\rangle = V_0\, I_1\, I_2$$

where

$$I_1 = \left\langle \phi_n(\alpha x) \left| \mathrm{e}^{-\frac{(x-x_0)^2}{d^2}} \right| \phi_n'(\alpha x) \right\rangle$$

$$= A \int_{-\infty}^{+\infty} H_n(\widetilde{\alpha_x} x) H_{n'}(\widetilde{\alpha_x} x) e^{-\widetilde{\alpha_x}^2 x^2} \mathrm{e}^{-\frac{(x-x_0)^2}{d^2}} \mathrm{d}x \qquad (35)$$

$$I_2 = \left\langle \phi_m(\beta y) \left| \mathrm{e}^{-\frac{(y-y_0)^2}{d^2}} \right| \phi_m'(\beta y) \right\rangle$$

$$= B \int_{-\infty}^{+\infty} H_m(\widetilde{\alpha_y} y) H_{m'}(\widetilde{\alpha_y} y) \mathrm{e}^{-\widetilde{\alpha_y}^2 y^2} \mathrm{e}^{-\frac{(y-y_0)^2}{d^2}} \mathrm{d}y \qquad (36)$$

With constants $A = \frac{\widetilde{\alpha_x}}{\left(2^{n+n'} n! n'! \pi\right)^{1/2}}$ and $B = \frac{\widetilde{\alpha_y}}{\left(2^{m+m'} m! m'! \pi\right)^{1/2}}$

to simplify the integrations, we use the transformations:

$$\eta_x^2 = \widetilde{\alpha_x^2} + \frac{1}{d^2}\,, \eta_y^2 = \widetilde{\alpha_y^2} + \frac{1}{d^2}\,, \lambda_x = e^{-\frac{x_0^2\left(\eta_x^2 - \frac{1}{d^2}\right)}{d^2\,\eta_y^2}}\,, \lambda_y = e^{-\frac{y_0^2\left(\eta_y^2 - \frac{1}{d^2}\right)}{d^2\,\eta_y^2}}\,,$$

yields

$$I_1 = A\lambda_x \int_{-\infty}^{+\infty} H_n(\alpha_x^* u) H_{n'}(\alpha_x^* u) \mathrm{e}^{-(u-\rho_x)^2} \mathrm{d}u \qquad (37)$$

$$I_2 = B\lambda_y \int_{-\infty}^{+\infty} H_n(\alpha_y^* v) H_{n'}(\alpha_y^* v) \mathrm{e}^{-(v-\rho_y)^2} \mathrm{d}v \qquad (38)$$

Where $\rho_x = \frac{x_0}{\eta_x d^2}$, $\rho_y = \frac{y_0}{\eta_y d^2}$, $\alpha_x^* = \frac{\widetilde{\alpha_x}}{\eta_x}$, $\alpha_y^* = \frac{\widetilde{\alpha_y}}{\eta_y}$, $u = \eta_x x$ and $v = \eta_y y$

With the help of the relation (Grandshteyn & Ryzhik, 1980)

$$\int_{-\infty}^{\infty} e^{-(x-y)^2} H_{n'}(\alpha x) H_n(\alpha x) dx$$

$$= \pi^{\frac{1}{2}} \sum_{k=0}^{\min(n',n)} 2^k k! \binom{n'}{k} \binom{n}{k} (1$$

$$- \alpha^2)^{\frac{n'+n}{2}-k} H_{n'+n-2k}\left[\frac{\alpha y}{(1-\alpha^2)^{\frac{1}{2}}}\right] \qquad (39)$$

It's now easy to write

$$I_1 = D_1 \sum_{k=0}^{min(n,n')} f(k,n,n') \tag{40}$$

$$I_2 = D_2 \sum_{l=0}^{min(m,m')} g(l,m,m') \tag{41}$$

where

$$f(k,n,n') = 2^k k!^n \, C_k C_k (1-\alpha^{*2})^{\frac{n+n'}{2}-k} \times H_{n+n'-2k}(\alpha_1 \, \rho_1) \tag{42}$$

$$g(l,m,m') = 2^l l!^m \, C_l C_l (1-\beta^{*2})^{\frac{m+m'}{2}-l} \times H_{m+m'-2l}(\beta_1 \rho_2) \tag{43}$$

With $D_1 = B\lambda_1 \pi^{1/2}/\eta_1$ and $D_2 = B\lambda_2 \pi^{1/2}/\eta_2$

Finally, the impurity matrix element will be evaluated using the relation:

$$\left\langle \Psi_{n_x n_y s} \middle| \hat{V}_{imp} \middle| \Psi_{n'_x n'_y s'} \right\rangle = D_1 D_2 \sum_{k=0}^{min(n,n')} \sum_{l=0}^{min(m,m')} f(k,n,n') \times g(l,m,m') \, \delta_{s,s'} \tag{44}$$

To evaluate the spin-orbit interaction terms: Rashba and Dresselhaus, we expand the vectors cross product, as

$$H_R = \frac{\alpha_R}{\hbar} [\boldsymbol{\sigma} \times (\mathbf{p} - \mathrm{e}\mathbf{A})]_z = \frac{\alpha_R}{\hbar} \left[\sigma_x \left(p_y - eA_y\right) - \sigma_y (p_x - \mathrm{e}A_x)\right] \tag{45}$$

$$H_D = \frac{\alpha_D}{\hbar} [\boldsymbol{\sigma}.(\mathbf{p} - e\mathbf{A})] = \frac{\alpha_D}{\hbar} \left[\sigma_y \left(p_y - \mathrm{e}A_y\right) - \sigma_x (p_x - \mathrm{e}A_x)\right] \tag{46}$$

Recalling that for the vector potential, we chose the symmetric gauge $\boldsymbol{A} = \frac{B}{2}\,(-y, x, 0\,)$, so equations (45 and 46) can be expressed respectively as,

$$H_R = \frac{\alpha_R}{\hbar}\left(\sigma_x \left(p_y - \frac{eB}{2}x\right) - \sigma_y \left(p_x + \frac{eB}{2}y\right)\right) \tag{47}$$

$$H_D = \frac{\alpha_D}{\hbar}\left(\sigma_y \left(p_y - \frac{eB}{2}x\right) + \sigma_x \left(p_x + \frac{eB}{2}y\right)\right) \tag{48}$$

It is appropriate to use ladder operators for the momentum, position, and spin angular momentum,

$$\sigma_x = \frac{1}{2}\,(\,\sigma_+ + \sigma_-) \tag{49}$$

$$\sigma_y = \frac{1}{2i}\,(\,\sigma_+ - \sigma_-) \tag{50}$$

as a result, the matrix element for Rashba Hamiltonian is evaluated to be in terms of the system's parameters and quantum numbers as follows :

$$\begin{aligned}
\frac{\alpha_R}{2\sqrt{2}\hbar}\Bigg(&\delta_{s,1+s'}\left(-i\delta_{m,-1+m'}\delta_{n,n'}\left(\frac{\omega_c}{\widetilde{\alpha_{\mathrm{y}}}}m^* + 2\hbar\widetilde{\alpha_{\mathrm{y}}}\right)\sqrt{m'}\right.\\
&+ i\delta_{m,1+m'}\delta_{n,n'}\left(-\frac{\omega_c}{\widetilde{\alpha_{\mathrm{y}}}}m^* + 2\hbar\widetilde{\alpha_{\mathrm{y}}}\right)\sqrt{1+m'}\\
&+ \delta_{m,m'}\delta_{n,-1+n'}\left(\frac{\omega_c}{\widetilde{\alpha_x}}m^* + 2\hbar\widetilde{\alpha_{\mathrm{x}}}\right)\sqrt{n'}\\
&\left.+ \delta_{m,m'}\delta_{n,1+n'}\left(\frac{\omega_c}{\widetilde{\alpha_{\mathrm{x}}}}m^* - 2\hbar\widetilde{\alpha_{\mathrm{x}}}\right)\sqrt{1+n'}\right)\\
&+ \delta_{s,-1+s'}\left(-i\delta_{m,-1+m'}\delta_{n,n'}\left(-\frac{\omega_c}{\widetilde{\alpha_{\mathrm{y}}}}m^* + 2\hbar\widetilde{\alpha_{\mathrm{y}}}\right)\sqrt{m'}\right.\\
&+ i\delta_{m,1+m'}\delta_{n,n'}\left(\frac{\omega_c}{\widetilde{\alpha_{\mathrm{y}}}}m^* + 2\hbar\widetilde{\alpha_{\mathrm{y}}}\right)\sqrt{1+m'}\\
&+ \delta_{m,m'}\delta_{n,-1+n'}\left(\frac{\omega_c}{\widetilde{\alpha_x}}m^* - 2\hbar\widetilde{\alpha_{\mathrm{x}}}\right)\sqrt{n'}\\
&\left.+ \delta_{m,m'}\delta_{n,1+n'}\left(\frac{\omega_c}{\widetilde{\alpha_{\mathrm{x}}}}m^* + 2\hbar\widetilde{\alpha_{\mathrm{x}}}\right)\sqrt{1+n'}\right)\Bigg)
\end{aligned} \tag{51}$$

From Eq. (51), one can see the missing of the states with different quantum numbers for the basis harmonic oscillators $(n = n' + 1\ \&\ m = m')$, $(n = n' - 1\ \&\ m = m')$, and same for y quantum numbers, $(n = n'\ \&\ m = m' + 1)$, $(n = n'\ \&\ m = m' - 1)$, where all the above contributions are taken into account for different spin orientations, mathematically $s \neq s'$.

And for the Dresselhaus Hamiltonian, going ahead with same procedures, the result is will be quite similar for the Rashba Hamiltonian, mathematically, the Dresselhaus term give a contribution when $s \neq s'$ and $(n = n' + 1\ \&\ m = m')$, $(n = n' - 1\ \&\ m = m')$, or $(n = n'\ \&\ m = m' + 1)$, $(n = n'\ \&\ m = m' - 1)$.

After simplification, the term will be:

$$\frac{\alpha_D}{2\sqrt{2}\hbar}\Bigg(\delta_{s,1+s'}\Bigg(\delta_{m,-1+m'}\delta_{n,n'}\left(-2\widetilde{\alpha_{\mathrm{y}}}\hbar+\frac{\omega_{\mathrm{c}}m^*}{\widetilde{\alpha_{\mathrm{y}}}}\right)\sqrt{m'}$$
$$+\delta_{m,1+m'}\delta_{n,n'}\left(2\widetilde{\alpha_{\mathrm{y}}}\hbar+\frac{\omega_{\mathrm{c}}m^*}{\widetilde{\alpha_{\mathrm{y}}}}\right)\sqrt{1+m'}$$
$$+\delta_{m,m'}\delta_{n,-1+n'}\left(2i\widetilde{\alpha_{\mathrm{x}}}\hbar-\frac{i\omega_{\mathrm{c}}m^*}{\widetilde{\alpha_{\mathrm{x}}}}\right)\sqrt{n'}$$
$$+\delta_{m,m'}\delta_{n,1+n'}\left(-2i\widetilde{\alpha_{\mathrm{x}}}\hbar-\frac{i\omega_{\mathrm{c}}m^*}{\widetilde{\alpha_{\mathrm{x}}}}\right)\sqrt{1+n'}\Bigg)$$
$$+\delta_{s,-1+s'}\Bigg(\delta_{m,-1+m'}\delta_{n,n'}\left(2\widetilde{\alpha_{\mathrm{y}}}\hbar+\frac{\omega_{\mathrm{c}}m^*}{\widetilde{\alpha_{\mathrm{y}}}}\right)\sqrt{m'}$$
$$+\delta_{m,1+m'}\delta_{n,n'}\left(-2\widetilde{\alpha_{\mathrm{y}}}\hbar+\frac{\omega_{\mathrm{c}}m^*}{\widetilde{\alpha_{\mathrm{y}}}}\right)\sqrt{1+m'}$$
$$+\delta_{m,m'}\delta_{n,-1+n'}\left(2i\widetilde{\alpha_{\mathrm{x}}}\hbar+\frac{i\omega_{\mathrm{c}}m^*}{\widetilde{\alpha_{\mathrm{x}}}}\right)\sqrt{n'}$$
$$+\delta_{m,m'}\delta_{n,1+n'}\left(-2i\widetilde{\alpha_{\mathrm{x}}}\hbar+\frac{i\omega_{\mathrm{c}}m^*}{\widetilde{\alpha_{\mathrm{x}}}}\right)\sqrt{1+n'}\Bigg)\Bigg) \qquad (52)$$

Now, combining all the energy matrix elements, our energy matrix $H_{nn'}$ is ready for diagonalization and extracting the desired quantum dot energy. These obtained energy spectra are used to investigate the dependence of system properties of the QD on the tunable physical parameters.

2.6 Quantum dot properties: magnetic and electronic

From the exact diagonalization output, one can use sufficient single electron's energy spectra to calculate the partition function using canonical definition

The partition function, denoted by Z, is a fundamental quantity in statistical mechanics that characterizes the equilibrium properties of a system. It is defined as the sum over all possible states of the system, weighted by their Boltzmann factors. In the case of a quantum system, the partition function is obtained by considering the energy spectra of single electrons within the system, mathematically,

$$Z=\sum_{n}^{\infty}e^{-\beta E_n} \qquad (53)$$

$\beta = 1/k_BT$, where k_B is a Boltzmann constant**.**

The average energy can be calculated by using the standard statistical expression:

$$\langle E\rangle = -\frac{\partial\, Ln(Z)}{\partial\beta} \tag{54}$$

This expression allows us to determine the average energy as a function of the temperature and the system's energy levels.

The average energy, denoted by ⟨E⟩, is defined as the expectation value of the energy operator over all possible states of the system. It represents the average value of the energy that the system possesses.

To comprehend the magnetic properties of materials, it is essential to investigate how they interact with an external magnetic field. When a magnetic field is applied, it influences the energy levels of the electrons within the quantum dot, leading to changes in the average mean energy of the system. By quantifying the relationship between the applied magnetic field and the resulting changes in energy, the magnetization can be determined.

The magnetization (M) of QD, a key feature that indicates the response of the material to an external magnetic field can be calculated by taking the derivative of the average energy with respect to the magnetic field. This calculation is crucial in understanding the magnetic properties of the materials:

$$\boldsymbol{M} = -\frac{\partial\,\langle E\rangle}{\partial B} \tag{55}$$

Similar to this, the magnetic susceptibility (χ) may categorize a material as diamagnetic when, ($\chi < 0$). and paramagnetic when ($\chi > 0$).

By using the derivate of magnetization (M) with respect to the magnetic field, it is possible to determine the material's magnetic susceptibility

$$\chi = \frac{\partial \mathrm{M}}{\partial \mathrm{B}} \tag{56}$$

It is worth mentioning that the exact derivative in analytical form is unobtainable since the result of the diagonalization process will give us the numerical values for the energy spectra, so we deal with the definition of the derivative; for example, the magnetization can be computed using the following definition,

$$M = \lim_{\Delta B\to 0} \frac{\langle E(B+\Delta B)\rangle - \langle E(B)\rangle}{\Delta B} \tag{57}$$

In the same manner, magnetic susceptibility can be calculated.

In addition to previous quantities, the effective Lande g factor ($g^*_{eff} = g$) will be computed for the low-lying state using the relation

$$g^*_{eff} = \frac{E_{G.s}(\, s \uparrow) - E_{G.s}(s \downarrow)}{\mu_B B} \tag{58}$$

The electronic density of state (DOS) for a QD is another quantity that can reveal much important information about the electronic structure of nanomaterial, which is given as the sum of a series of δ functions as,

$$DOS(E) = \frac{1}{V}\sum_{n=1}^{N} \delta(E - E_{\mathrm{n}}) \tag{59}$$

which we numerically calculated with a Gaussian distribution as,

$$\mathrm{DOS}(E) = \frac{1}{\sqrt{2\pi\Gamma^2}}\sum_{n} \exp\left[\frac{-(E - E_n)^2}{2\Gamma^2}\right] \tag{60}$$

where Γ is the broadening factor, and E_n is the energy of the system, which was shown a result of the diagonalization process.

The algorithm of our work can be visualized by the scheme given in Fig. A.5.

2.7 Convergence tests

The completeness of the wavefunctions in the one-dimensional harmonic oscillator implies that any function, including the arbitrary wave function can be expressed precisely as a linear combination of the basis wavefunctions. This property allows us to decompose complex wave functions into simpler components, facilitating the analysis and understanding of quantum mechanical systems.

The wavefunctions, or basis, of the one-dimensional harmonic oscillator are considered as a complete set so that any function can be expressed in terms of a linear combination of them, yielding that any arbitrary wave function ψ, can be written as,

$$\psi(x, y) = \lim_{N\to\infty}\sum_{n,m}^{N} C_{n,m}\phi_n(\alpha_x, x)\phi_m(\alpha_y, y) \tag{61}$$

Ideally, we have to construct a matrix with infinite dimension for the Hamiltonian to get the exact energy spectra, but in practice, the size of the basis, and hence the dimension

of the Hamiltonian matrix, has to be large enough to ensure the convergence of the state vectors we are interested in. As N becomes large, any further increase of the Hilbert space dimension will not have a noticeable effect on the calculated low-lying excited states, so it is sufficient to take the value of N to ensure that the highest desired energy, let us call it E_f, converges to a specific value as N increases, and this convergence condition is given mathematically as,

$$\left|E_f(\,N+1\,)-E_f(N)\right|=\delta_1<\epsilon_1 \tag{62}$$

Here, ϵ_1 represents the maximum energy value tolerance and depends on our calculation's desired accuracy. For this reason, the numerical method is called exact diagonalization method.

We aim to calculate the energy for low-laying states and then use these energies to investigate the temperature-dependent properties, mainly the partition function (Z). The Z-expression is also an infinite sum over the system energies (ideally, the sum over all the energy spectra of the system), as given later by Eq. (27). The second critical stage is to ensure the issue of convergence at any temperature value; we have to test the effect of larger states above E_f, by applying the condition:

$$Z\,(\,E_f)-Z\,(E_{f-1}\,)=\delta_2\;<\epsilon_2 \tag{63}$$

ϵ_2 represents the maximum tolerance in the partition function value. It is worth mentioning here that as the temperature increases, the electron has a chance to be in the higher state, so the higher state (f) must be increased, and more energy states will be included in the partition function to ensure the converged results, therefore, to have acceptable accuracy in the new E_f , we should reinvestigate the convergence condition given by Eq. (62) and increase the Hilbert space dimension (N). Our two-stage convergence test is summarized in Fig. A.6.

Since the total Hamiltonian in this project contains the combined effects of many physical terms (anisotropic confinement potential, impurity, external magnetic field, and spin orbit interaction effect) we can fix or neglect, temporarily, one or more terms to compare the result and ensure the accuracy of our code and method. One of the essential quantitative checks is taking the isotropic case (by setting $\omega_x=\omega_y$) so, and neglecting the impurity term, the calculated energies using exact diagonalization method in case,

the parabolic quantum dot, will give the same energy are expected to match the analytical energy given by Eq. (4).

Chapter Three
Results and Discussions

This chapter presents the computed numerical results for the energy spectra, magnetization, magnetic susceptibility, effective g factor, and density of state for InAs anisotropic QD presented in the perpendicular magnetic field, taking into account the doping process with acceptor impurity, which has been modeled to Gaussian form. The material parameters for InAs in this work have been chosen to be : $m^* = 0.0239m_0$ and g_0 = -15 (Sanjay Prabhakar et al., 2011).

3.1 Hamiltonian matrix and diagonalization

In Fig.2, the Hamiltonian matrix has been displayed to investigate the effect of each term on the system's electronic properties; as previously mentioned, the isotropic (circular) quantum confinement in the spatial direction has an analytical solution in terms of the used HO bases, so as expected result to give a contribution to main diagonal of the Hamiltonian as shown in Fig. 2(a), the value of the energy equals the two-dimensional harmonic oscillator energy. The presence of the magnetic field causes a new mixing between the eigenstates as appeared in the last term in Eq. 30, so mixing the state with $\Delta n = \pm 1$, $\Delta m = \pm 1$, and $\Delta s = 0$, so from this point, the well-known n_x, n_y will not be longer a good quantum numbers to describe the system states; this remark can be seen in Fig. 2(b). it's worth mentioning here that the solution for the anisotropic HO is previously discussed; the analytical solution has been found using appropriated canonical transformation with new rotated bases, for the interested reader can refer to (S. Avetisyan et al., 2012). The SOI terms: Rashba and Dresselhaus give a new mixing between the state and the interesting remark that the SOI mixes the states with a different spin as shown in Fig. 2(c) and d, finally, the on-center Gaussian impurity contributed to mixing the states, as shown in Fig. 2(e) the combined matrix for the above matrix terms has been collected in Fig 2(f).

from Fig. 2(f), one can see that the combined effect of the Gaussian impurity and the both type of the SOI, give more contribution for the of diagonal terms, means they significantly mixed the original harmonic oscillator's states, as result a higher matrix dimension is required to ensure the convergence issue.

Figure 2:

Hamiltonian matrix for the anisotropic quantum dot a) the diagonal term b) mixing term $\left\langle \Psi_{nms} \left| \frac{1}{2}\omega_c(P_x y - P_y x) \right| \Psi_{n'm's'} \right\rangle$ *c) Rashba SOI d) Dresselhaus SOI e) on center impurity elements f) the total Hamiltonian matrix*

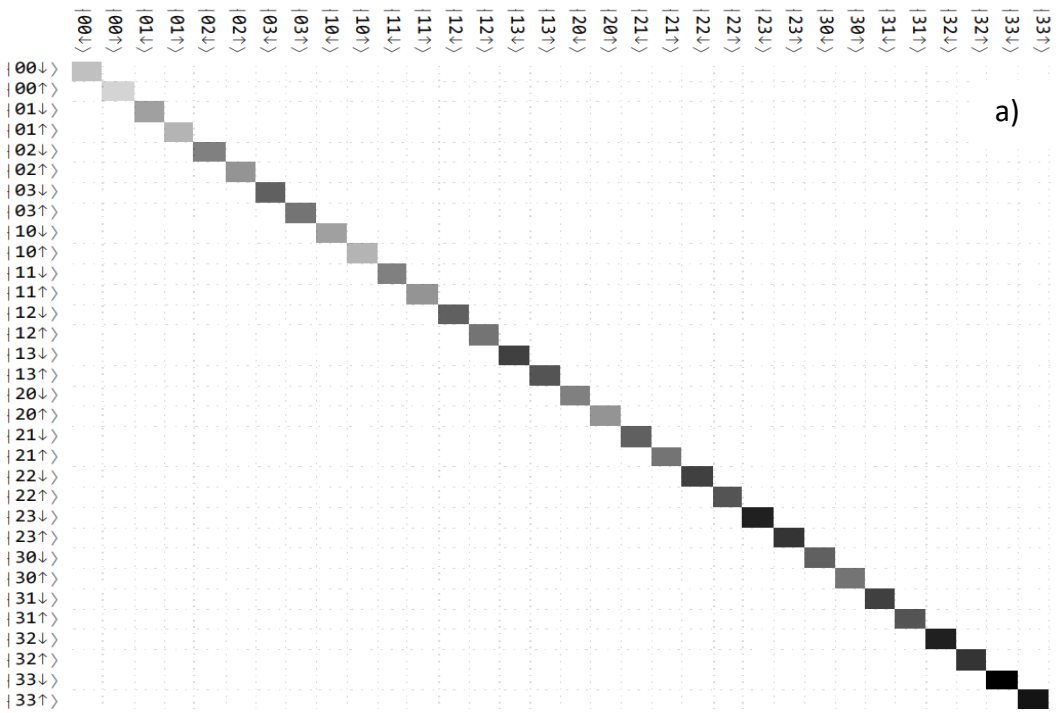

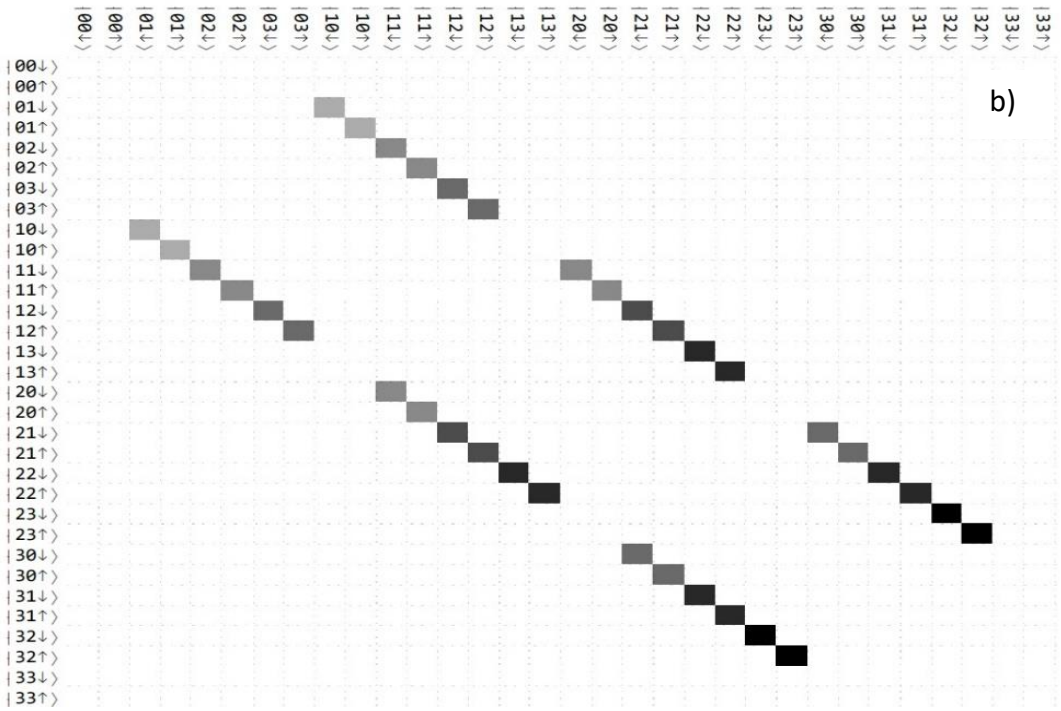

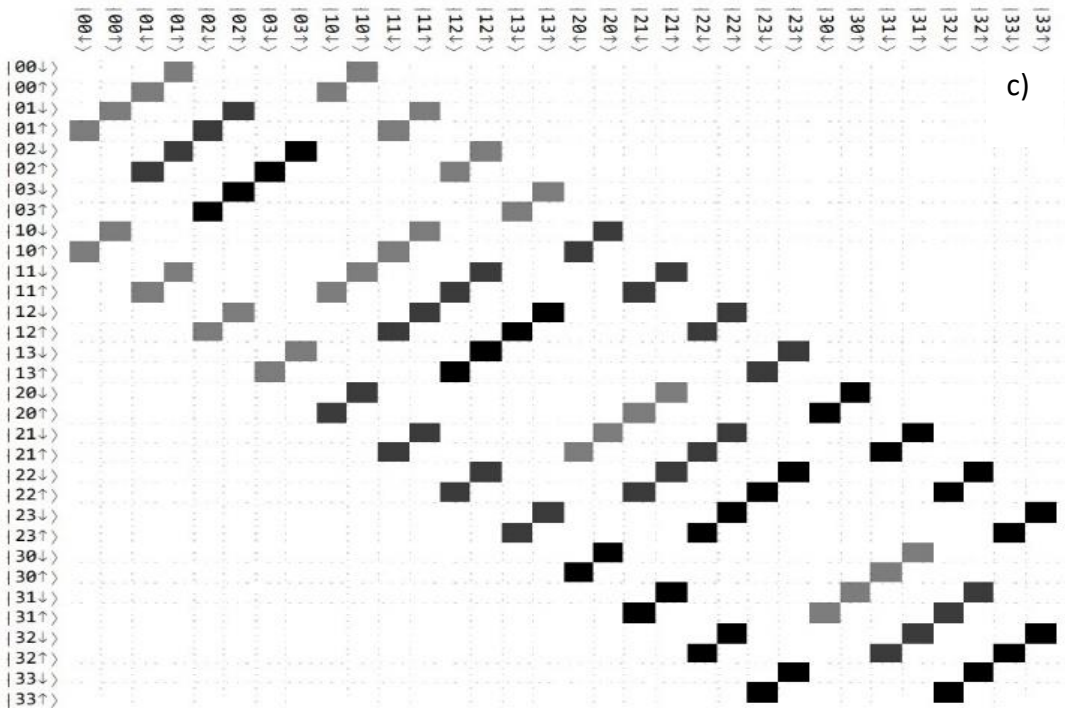
c)

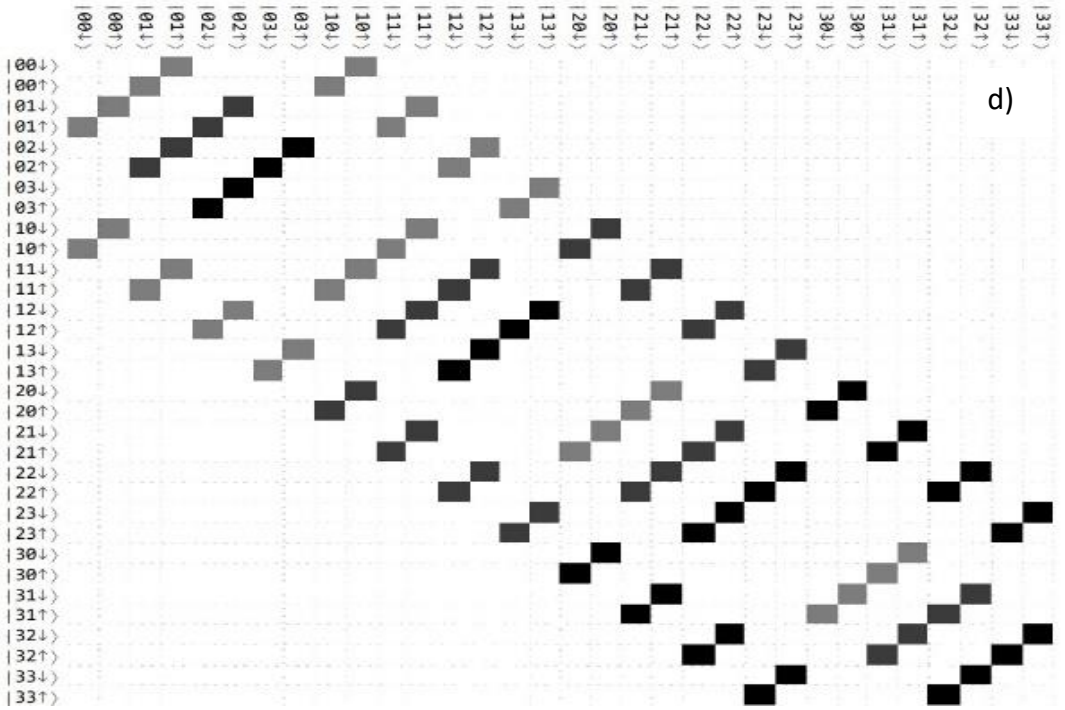
d)

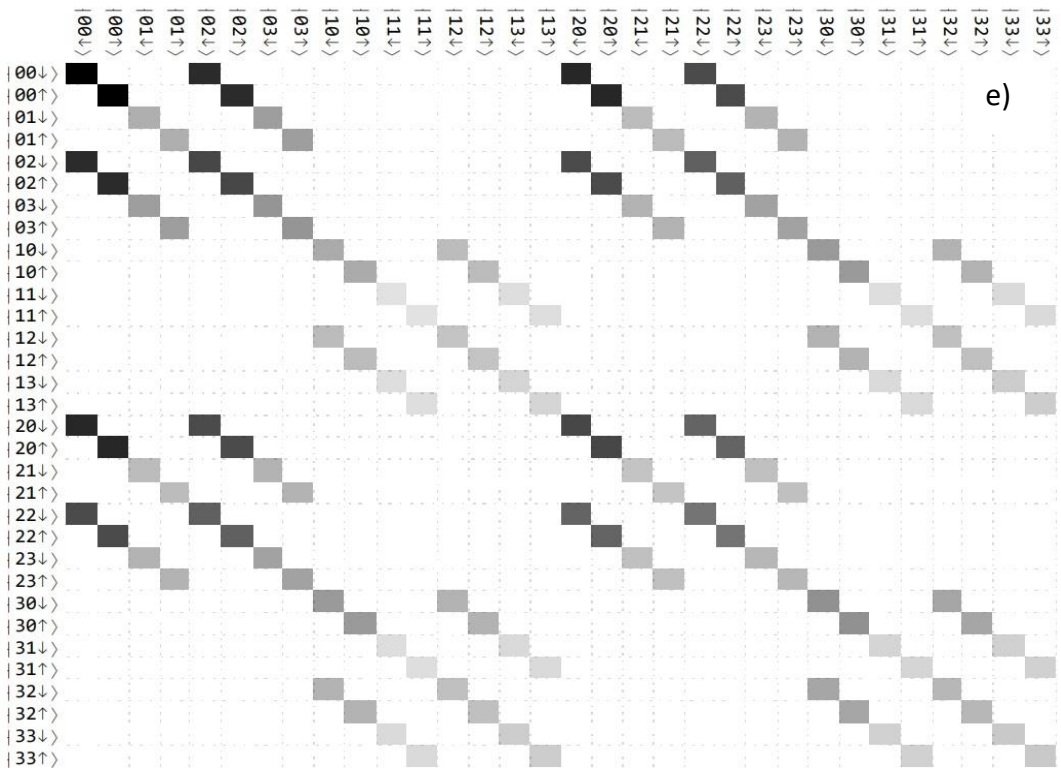
e)

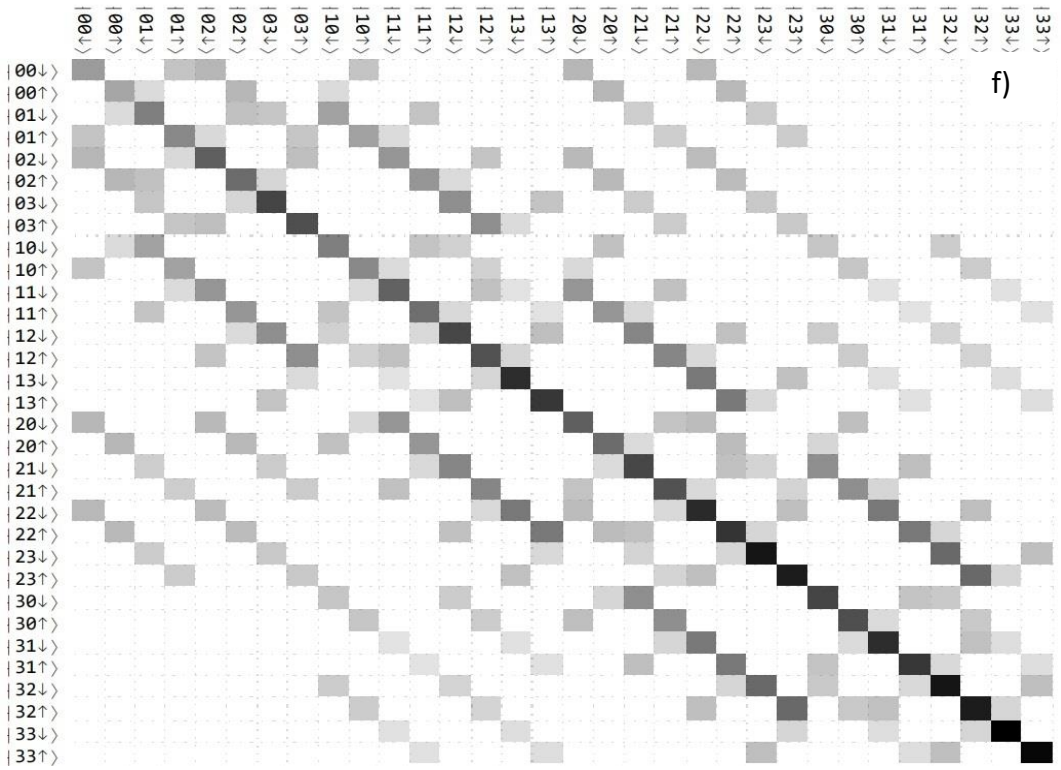
f)

Another crucial point is that using a closed analytical form for evaluating the Hamiltonian matrix elements significantly speeds up computation processes. For instance, the impurity matrix element term in Eq. 34 was calculated using the numerical integration method, and using the output from Eq. 44. the computation time and the matrix elements values for some low-lying states are given in Table 2.

For example, the analytical evaluation of the matrix element of the impurity $\langle 1,1 \left| H_{imp} \right| 1,1 \rangle$ is 62 times faster than the numerical integration. It is worth to mention that in case of on center impurity, the impurity Hamiltonian is even in each spatial dimension, so it's expected to get zero contribution if at least the bra and ket of the x or y harmonic oscillator basis have different parity as $\langle 1,1 \left| H_{imp} \right| 1,2 \rangle$ and $\langle 2,1 \left| H_{imp} \right| 3,2 \rangle$.

In case the impurity Hamiltonian makes zero contribution, numerical integration methods often require a considerable amount of time to ensure accurate zero values. This is because numerical integration involves discretizing the problem domain and evaluating the integrand at multiple points, which can be computationally expensive. It requires a fine-grained sampling to capture the small variations in the integrand that may lead to non-zero values, even when the impurity Hamiltonian is expected to contribute nothing.

However, when a closed analytical expression is available, the computation time can be significantly reduced. Analytical expressions provide a direct mathematical formula or equation to calculate the desired quantity without the need for numerical approximations. By substituting the necessary variables and parameters into the analytical expression, the result can be obtained promptly, often with a lower computational cost compared to numerical methods.

The basis-functions with n_x, n_y were taken from $0 - 30$ for each direction in the linear variational calculation. The direct product of the basis gave a 30 X 30-dimensional space. We confirmed that the basis functions cover the two-dimensional space, at least in expressing the observables under investigation. A larger number of basis functions were used in the convergence test. Table 3 shows the eigenenergies for the ground and the first two excited states for a range of basis functions.

Table 2

On-center impurity matrix element for $\boldsymbol{\omega_x = 6\ meV}$, $\boldsymbol{\omega_y = 3\ meV}$, $\boldsymbol{d = 10\ nm}$, *using numerical integration and closed form given in Eq 44*

	Numerical matrix elements		Analytical matrix elements	
$(H_{imp})_{n,m,n',m'}$	Time (sec)	element value (arb. unit)	Time (sec)	element value (arb. unit)
1,1,1,1	0.019907	1.56501869	0.0003211	1.565019
1,1,1,2	0.002576	0	0.0002766	0
1,1,1,3	0.057623	-0.742598035	0.0003056	-0.7426
1,1,2,1	0.032559	0	0.0003129	0
1,1,2,2	0.071604	0	0.0003115	0
1,1,3,1	0.066772	-0.474280457	0.0003008	-0.47428
1,1,3,2	0.133869	0	0.0003289	0
1,1,3,3	0.215458	0.225045131	0.0003257	0.225045
1,2,1,1	0.002405	0	0.0002741	0
1,2,1,2	0.024303	1.150427913	0.0003658	1.150428
1,2,1,3	5.461316	0	0.0003951	0
1,2,2,1	0.081158	0	0.0002921	0
1,2,3,1	0.155340	0	0.0003213	0
1,2,3,2	0.098687	-0.348639	0.0003433	-0.34864
1,2,3,3	6.420399	0	0.0004045	0
2,1,1,1	0.040773	0	0.0002983	0
2,1,1,3	0.11347	0	0.00036	0
2,1,2,1	0.026372	1.241433	0.0003509	1.241433
2,1,2,2	0.002800	0	0.0003636	0
2,1,2,3	0.089877	-0.58906	0.0003739	-0.58906
2,2,1,1	0.088176	0	0.0003478	0

Table 3

The low-lying state energies for different basis numbers at $\boldsymbol{V_0 = 16\ meV, d = 10\ nm, \omega_x = 4meV, \omega_y = 6\ meV}$, *and* $\boldsymbol{B = 2T}$

Dimensional space	G. S	1st excited state	2nd excited state
5×5	10.2834	12.9467	20.3453
10×10	10.0443	11.0118	11.3830
12×12	10.0311	10.9846	11.3798
15×15	10.0140	10.9043	11.3779
17×17	10.0093	10.9008	11.3766
20×20	10.0025	10.8960	11.3750
22×22	10.0025	10.8960	11.3750
25×25	9.9996	10.8938	11.3747
27×27	9.9995	10.8938	11.3746
30×30	9.9995	10.8938	11.3746
35×35	9.9995	10.8938	11.3746
40×40	9.9995	10.8938	11.3746
45×45	9.9995	10.8938	11.3746

3.2 Energy spectra and electron probability

In Fig. 3 (a and b), we have shown the Fock-Darwin states of a single electron in the absence of impurity ($V_0 = 0$), for circular QD Fig. 3(a) and elliptical QD Fig. 3(b). The figures show quite similar behavior of the energies as a function of B, except that the degeneracies of the states are lifted at B=0 due to different confinement strengths in x and y directions; this result has been previously reported in Ref (Siranush Avetisyan et al., 2012). At $B \neq 0$ the most characterized feature of the figures is that the Fock Darwin levels are split due to Zeeman interaction into two substates corresponding to different spin orientations. This separation between the two sublevels shows linearly behavior with the applied magnetic field as $|\mu_B g\ B|$. Fig. 3(c and d) highlights the effect of an on-center gaussian impurity on the state's energies of the system as a function of

$\boldsymbol{B}$. An interesting level crossing between the ground state and the first excited state has appeared at a particular B. In the isotropic (anisotropic) potential case, this crossing occurs at $B \approx 2.4\,T$ $(2.8T)$.

We have studied the dependence of low-lying states on the impurity profiles (strength, influence domain, and position). Fig. 3(e, f, g) shows the effect of the acceptor impurity domain on the level crossing; as d increases, the intersection point occurs at a lower magnetic field value. Also, by comparing Figs. 3(d, e, and h), it is revealed that increasing the impurity strength for a fixed influence domain moves the crossing to a lower B value.

In Fig. 3(i and j) we plot the low-lying states as a function of impurity strength (Fig. 3(i)) and impurity domain (Fig. 3(j)). The on-center impurity affects the ground state ($|0,0\rangle$) more than other states, and this increase in the ground state energy makes the levels cross. As V_0 increases, the repulsive force between the impurity and the electron increases; as a result, the electron is pushed from the center to be at a higher energy state. In the same way, as d increases, the impurity effect is speared from the center, so the electron is being pushed further away. Another observation is that when d increases, the excited states are also significantly affected by the impurity potential.

To explain this observation, the electron probability density has been plotted in Fig. A.7 for different impurity profiles (strength, position, and domain). As the top panel shows, in the absence of impurity, the electron in the state $|0,0\rangle$ has a higher probability of being at the center of the quantum dot. Since, $\omega_x < \omega_y$. The first excited state ($|1,0\rangle$) has a node in the x-direction, while the state $|0,1\rangle$ is the second excited state (which has a node in the y-direction), These distinct nodal patterns in the excited states underscore the different behaviors resulting from the anisotropic nature of the confinement potential in the x and y directions. In the presence of an on-center impurity, the charge density distributes away due to electron-impurity repulsion, so the electron has a greater probability of being further from the center, while for the excited states $|1,0\rangle$ and $|0,1\rangle$ the electron probability at the center is zero, so the presence of the impurity has an insignificant effect on these excited states' probability, therefore, a minor effect on the state's energy, especially for low values of d.

Figure 3

Low-lying state energies of the QD: (a - h) as a function of B, (i) as function of $\boldsymbol{V_0}$ *and (j) as function of d.*

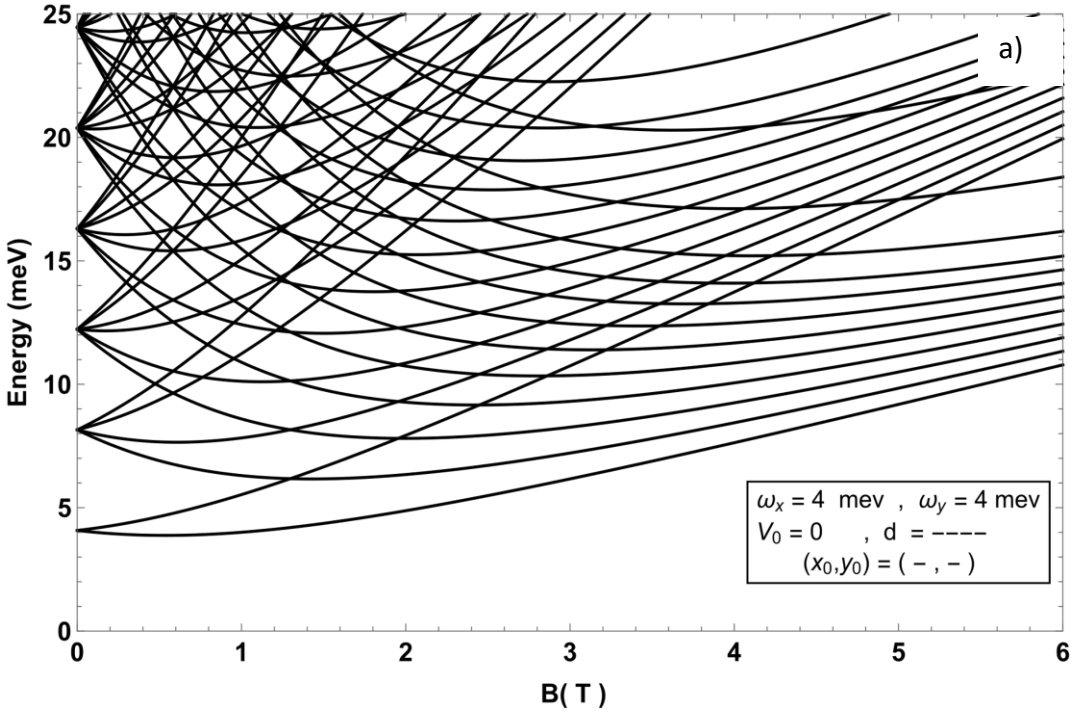

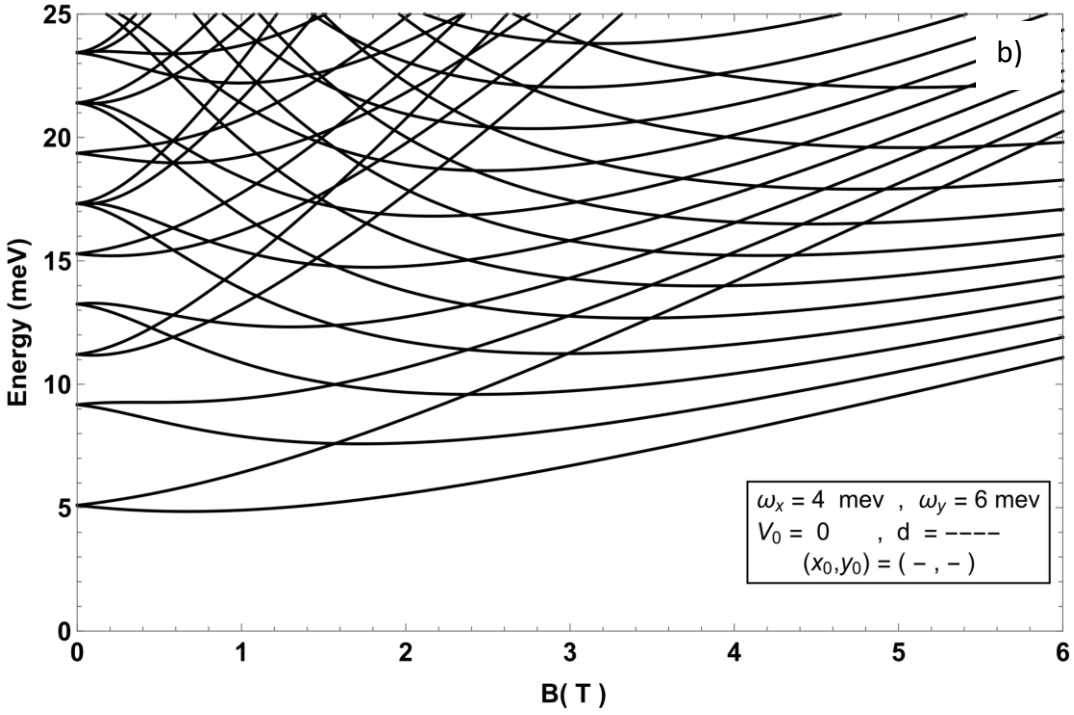

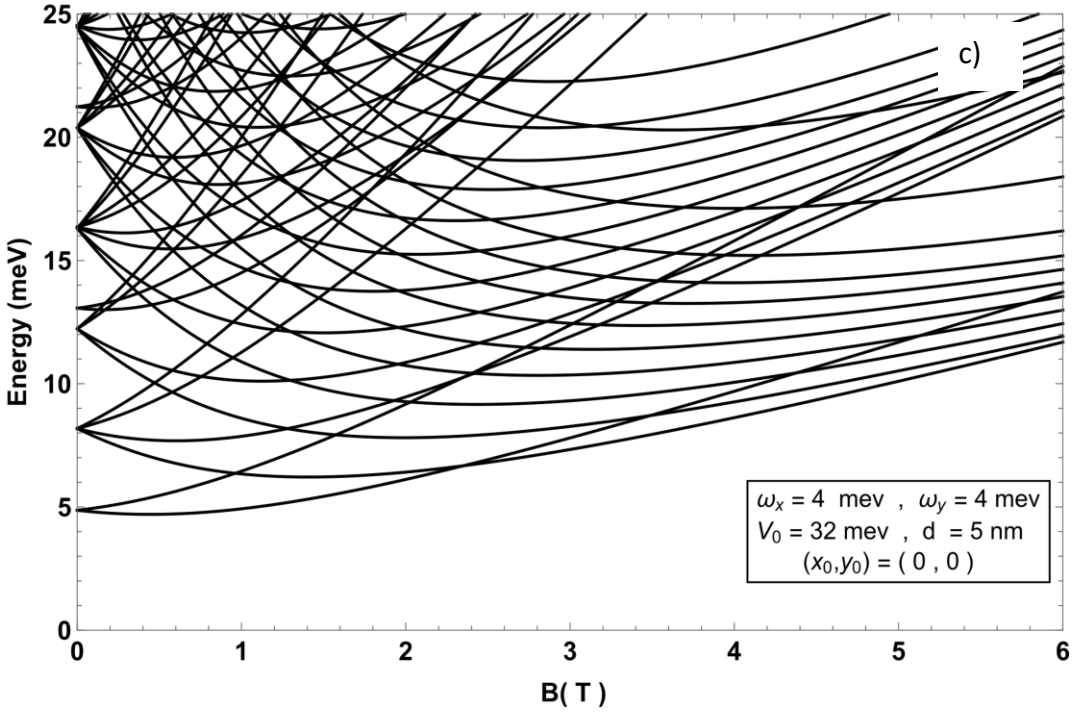
c)
Energy (meV)
B(T)
ω_x = 4 mev , ω_y = 4 mev
V_0 = 32 mev , d = 5 nm
(x_0,y_0) = (0 , 0)

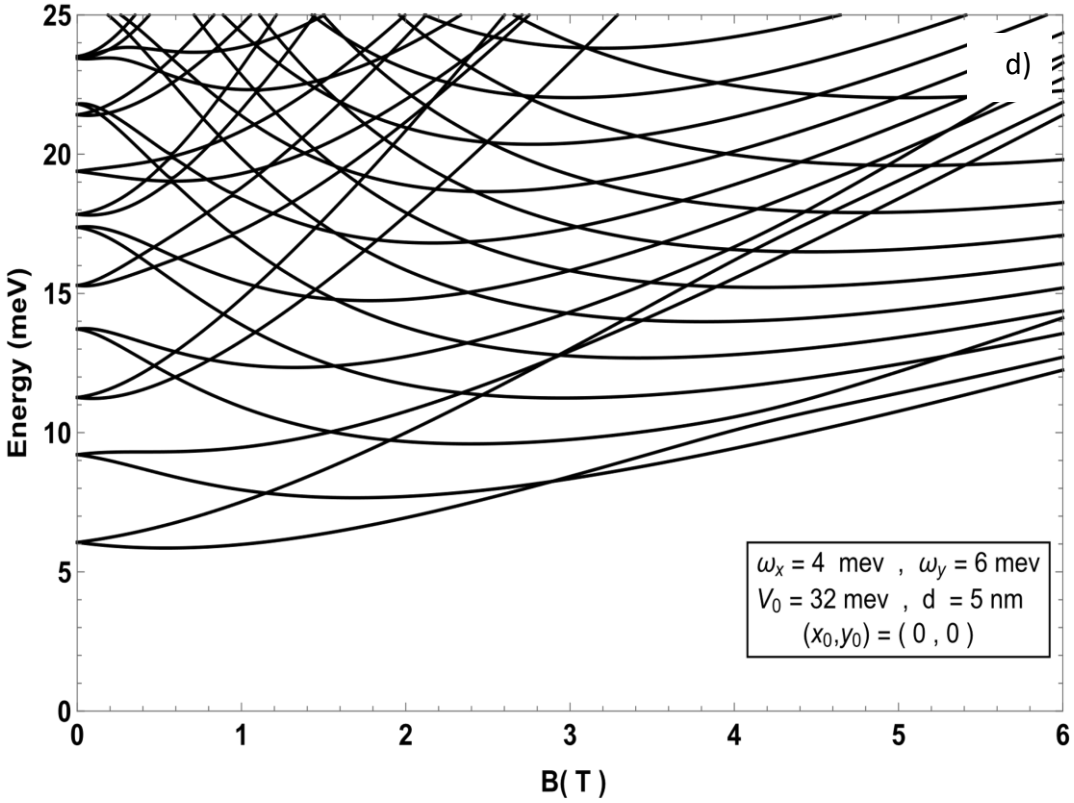
d)
Energy (meV)
B(T)
ω_x = 4 mev , ω_y = 6 mev
V_0 = 32 mev , d = 5 nm
(x_0,y_0) = (0 , 0)

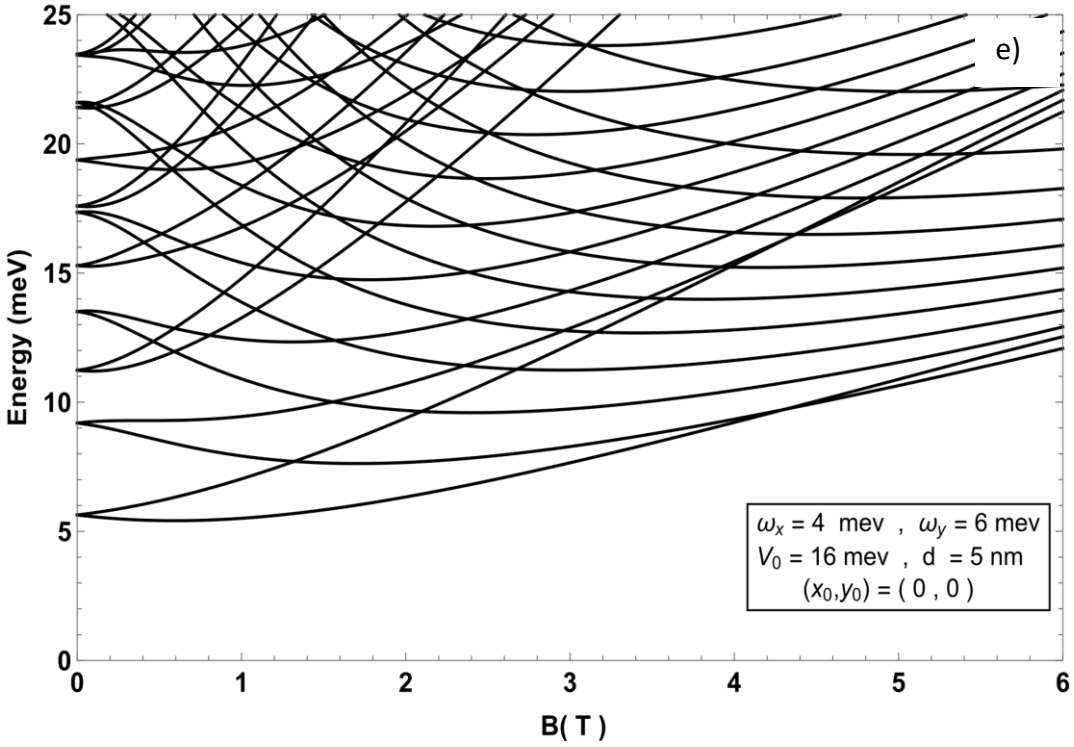
e)
Energy (meV)
B(T)
ω_x = 4 mev , ω_y = 6 mev
V_0 = 16 mev , d = 5 nm
(x_0,y_0) = (0 , 0)

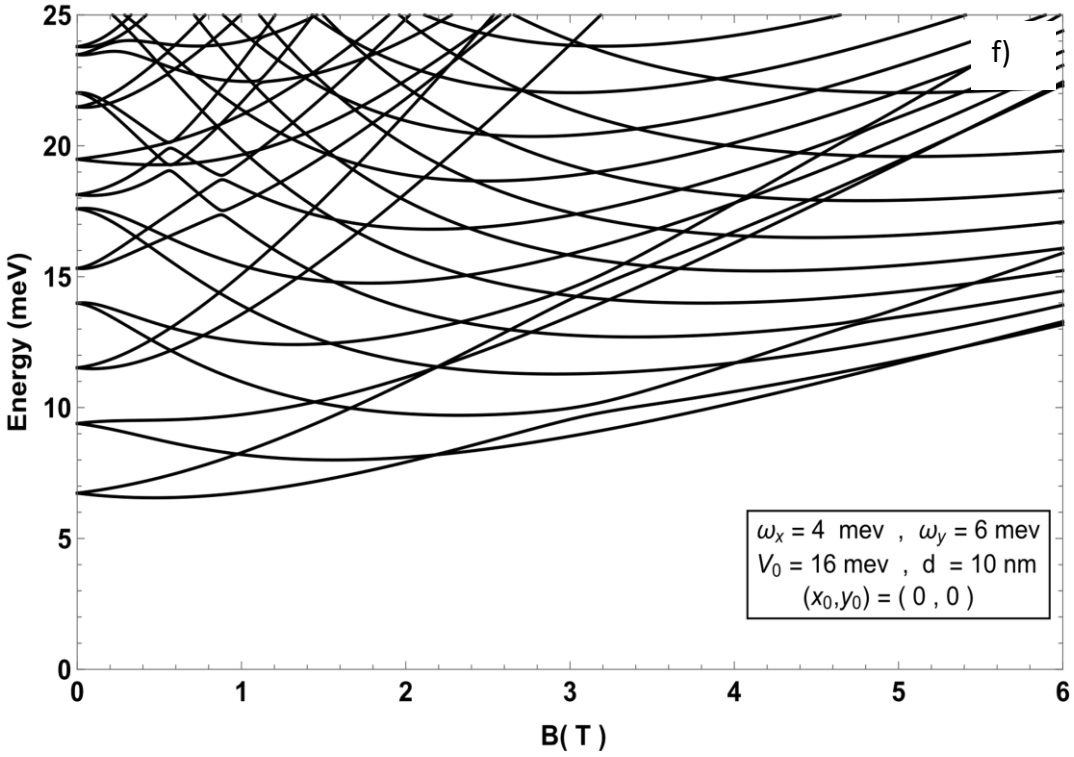
f)
Energy (meV)
B(T)
ω_x = 4 mev , ω_y = 6 mev
V_0 = 16 mev , d = 10 nm
(x_0,y_0) = (0 , 0)

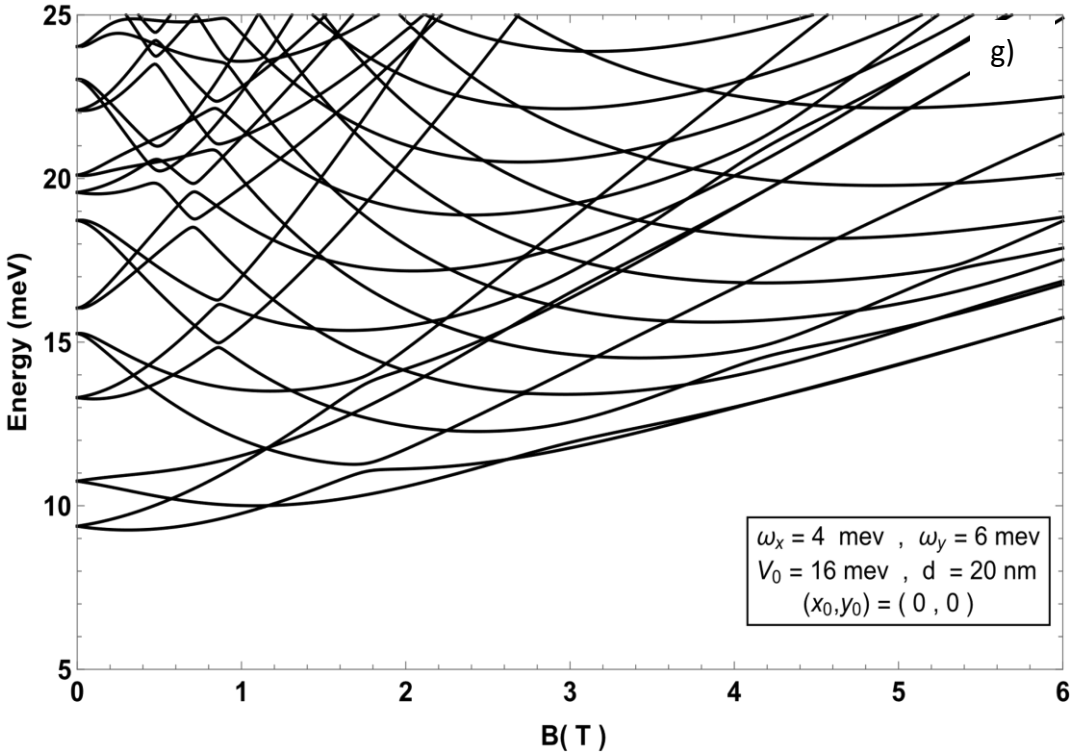
g)
Energy (meV)
B(T)
ω_x = 4 mev , ω_y = 6 mev
V_0 = 16 mev , d = 20 nm
(x_0,y_0) = (0 , 0)

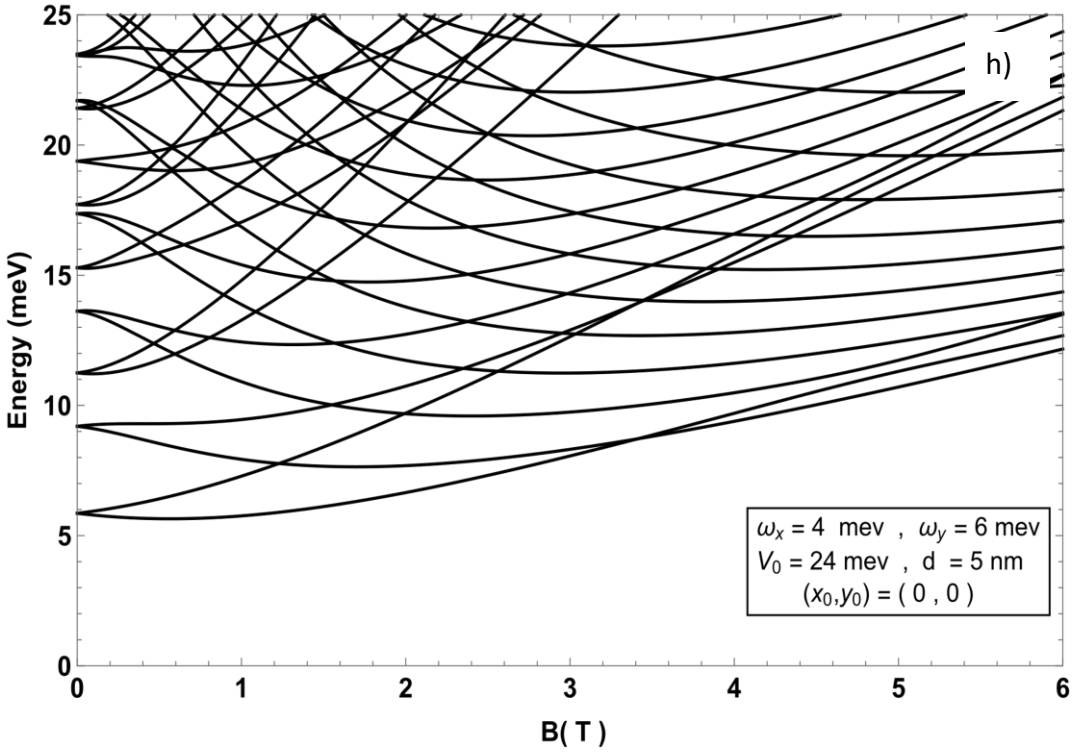
h)
Energy (meV)
B(T)
ω_x = 4 mev , ω_y = 6 mev
V_0 = 24 mev , d = 5 nm
(x_0,y_0) = (0 , 0)

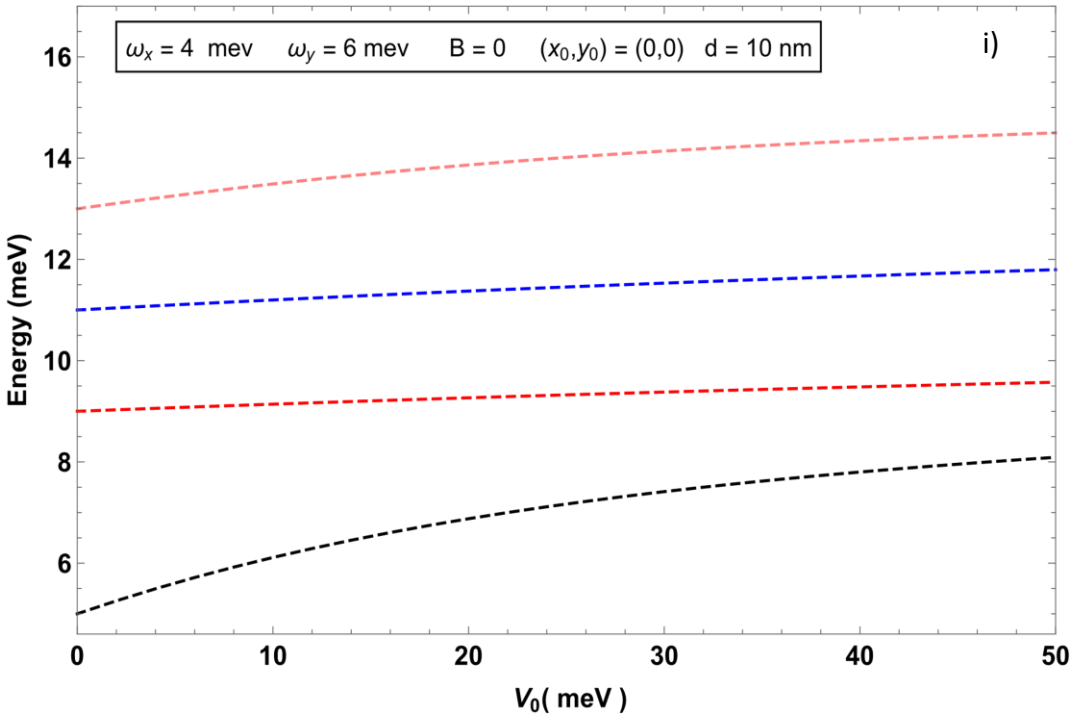
ω_x = 4 mev ω_y = 6 mev B = 0 (x_0,y_0) = (0,0) d = 10 nm
i)
Energy (meV)
16
14
12
10
8
6
0
10
20
30
40
50
V_0(meV)

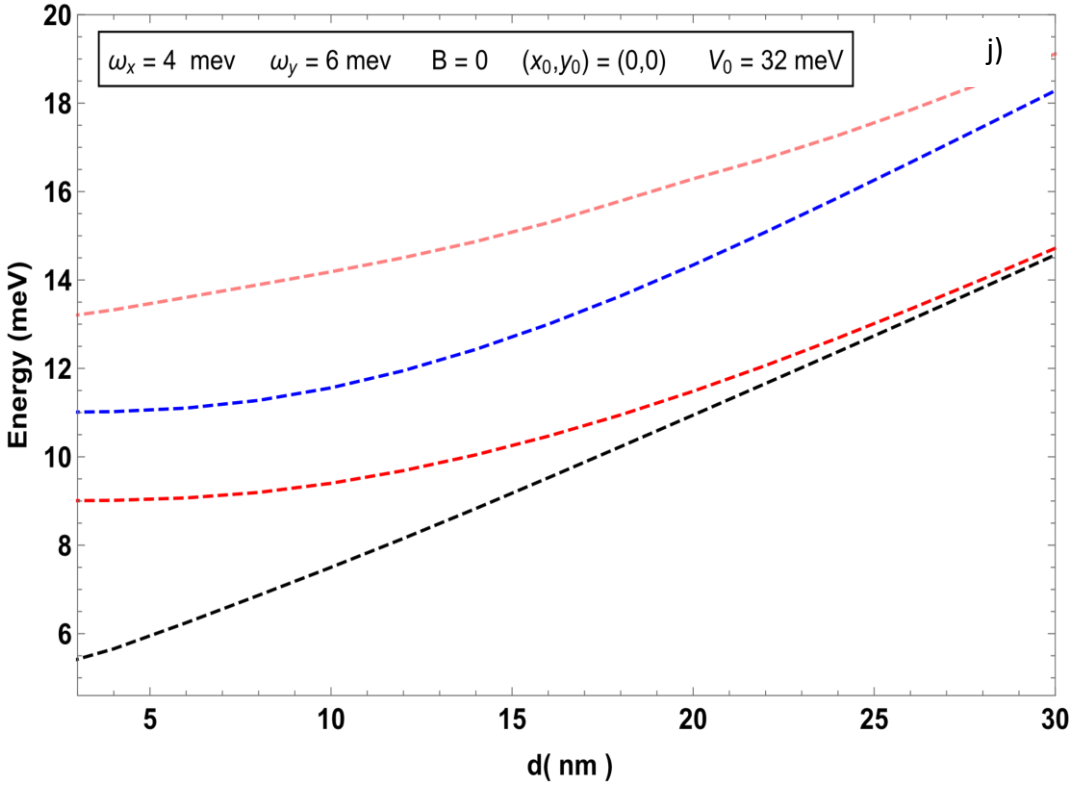
ω_x = 4 mev ω_y = 6 mev B = 0 (x_0,y_0) = (0,0) V_0 = 32 meV
j)
Energy (meV)
20
18
16
14
12
10
8
6
5
10
15
20
25
30
d(nm)

As the impurity strength increases, the probability becomes less at the center, so the electron is obligated to be at a higher confined point due to the parabolic well in the x and y directions. On the other hand, for a larger value of d (bottom panel of Fig. A.7), the effects of impurity on the excited states are apparent, and the effects on the state $|1,0\rangle$ and $|0,1\rangle$ varies due to the isotropy of the QD.

From Fig. 4(a), it is clear that the $E_{G.S}$ increases as the impurity strength increases, and the cusp, which corresponds to the crossing, shifts to the left towards a lower magnetic field due to available repulsive energy as the strength increases. In Fig. 4(b), the effect of the impurity domain on the $E_{G.S}$ has been displayed. As d increases, more cusps appear in the $E_{G.S}$. For example, two cusps for $d = 20\,nm$ correspond to the two crossings in Fig. 3(c).

In Fig. 4(c and d), we have displayed the effect of impurity position on the energy level for the four low-lying states. From these two plots, we can conclude that the off-center impurity position affects the states with a larger probability of the electron being at the impurity position; when the impurity is located at x (y) = 22 nm from the origin, the energy of the state $|1,0\rangle$ ($|0,1\rangle$) is significantly affected, while the sates $|0,1\rangle$ ($|1,0\rangle$) are minorly affected due to their node at $x\,(y) = 0$, whereas the third excited state $|2,0\rangle$ is more affected by the on-center impurity than the lower excited states due to its electron probability at $x = 0$.

The electron's probability density was calculated and plotted in Fig. A.8 for the previous four orbits (ground state and the first, second and third excited states) for anisotropic quantum dot ($\omega_x = 4\,meV, \omega_y = 6\,meV$) in presence and absence of impurity to support the result of Fig. 4 and make it more understandable. The density extends perpendicular to the axis, which contains the impurity. for example, as the impurity located at (22 nm,0), which approximately the position of the anti-node of the first excited state $|1,0\rangle$ of the harmonic oscillator basis at given system parameters and the electron has a high probability to be there, the electron is pushed away from the impurity location and the probability density is redistributed to be extended in the y-direction, so the electron has a larger probability to be at further point from the origin, As a consequence, the energy value increases, on other hand.

Figure 4

$E_{G.S}$ *as a function of B for different impurity profiles (a and b), Impurity position effect on the low-lying energy state (c and d)*

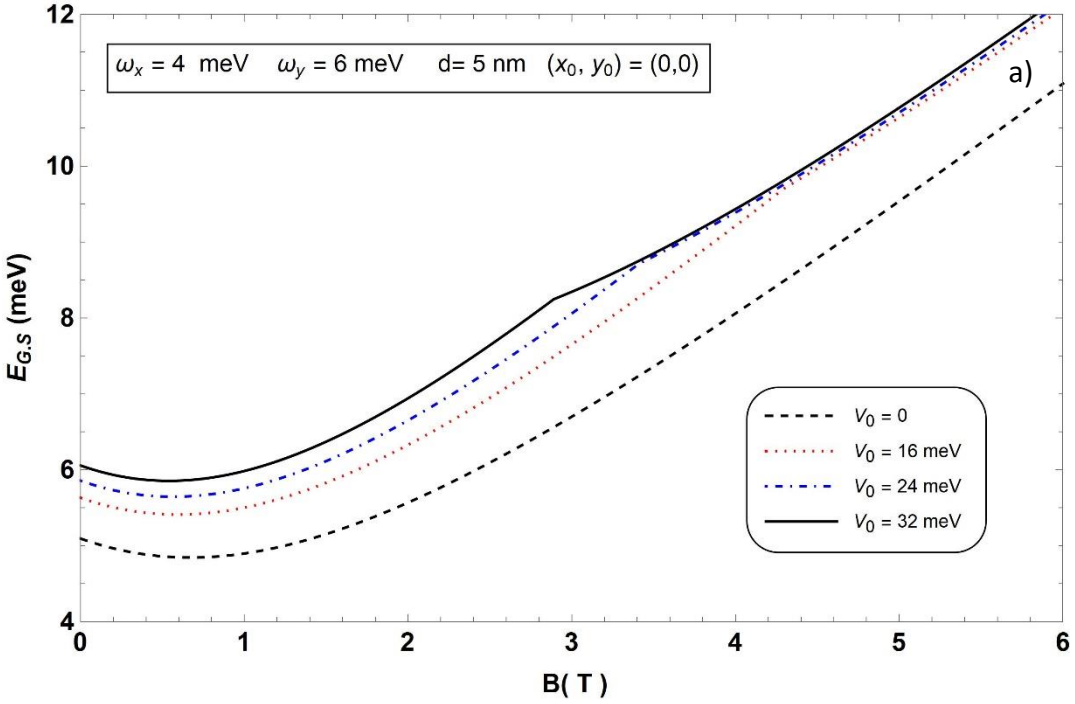

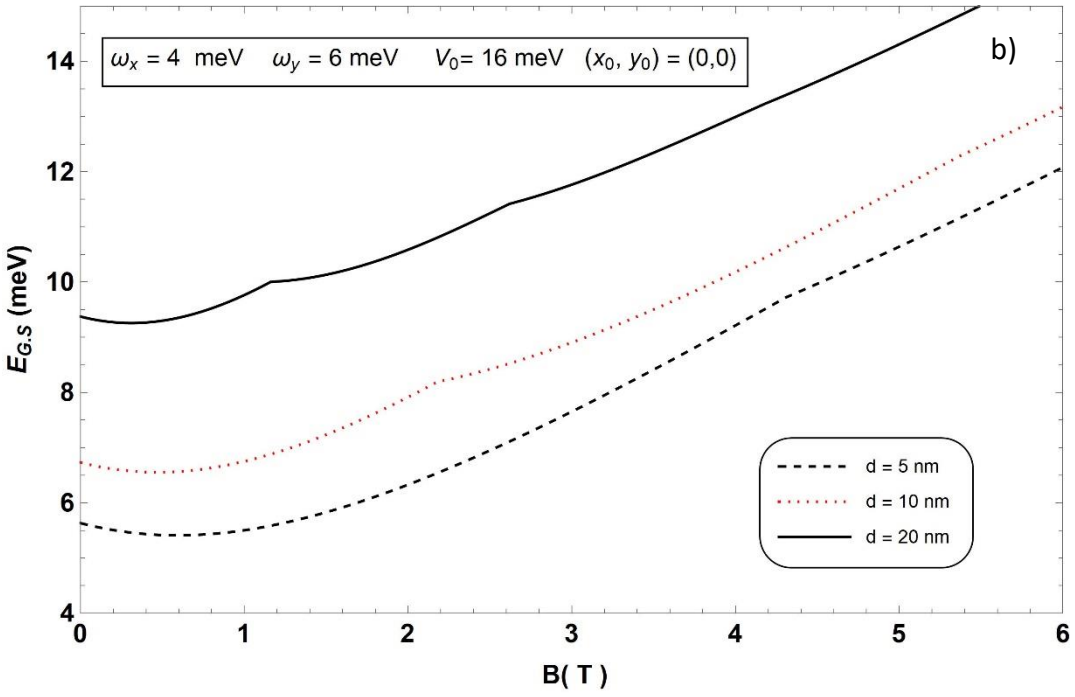

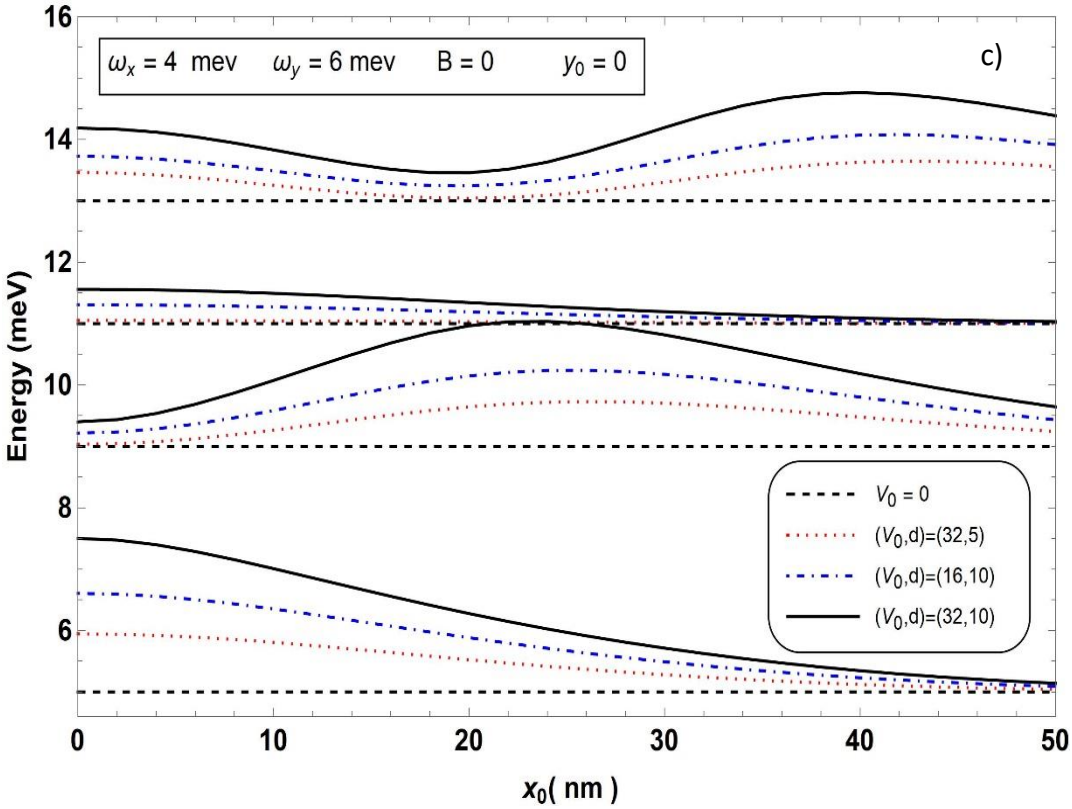
ωx = 4 mev ωy = 6 mev B = 0 y0 = 0
c)
Energy (meV)
x0(nm)
V0 = 0
(V0,d)=(32,5)
(V0,d)=(16,10)
(V0,d)=(32,10)

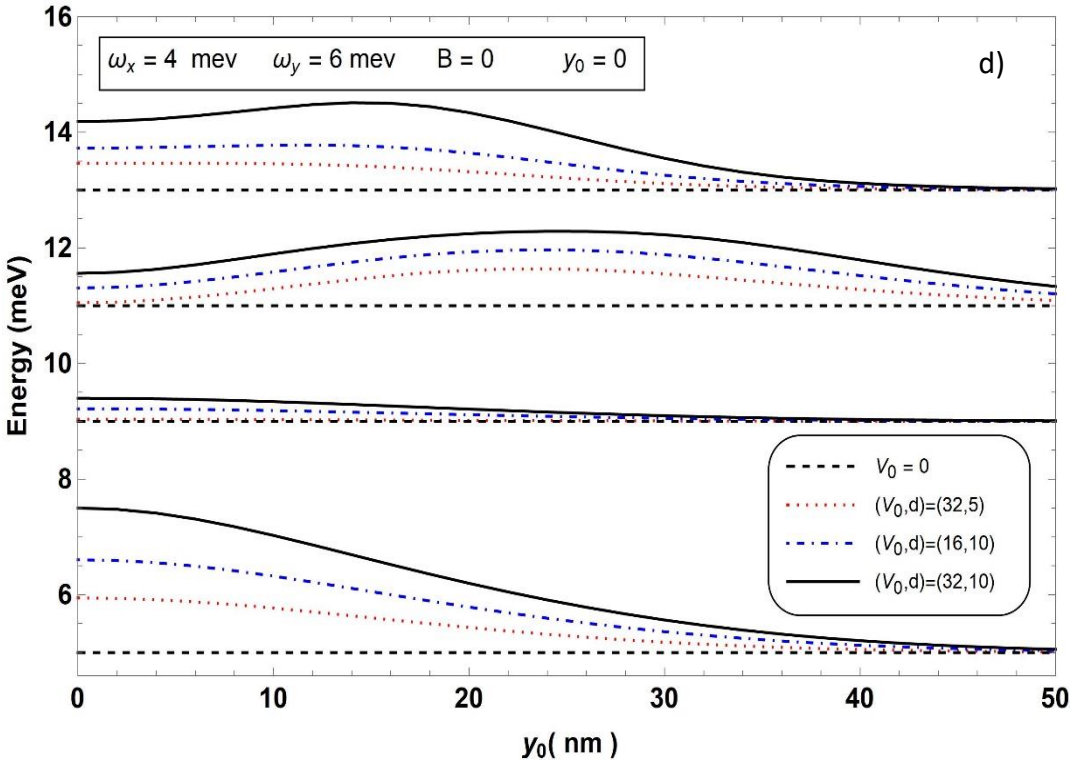
ωx = 4 mev ωy = 6 mev B = 0 y0 = 0
d)
Energy (meV)
y0(nm)
V0 = 0
(V0,d)=(32,5)
(V0,d)=(16,10)
(V0,d)=(32,10)

3.3 Magnetic properties of the Quantum dot system

The average statistical energy has been plotted in Fig.5 in the presence of on-center impurity for different temperatures, and the figure shows that the $\langle E \rangle$ is very similar to the ground state energy at low temperatures $T \to 0$, $E_{G.S}$ has cusps at the level crossings, where the states are degenerate.

In Fig. 5(b). The average statistical energy has been plotted as a function of T for different numbers of states. The results show that at low temperatures, there is no need to take a greater number of states since, at low temperatures, the probability of the electron to be in the higher states is neglectable. However, as the temperature increases, an interesting phenomenon occurs. The electron now possesses a notable probability of occupying higher energy states. Consequently, to ensure proper convergence and accuracy in describing the system's statistical energy, the summation must be extended to larger values of N_{max}. By including a greater number of states, the calculation encompasses a wider range of possible electron configurations, thereby accounting for the increased likelihood of the electron residing in higher energy levels at elevated temperatures.

These results highlight the crucial role of temperature in determining the necessary number of states to consider for an accurate representation of the system's statistical energy. It showcases the importance of carefully selecting N_{max}. based on the temperature regime of interest to effectively capture the behavior of the electron in different thermal conditions.

Numerically, when the temperature (T) is within the low range (T < 20 K), it is observed that the average energy curves exhibit a high degree of similarity regardless of the chosen value for N_{max}. In this regime, the system's behavior is such that the probability of the electron occupying higher energy states is significantly diminished at these lower temperatures.

However, as the temperature enters the higher range (T > 20 K), a distinct change in behavior is observed. At these elevated temperatures, the electron gains a substantial probability of occupying higher energy states. As a consequence, the convergence of the average energy curves becomes dependent on the value of N_{max}.

Figure 5

a) $\langle \boldsymbol{E} \rangle$ *vs. the magnetic field for fixed impurity profiles b)* $\langle \boldsymbol{E} \rangle$ *vs. the T for different* $\boldsymbol{N_{max}}$

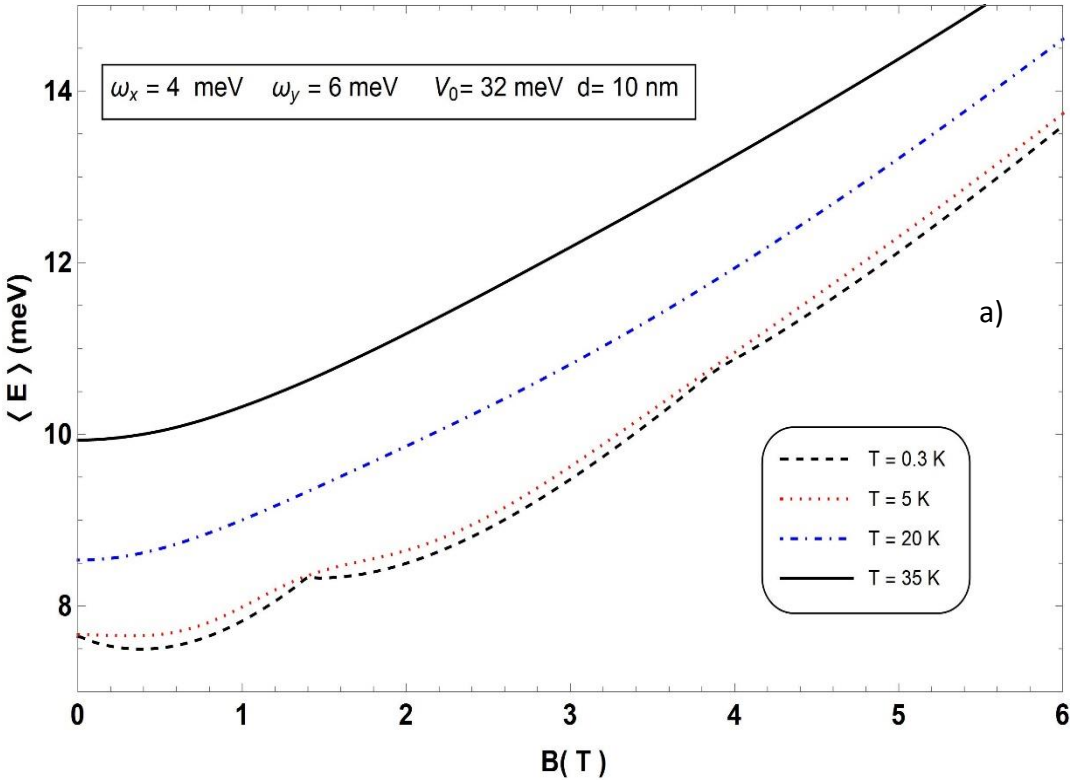

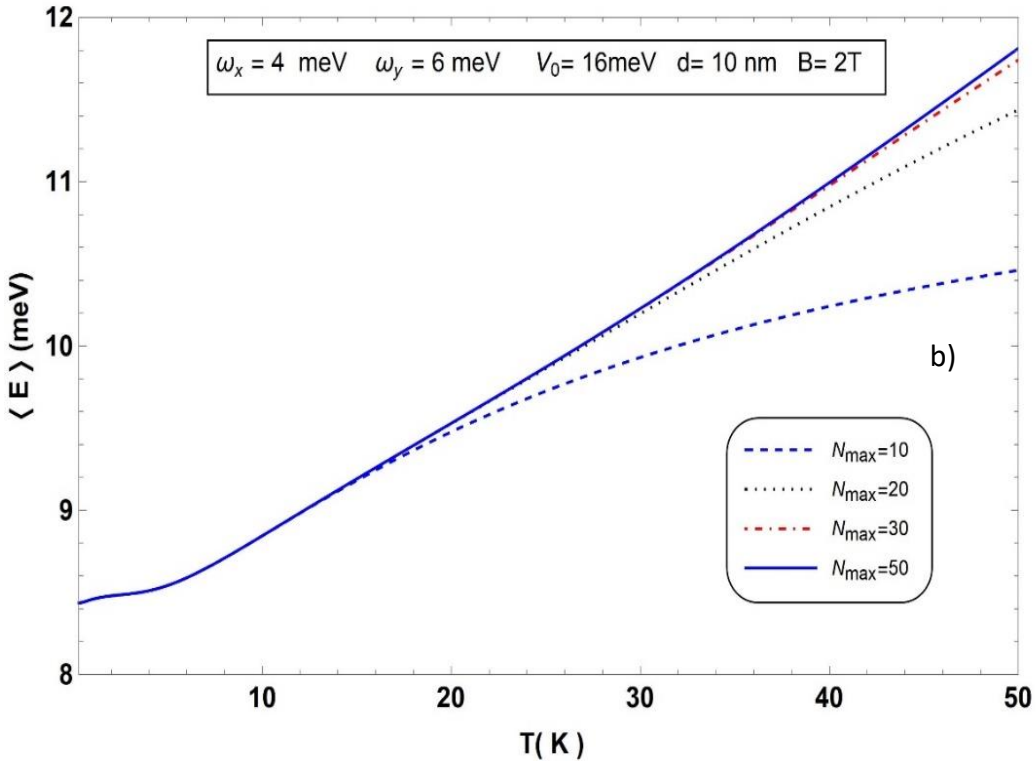

The dependence of the magnetization on the magnetic field and the impurity profile was studied in Fig. 6. The results show the presence of oscillation in the magnetization curve due to the intersection of the low-lying states' energies. In Fig. 6(a), the effect of the impurity strength is shown; the increase in the impurity strength pulls the intersection in the energy levels shown in previous figures towards a lower magnetic field value, as expected.

The influence of impurity extension has been investigated in Fig. 6(b). It is noticed that there are many peaks in the magnetization curve at larger values of d due to the occurrence of multiple cusps in the ground state energy curves, which appeared in Fig. 5(b).

The effect of the impurity's position was investigated in Fig. 6(c) since the major effect on magnetization is attributable to the ground state at temperatures near zero. As a result, the impurity's existence away from the center reduces the oscillation peaks hight.

The results revealed that when the impurity was positioned away from the center, there was a noticeable reduction in the height of the oscillation peaks. This observation indicates that the presence of the impurity, when situated at a distance from the central region, influences the magnetization characteristics, leading to a dampening effect on the oscillation amplitudes.

In Fig. 6(d), the effect of the temperature has been illustrated. For $T \to 0$, At the level crossings, the magnetization is discontinuous; consequently, the susceptibility diverges. On the other hand, at finite temperatures, thermal excitations make the magnetization a continuous and smooth function, and the susceptibility then has the spectral line form with a temperature dependence linewidth, as presented in Fig. 7(a). The number and position of the peaks depend on the impurity profile, as shown in Fig. 7(b).

From the previous figures (Fig. 6 and Fig. 7), we can conclude that the impurity plays a significant role in controlling the magnetic properties of the nanomaterials, by flip the magnetic susceptibility sign as result the material shows a diamagnetic to paramagnetic shift depends on the impurity profiles (strength, position, and stretch).

Figure 6

M *vs. B for a) different impurity strengths, b) different impurity stretches, c) different impurity positions, and d) different temperatures, where all other parameters have been fixed*

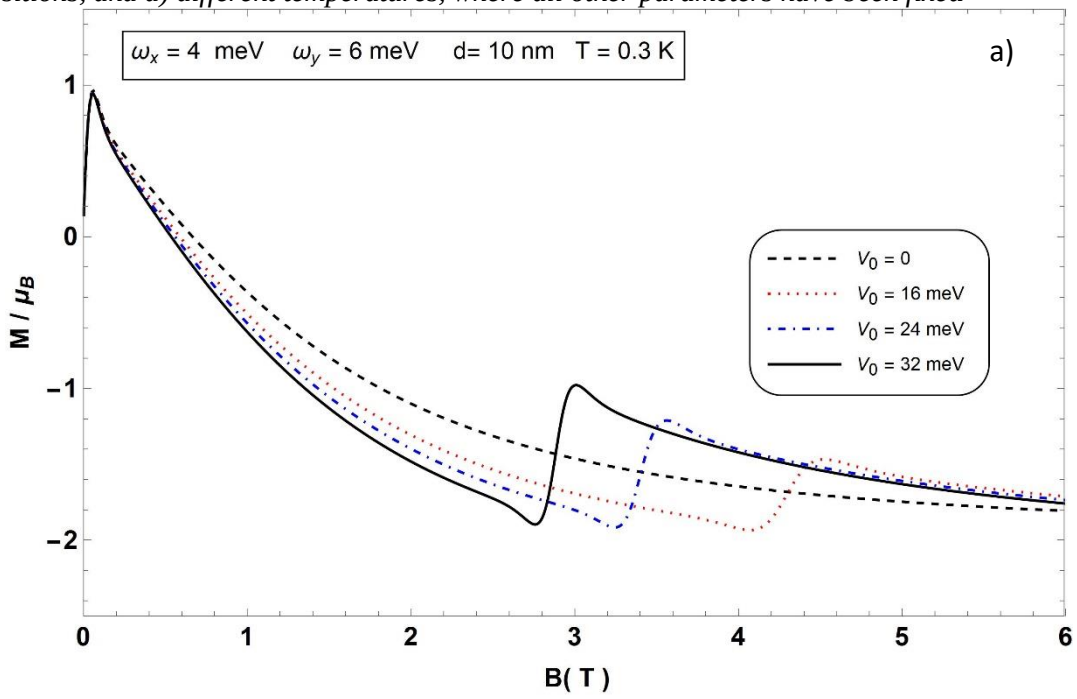

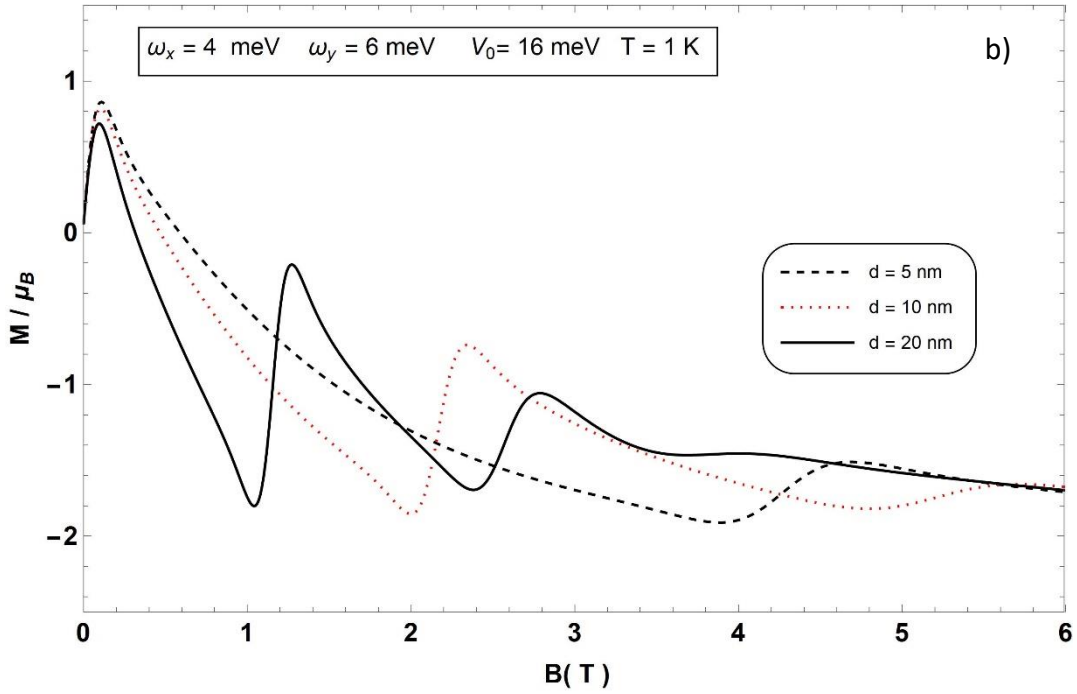

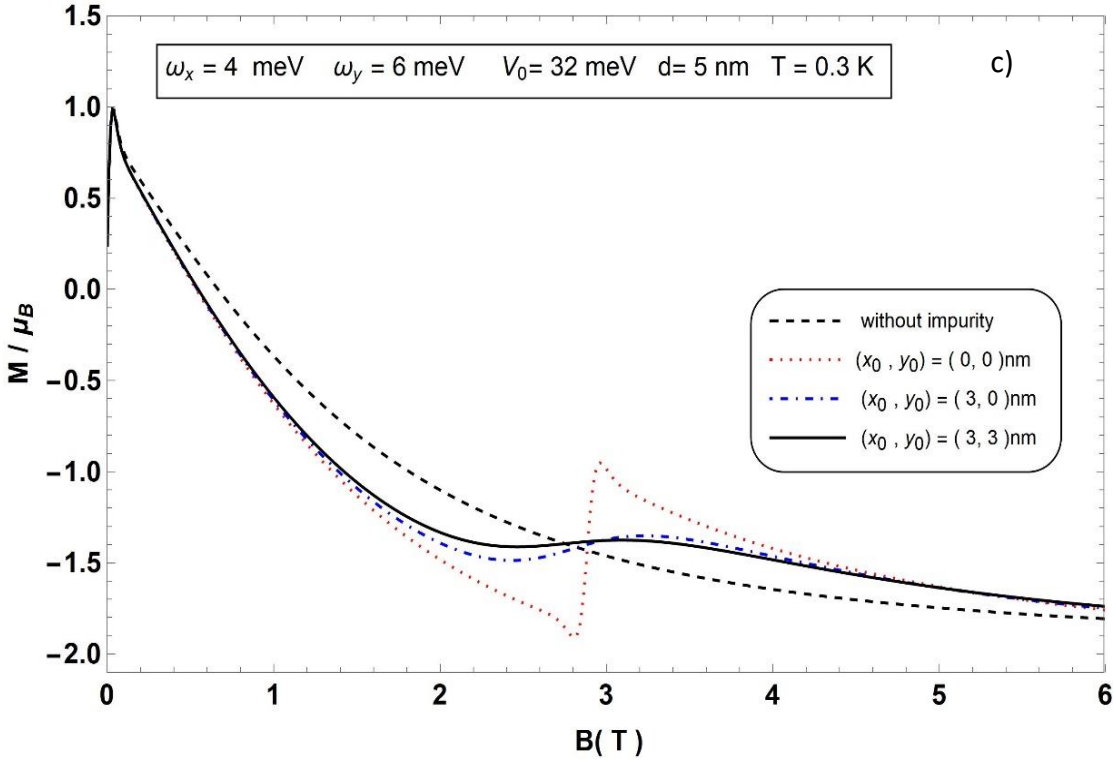
ω_x = 4 meV ω_y = 6 meV V_0= 32 meV d= 5 nm T = 0.3 K
c)
without impurity
(x_0 , y_0) = (0, 0)nm
(x_0 , y_0) = (3, 0)nm
(x_0 , y_0) = (3, 3)nm
M / μ_B
B(T)

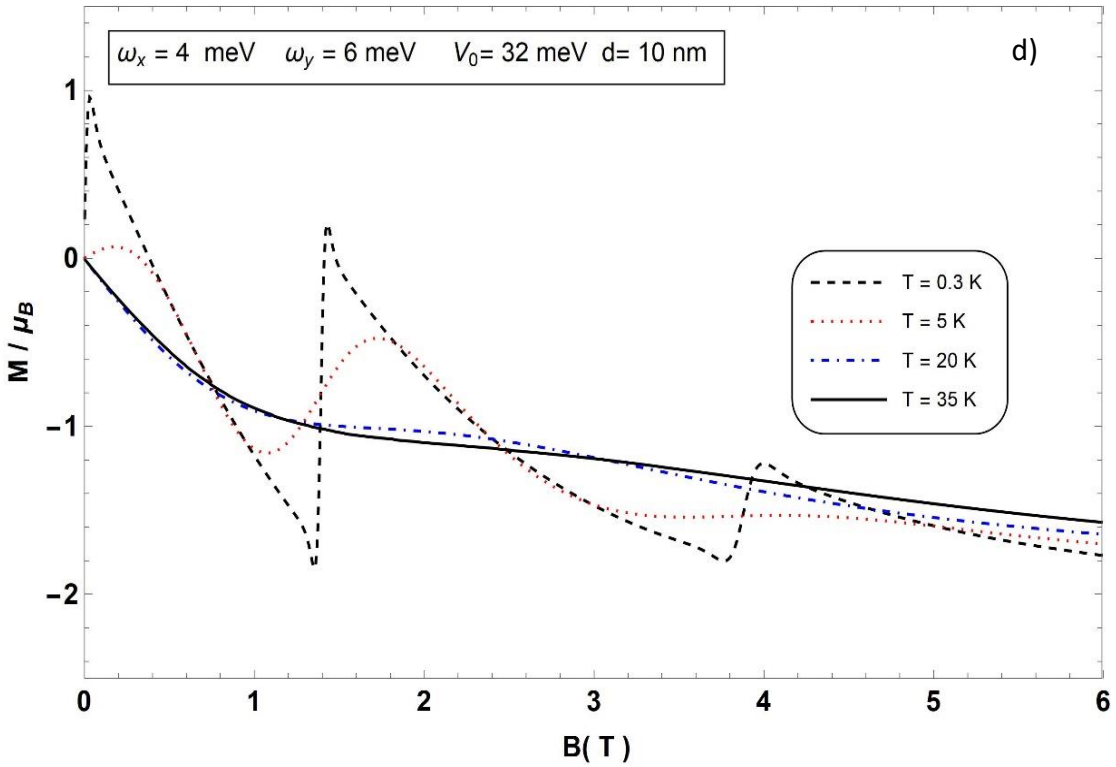
ω_x = 4 meV ω_y = 6 meV V_0= 32 meV d= 10 nm
d)
T = 0.3 K
T = 5 K
T = 20 K
T = 35 K
M / μ_B
B(T)

Figure 7

χ vs. B for a) different temperatures and b) different impurity stretches c) FWHM of χ as function of T

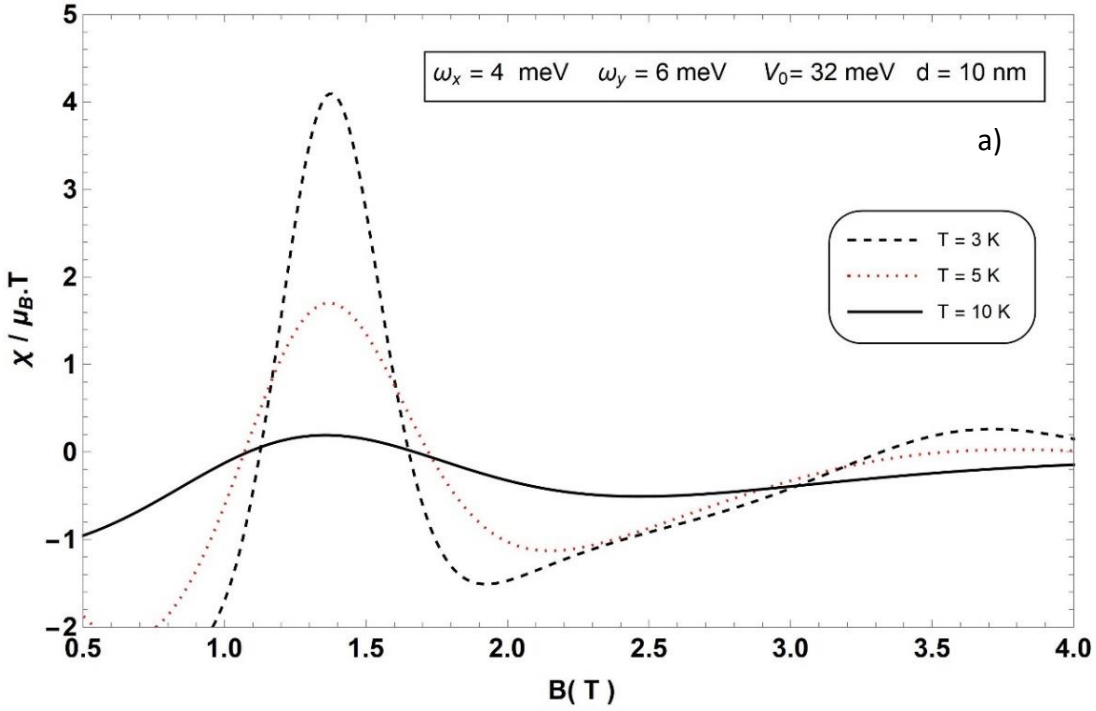

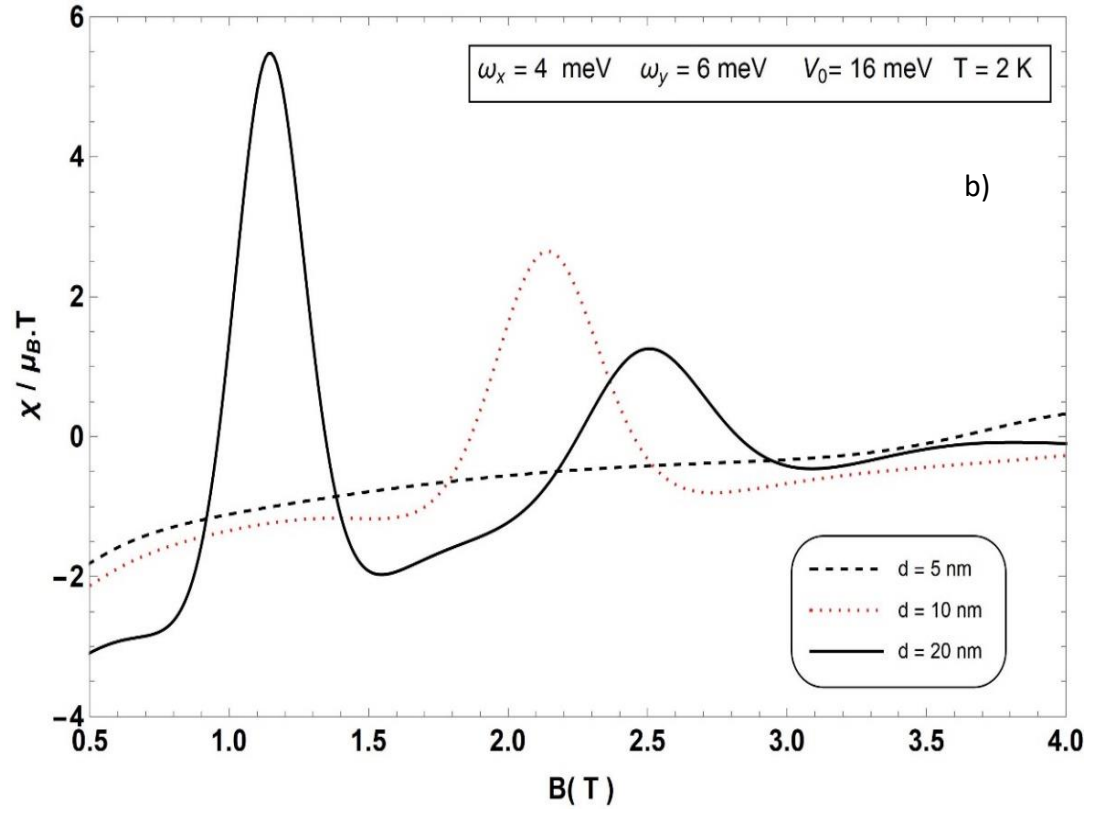

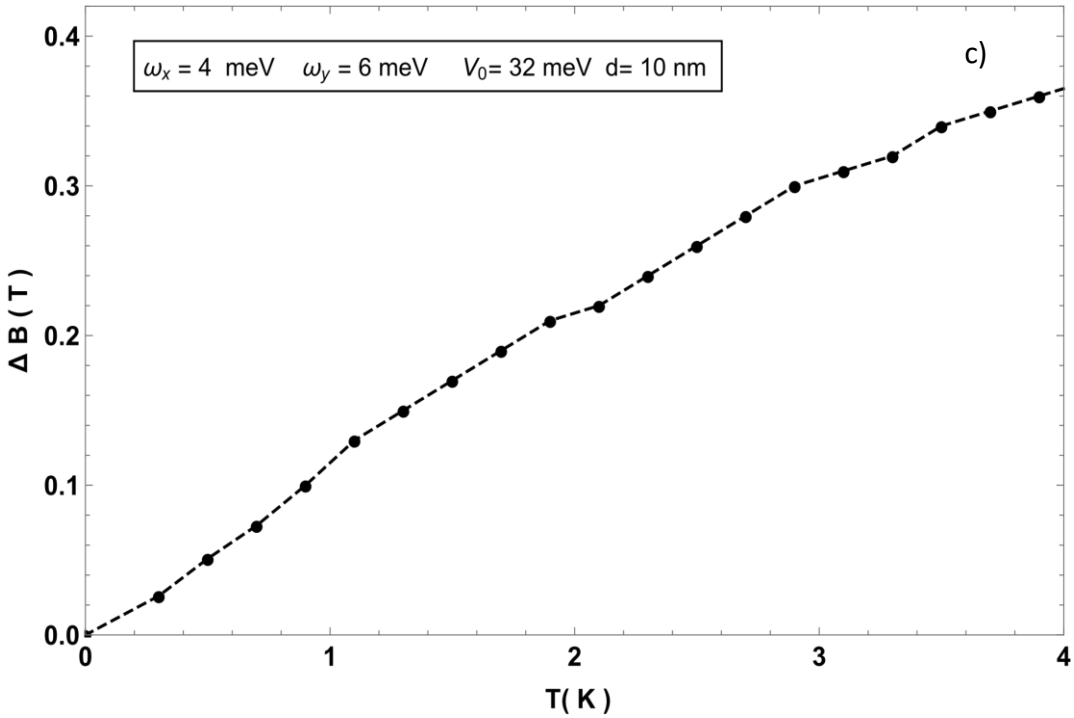

To investigate further the effect of the temperature on the magnetic susceptibility of the QD, the full width at half maximum of the spectral line of the susceptibility (FWHM) is shown as a function of temperature in Fig 7(c). One can see that the temperature changes the spectral linewidth linearly.

To investigate the effects of the SOI terms on the energy spectra and the magnetic properties of the InAs QD system, we have first, plotted the Rashba and Dresselhaus parameters as a function of the induced electric field in Fig.8(a). According to Eqs. 11 and 12, the ratio between Rashba and Dresselhaus for InAs $\frac{\alpha_R}{\alpha_D} = 0.015\, E^{1/3}$, the dashed line in Fig.8(a) indicates the range for the electric field in which the Dresselhaus SOI dominates over Rashba SOI, where the solid line (higher electric field) for which the Rashba has the main contribution in the spin splitting energy, the point between the two regions at, $E = 3.04 \times 10^3$ V/cm, the two parameters became equal.

Figure 8

a) Rashba to Dresselhaus ratio ($\boldsymbol{\alpha_R/\alpha_D}$) vs. the electric field. RSO and DSO couplings become equal at the electric field, $\boldsymbol{E = 3.04 \times 10^3}$ V/cm. b) *The energies of the low-lying states as a function of the magnetic field strength c) Ground state energy d) The statistical average energy of the lateral QD as a function of the magnetic field strength for different electric field values.*

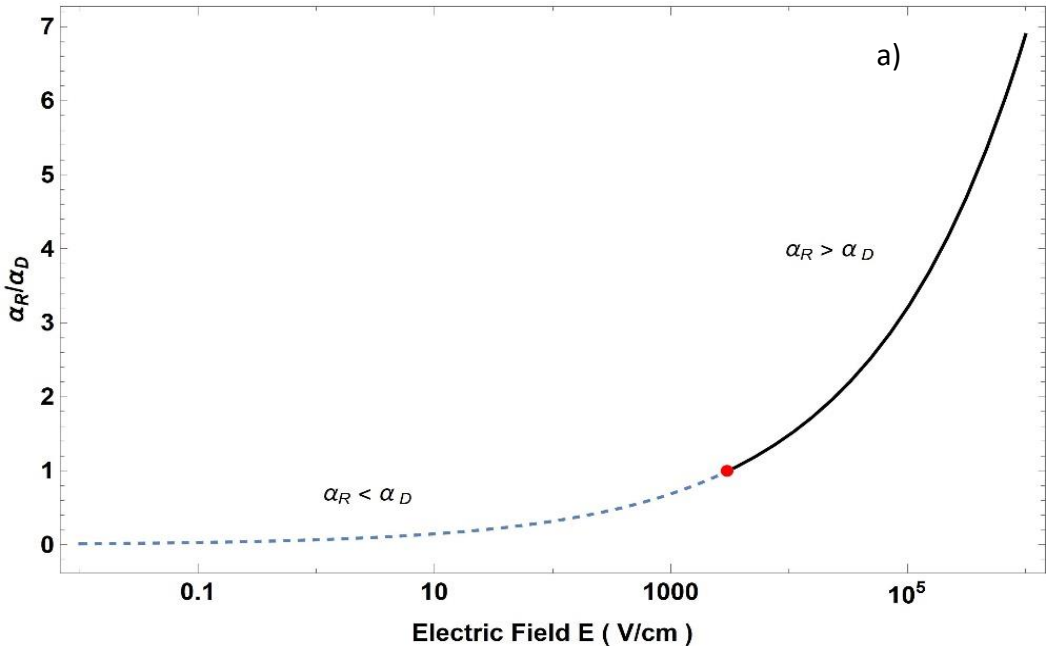

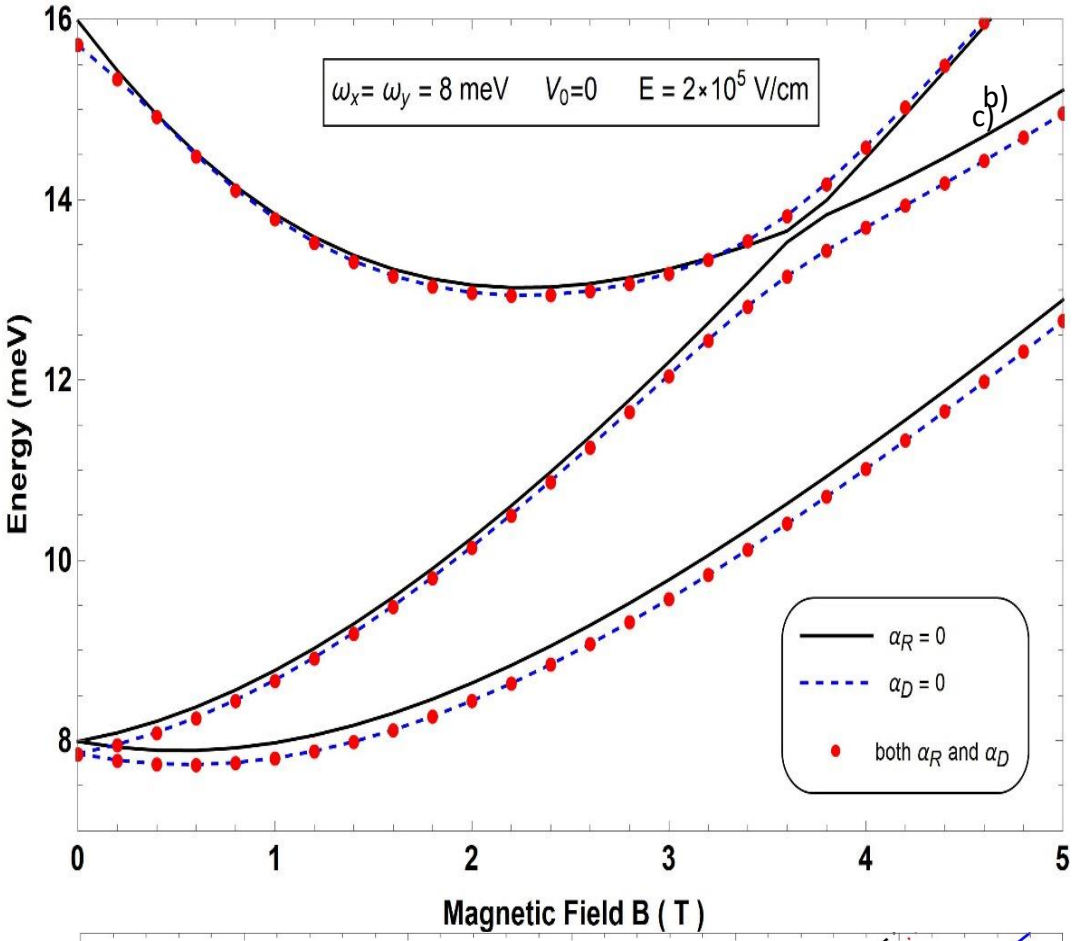
$\omega_x = \omega_y$ = 8 meV V_0=0 E = 2×10^5 V/cm
b)
c)
Energy (meV)
Magnetic Field B (T)
α_R = 0
α_D = 0
both α_R and α_D

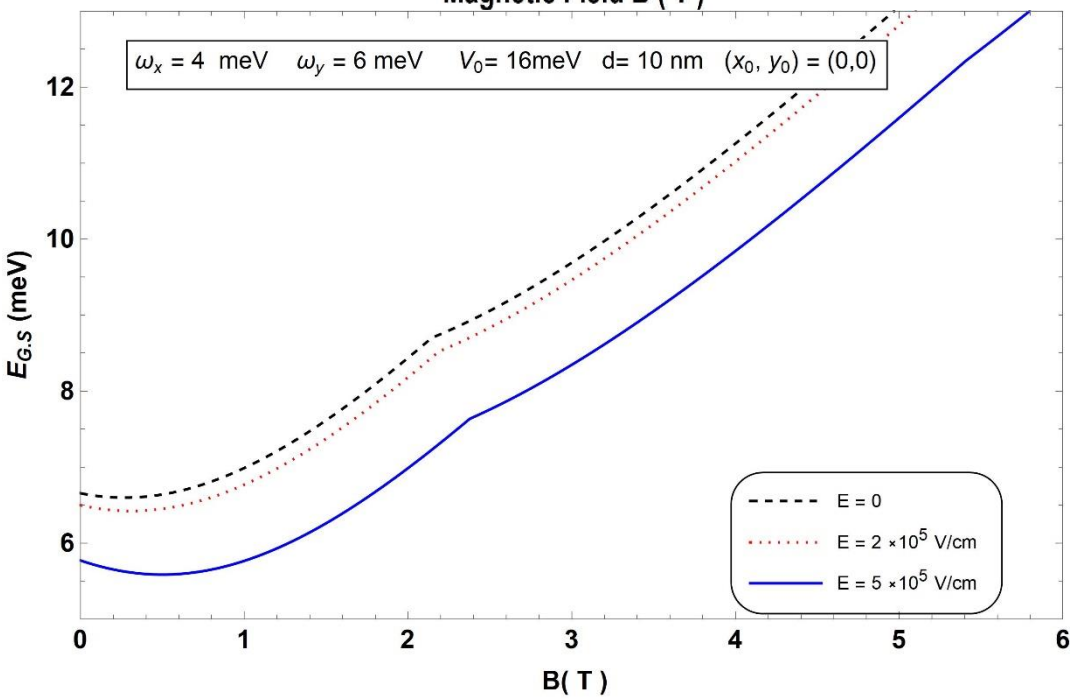
ω_x = 4 meV ω_y = 6 meV V_0= 16meV d= 10 nm (x_0, y_0) = (0,0)
$E_{G.S}$ (meV)
B(T)
E = 0
E = 2 ×10^5 V/cm
E = 5 ×10^5 V/cm

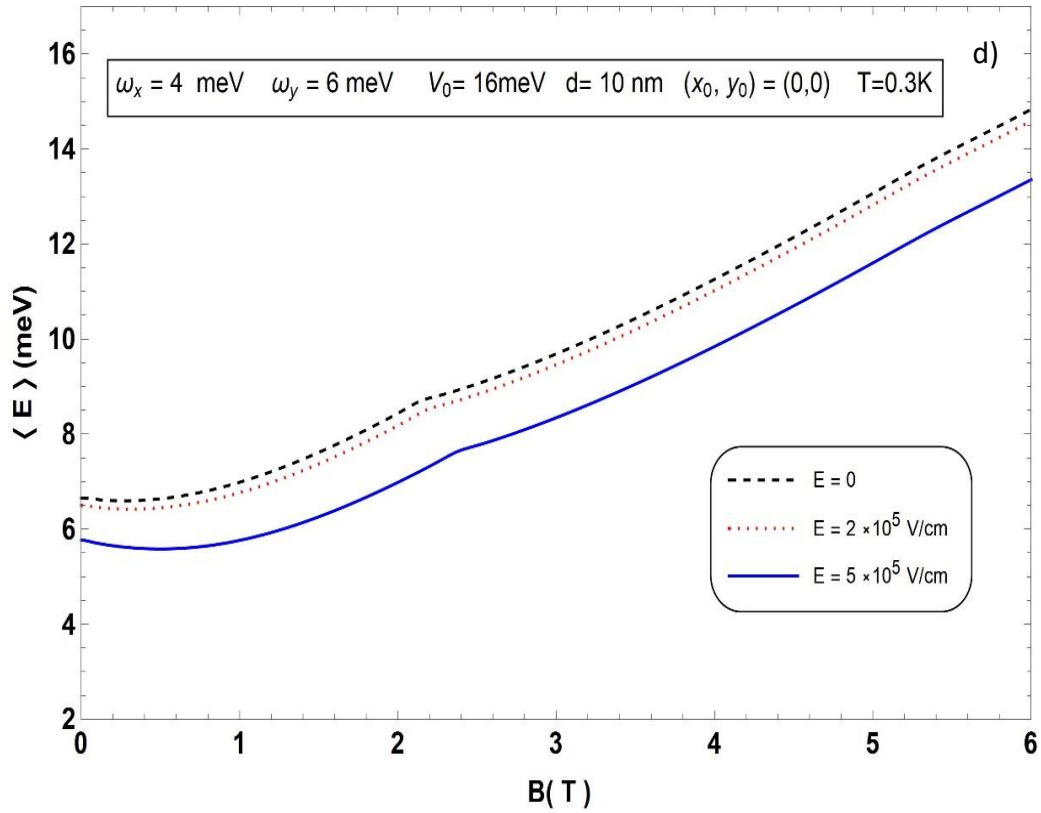

Figure 8(b) illustrates the eigenenergies for the low-lying states at $E = 2 \times 10^5\ V/cm$, for isotropic quantum dot in the absence of the impurity, it can be seen that the most contribution is attributed to Rashba, while the Dresselhaus SOI has minor contribution at this particular value of the electric field.

The shifting in the ground state energy is apparent In Fig. 8(c), even at zero magnetic fields, which is attributed to the SOI (primally Rashba SOI). In contrast, the cusp is shifted to a larger magnetic field value as the spin-orbit interaction (i.e., electric field) is increasing, which results in more significant shifting in the state $|0,0>$ relative to the first excited state, making the crossing/ anticrossing of the states appears at a larger magnetic field.

For low temperatures, the statistical average energy has been plotted in Fig. 8(d), and the same cusps (corresponding to the ground state energy cusps) appeared, which again attributed to the high probability of the electron being localized in the ground state,

To investigate the effect of the SOI on the magnetic properties of the QD system, the magnetization (M) and magnetic susceptibility (χ) have been plotted in Fig. A.9(a) and A.9(b), respectively; the plot shows an expected shift in the peaks of the curves

corresponding to the previously mentioned change in the ground state energies crossings/ anticrossing, where the magnetic phase transition still presents.

3.4 Effective Lande g factor

In Fig. 9(a) the effective Lande g factor has been plotted as a function of the magnetic field, at a fixed value of the electric field, for different SOI cases. For $\alpha_R = 0$ case (solid line), even $\alpha_D \neq 0$, the curves show a constant value for the Lande g factor, which matches the value of the bulk InAs material, since the Dresselhaus SOI has a minor contribution to small band gap semiconductors. For the dashed line, the presence of RSOI enhances the value of the g factor due to the more significant separation of the states with different spin orientations, $\Delta E = E\uparrow - E\downarrow$

Figure 9

Effective Lande' g factor vs.a) magnetic fields b) electric field c) $\boldsymbol{\omega_0}$ *d) anisotropy of QD without impurity (a – g) and in presence of acceptor impurity (h and I)*

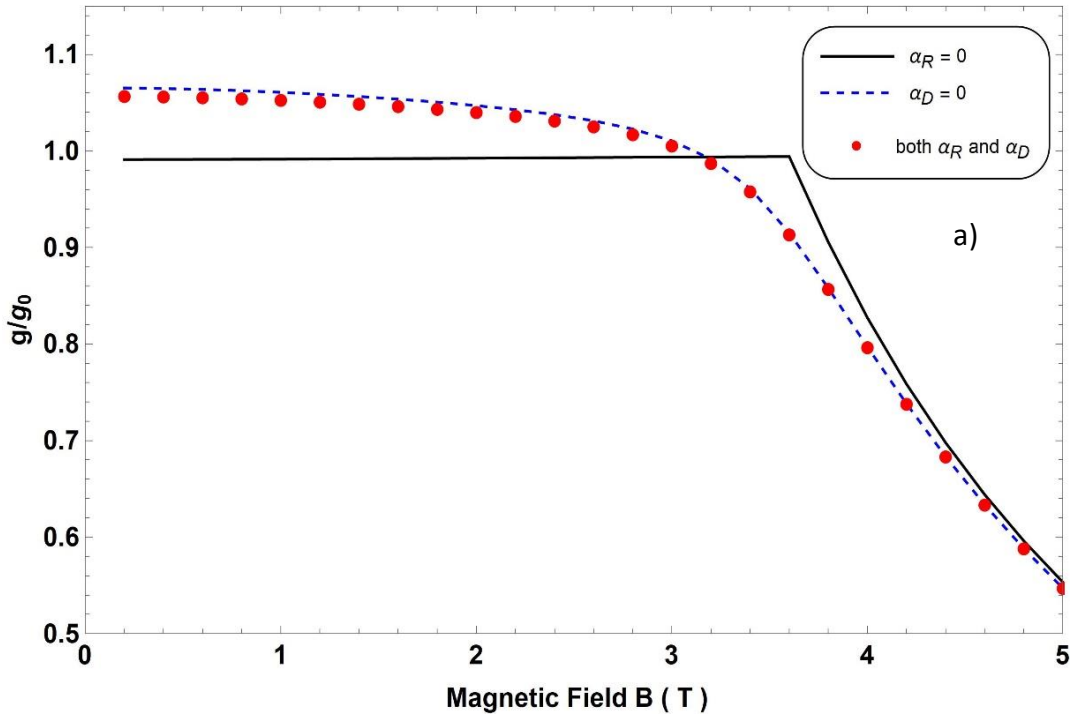

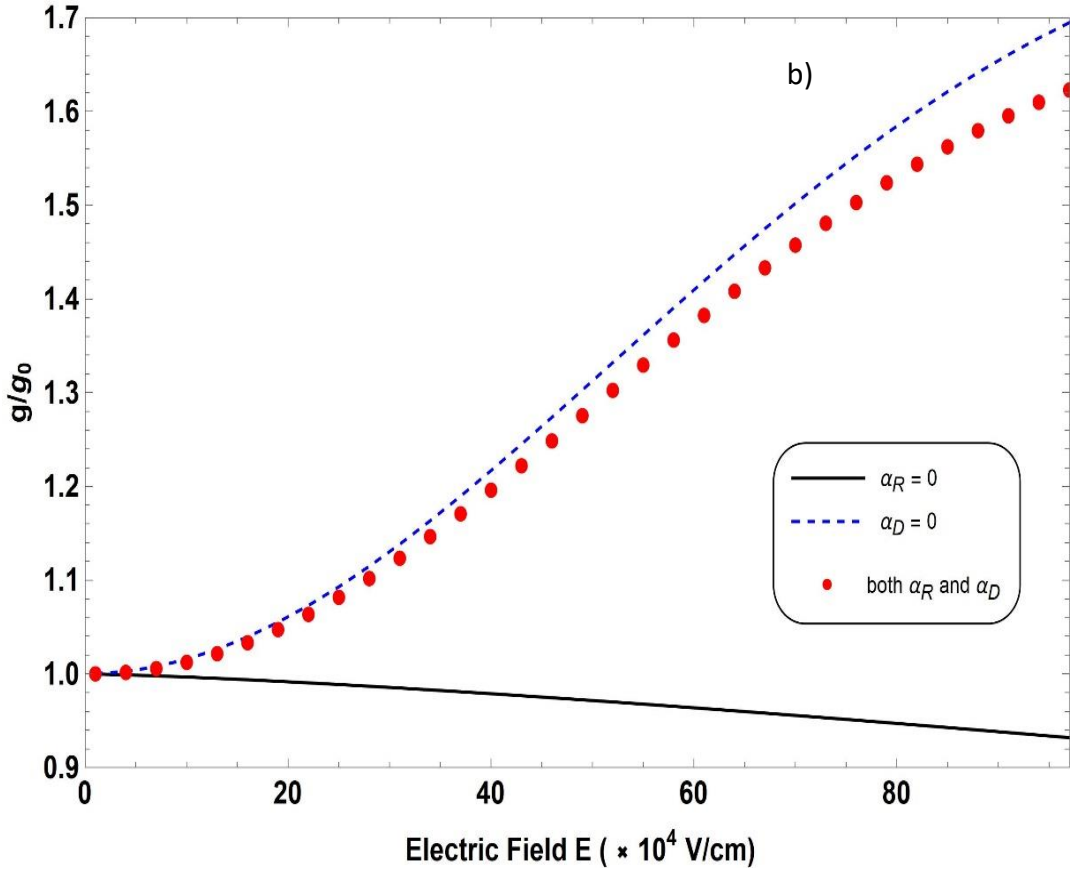

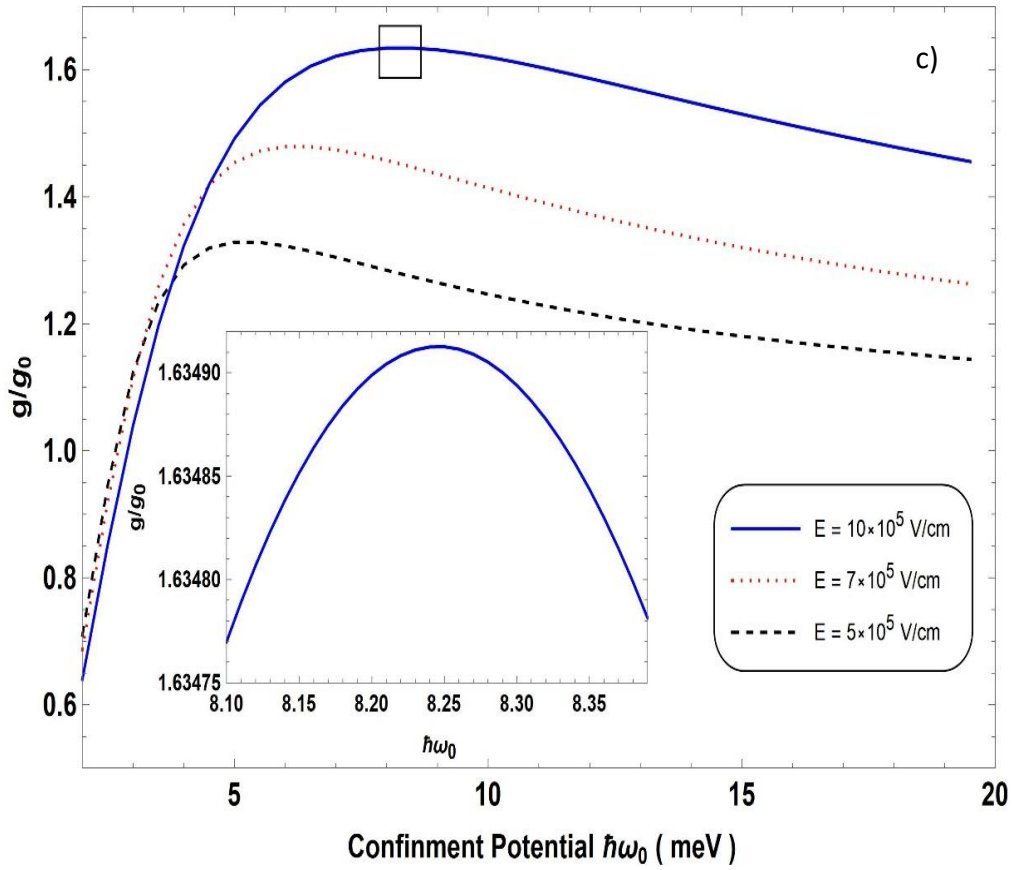
c)
g/g0
1.6
1.4
1.2
1.0
0.8
0.6
5
10
15
20
Confinment Potential ħω0 (meV)
1.63490
1.63485
1.63480
1.63475
8.10
8.15
8.20
8.25
8.30
8.35
ħω0
E = 10×10^5 V/cm
E = 7×10^5 V/cm
E = 5×10^5 V/cm

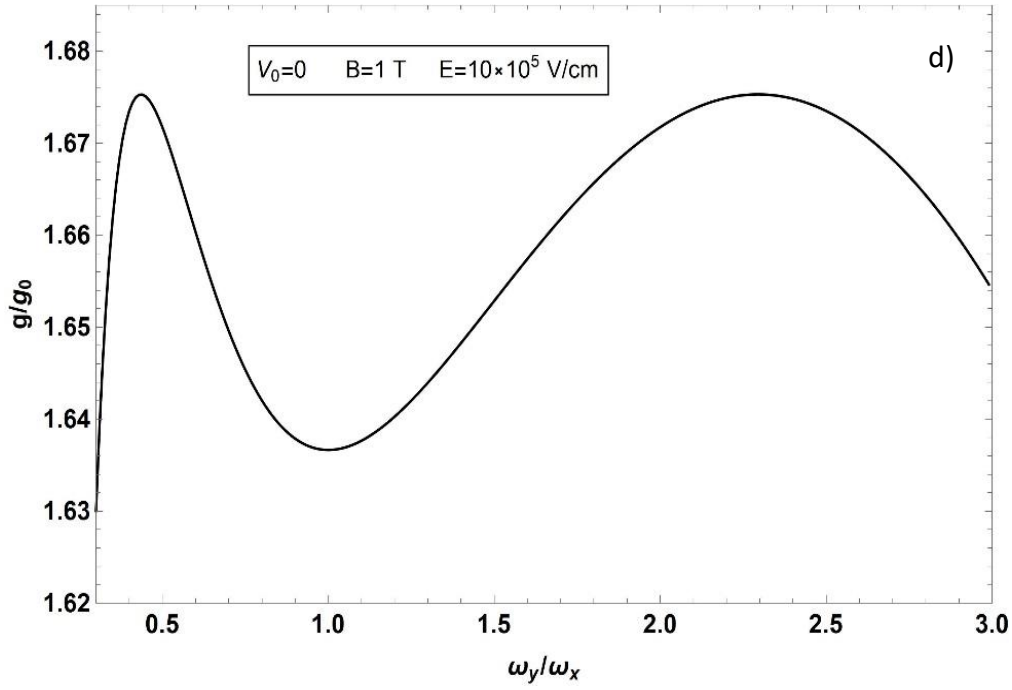
d)
V0=0 B=1 T E=10×10^5 V/cm
g/g0
1.68
1.67
1.66
1.65
1.64
1.63
1.62
0.5
1.0
1.5
2.0
2.5
3.0
ωy/ωx

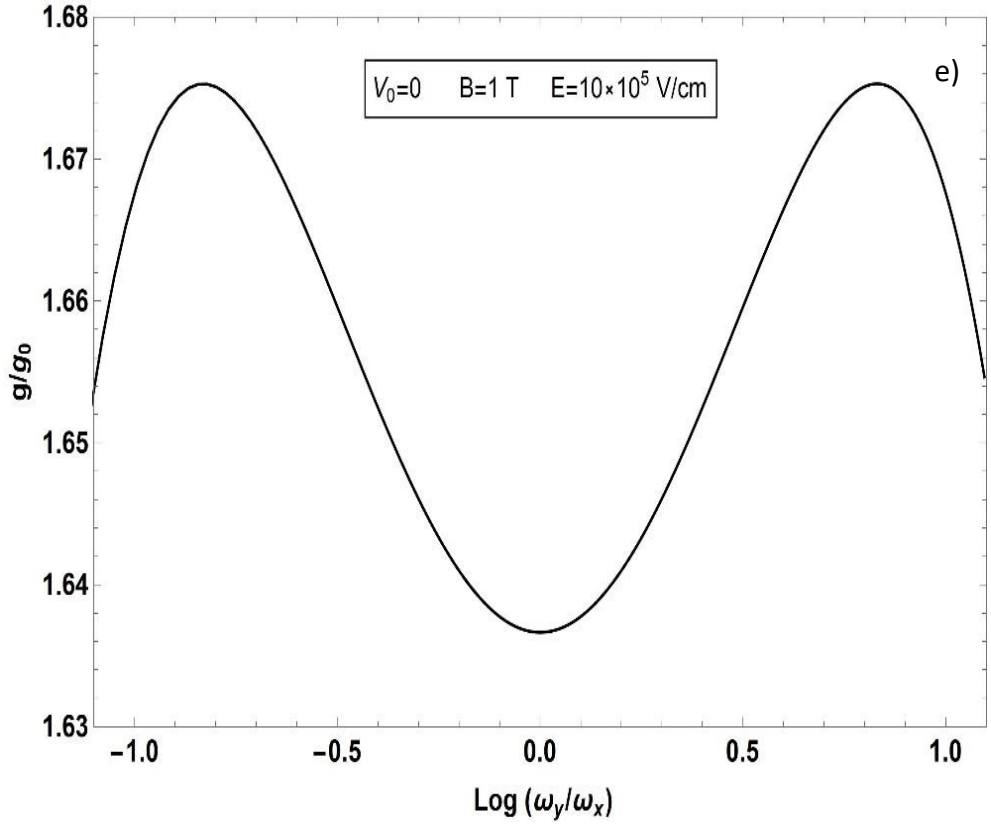
e)
V_0=0 B=1 T E=10×10^5 V/cm
1.68
1.67
1.66
1.65
1.64
1.63
g/g$_0$
−1.0
−0.5
0.0
0.5
1.0
Log (ω_y/ω_x)

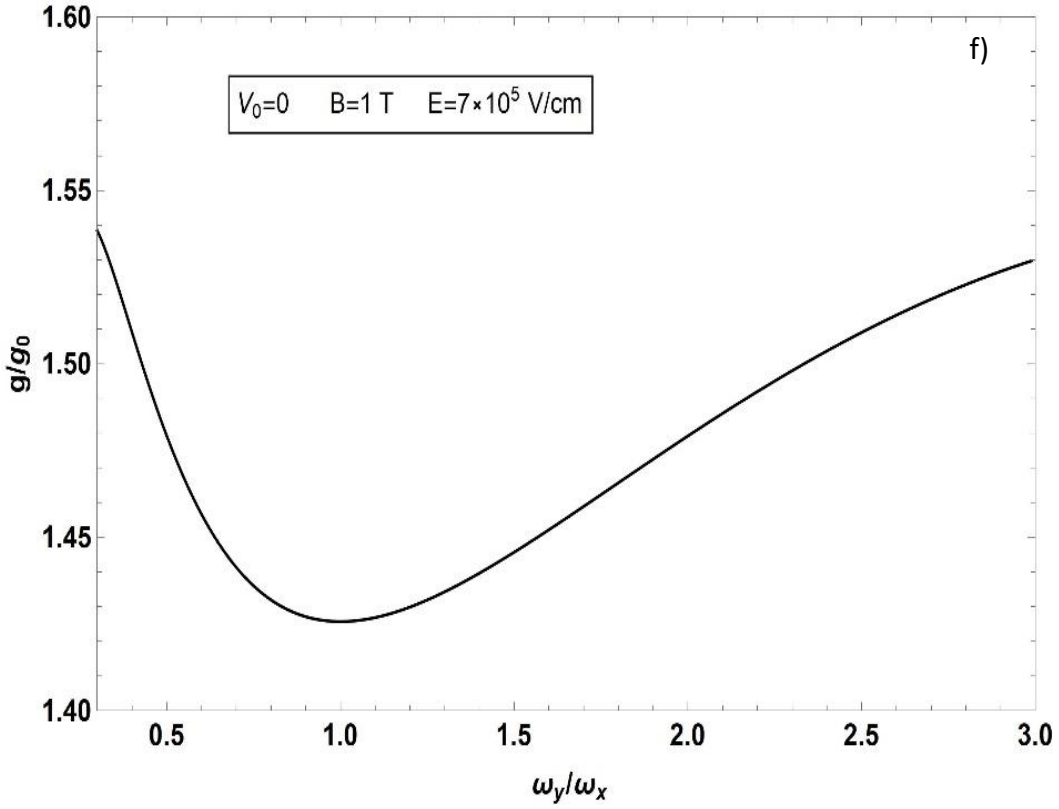
f)
V_0=0 B=1 T E=7×10^5 V/cm
1.60
1.55
1.50
1.45
1.40
g/g$_0$
0.5
1.0
1.5
2.0
2.5
3.0
ω_y/ω_x

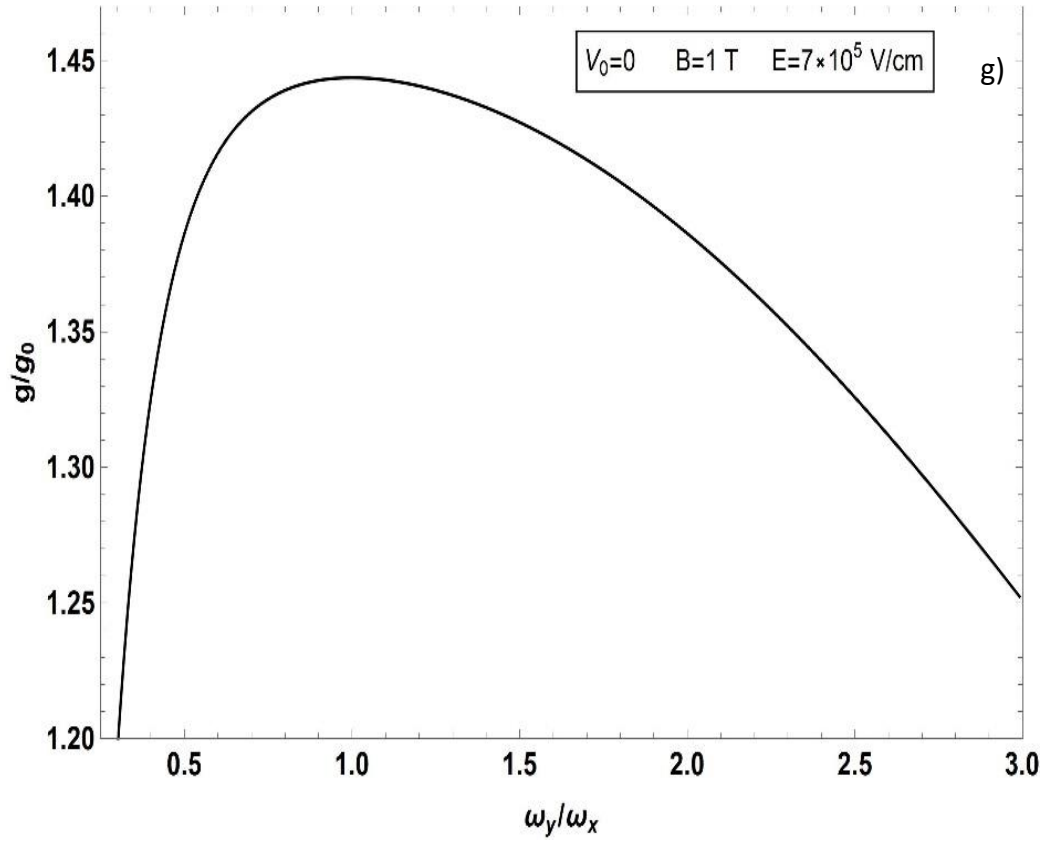
V_0=0 B=1 T E=7×10^5 V/cm
g)
1.45
1.40
1.35
1.30
1.25
1.20
g/g$_0$
0.5
1.0
1.5
2.0
2.5
3.0
ω_y/ω_x

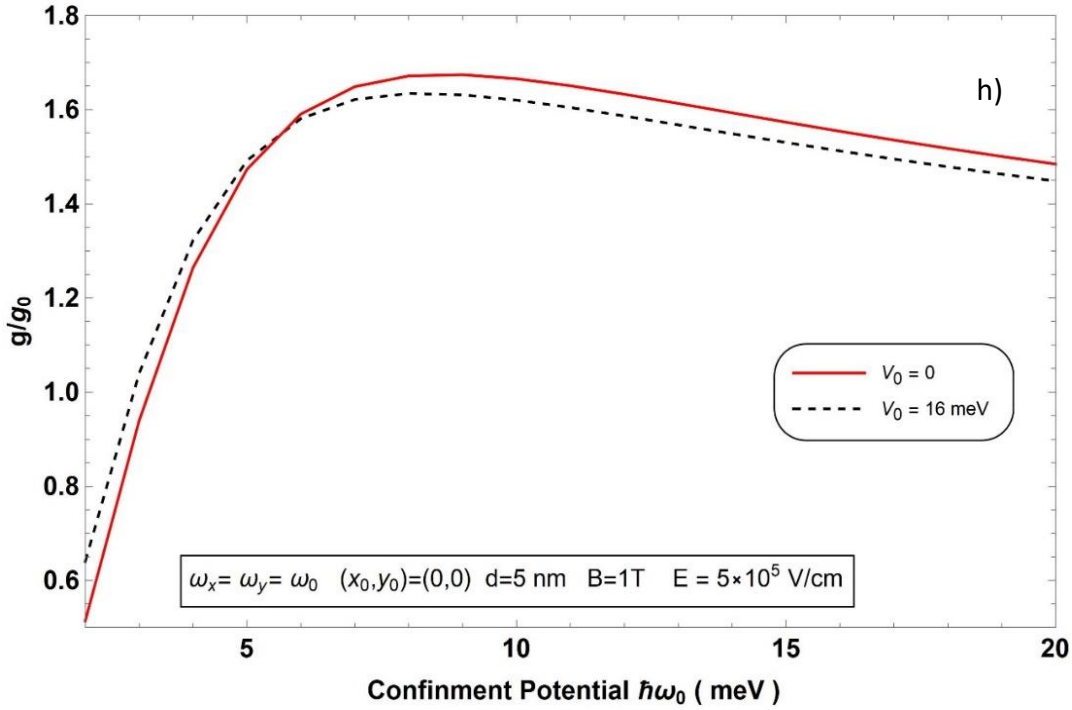
h)
1.8
1.6
1.4
1.2
1.0
0.8
0.6
g/g$_0$
V_0 = 0
V_0 = 16 meV
ω_x= ω_y= ω_0 (x_0,y_0)=(0,0) d=5 nm B=1T E = 5×10^5 V/cm
5
10
15
20
Confinement Potential $\hbar\omega_0$ (meV)

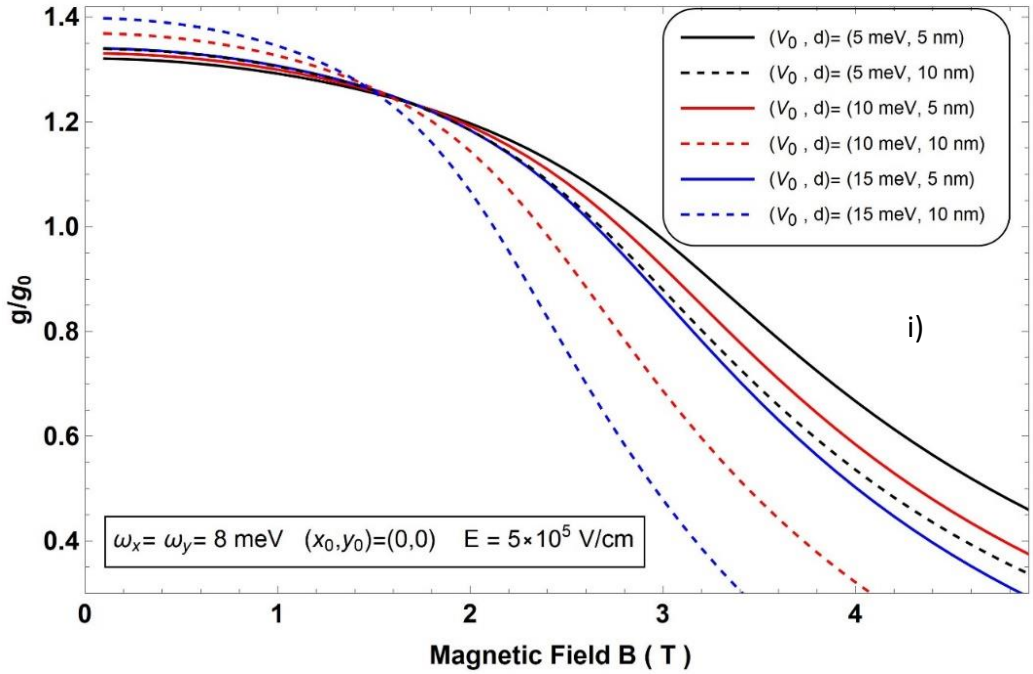

For fixed parameters,$B = 1T, \omega_x = \omega_y = 8\,meV$, the two types of SOI can be manipulated by changing the electric field strength. The SOI strength effect on the Lande g factor has been investigated in Fig 9(b). In the first case, we neglected the Dresselhaus effect $\alpha_D = 0$, the Rashba SOI enhanced the g value as the electric field increases, which is clearly shown in the dashed line in the figure. This result shows the role of the Rashba SOI in the area of spintronics devices. On the other hand, by neglecting the Rashba effect $\alpha_R = 0$, the Dresselhaus SOI slightly reduces the absolute value of g as the electric field increases, as shown in the solid line in the figure. The combined effect displayed in the dotted points shows the dominance of the Rashba SOI effect over the Dresselhaus SOI one.

The size of the symmetric quantum dot ($\omega_x = \omega_y = \omega_0$) significantly affects the value of the g factor at a fixed value of the electric field, as shown in Fig. 9(c), at a particular value of the confinement strength (which is inversely proportional to quantum dot size), the g factor curve has its maximum value, for example, at $E = 10 \times 10^5 V/cm$ the g factor has a peak value $g \approx 1.64 g_0$ for $\omega_0 = 8.15 meV$, the numerical data also given in Table 4, this peak value of the g factor became smaller and shifted to smaller confinement strength when the electric field decreased.

Table 4

Absolute value of g factor as function of the confinement strength for fixed magnetic field value

ω_0	$\left\|\frac{g}{g_0}\right\|$
2	0.635964
3	1.04601
4	1.336727
5	1.507444
6	1.593824
7	1.629756
7.6	1.636783
7.7	1.637212
7.8	1.637463
7.9	**1.637545**
8	1.637469
8.1	1.637244
8.2	1.63688
9	1.629859
10	1.614154
11	1.594399
12	1.572875
13	1.550874

In Fig. 9(d) and Fig. 9(e), the effect of anisotropy of the QD has been investigated. For a fixed quantum dot area $(\omega_x \times \omega_y)$, the g factor has been plotted as a function of the ratio of y to x confinement strength $(\frac{\omega_y}{\omega_x})$. The figure shows an interesting behavior for different values of x-direction confinement strength. In Fig. 9(c), the anisotropy slightly enhances the absolute value of the g factor; then the anisotropy reduces the value of the g factor as the quantum dot extends to be an elliptical shape. To show the geometric symmetry of the ratio effect, we plot in Fig. 9(e) the g factor as a function of the

$Log(\frac{\omega_y}{\omega_x})$, the figure exhibits an expected symmetry around $\omega_x = \omega_y$, equivalent to $Log(\frac{\omega_y}{\omega_x})$=0.

In Fig. 9(f and g) , the g factor shows different behavior with respect to the anisotropy of the QD. In Fig. 30(f), for $E = 7 \times 10^5\ V/cm$ and $\sqrt{\omega_x \times \omega_y} = 8.25\ meV$, the anisotropy enhances the g factor value as $\left|Log\left(\frac{\omega_y}{\omega_x}\right)\right|$ increases, whereas, for $E = 7 \times 10^5\ V/cm$ $\sqrt{\omega_x \times \omega_y} = 5\ meV$, the anisotropy decreases the g factor value as $\left|Log\left(\frac{\omega_y}{\omega_x}\right)\right|$ increases, as shown in Fig. 9(g). This conclusion has been previously partially discussed in Ref (S. Prabhakar et al., 2011), as the anisotropy of the confinement potential increases, the $|g|$ decreases.

From figures 9(c - g), one can observe the combined effects of the electric field, the confinement strength, and the anisotropy of the quantum dot on the absolute value of the effective Lande g factor. In practice, the value of the g factor is considered an important key by manipulating the relaxation time on the quantum computing area (de Sousa & Das Sarma, 2003), so further investigation about how to enhance or reduce the value by external parameters is considered a hot research subject and may be investigated in future work.

The presence of an acceptor impurity in the QD has been studied and shown in Figs. 9(h and i). In Fig 9(h), the on-center impurity slightly increases the g factor of symmetric QD with low confinement potential; however, the g factor decreases as the confinement potential strengthens.

For symmetric QD, the impurity profile (strength and stretch) effect has been shown in Fig. 9(i) as a function of the magnetic field. For a fixed value of d, the g factor can be increased as the impurity strength increases at a low magnetic field value (before the crossing/ anticrossing occurs. By the way, the more considerable value of d gives a similar effect by increasing the g factor.

3.5 The density of state DOS

The density of state has been studied to describe the system responses to Hamiltonian parameters, like the magnetic field, electric field, confinement anisotropy, and impurity profile.

In Fig. 10(a), at $\boldsymbol{B = 0}$ and for the fixed value of the x-direction confinement strength $\boldsymbol{\omega_x = 4meV}$, the density of state has been plotted as a function of the energy; for the isotropic case (dashed line), the energy spectra are given by $\boldsymbol{(n_x + n_y + 1)\hbar\omega_X}$ the figure shows an increasing state degeneracy as the energy increase; for example, the states $\left|\boldsymbol{0, 0, \frac{1}{2}}\right\rangle, \left|\boldsymbol{0, 0, -\frac{1}{2}}\right\rangle$ are degenerate with energy $\boldsymbol{\hbar\omega_x}$ since the spin degeneracy remains in the absence of the magnetic field, the states $\left|\boldsymbol{0, 1, \frac{1}{2}}\right\rangle, \left|\boldsymbol{0, 1, -\frac{1}{2}}\right\rangle, \left|\boldsymbol{1, 0, \frac{1}{2}}\right\rangle, \left|\boldsymbol{1, 0, -\frac{1}{2}}\right\rangle$ are degenerated states with energy $\boldsymbol{2\hbar\omega_x}$, and $\left|\boldsymbol{0, 2, \frac{1}{2}}\right\rangle, \left|\boldsymbol{0, 2, -\frac{1}{2}}\right\rangle, \left|\boldsymbol{1, 1, \frac{1}{2}}\right\rangle, \left|\boldsymbol{1, 1, -\frac{1}{2}}\right\rangle, \left|\boldsymbol{2, 0, \frac{1}{2}}\right\rangle, \left|\boldsymbol{2, 0, -\frac{1}{2}}\right\rangle$ are degenerate states with energy $\boldsymbol{3\hbar\omega_x}$, and so on. By contrast, for the anisotropic case, the degeneracy has been partially lifted, and two-state degeneracy remains since the different spin states have the same energy at zero magnetic fields in the absence of the SOI. Accidentally, at $\boldsymbol{E_n = 17meV}$ there are four degenerate states, namely ($\left|\boldsymbol{3, 0, \frac{1}{2}}\right\rangle, \left|\boldsymbol{0, 2, \frac{1}{2}}\right\rangle, \left|\boldsymbol{3, 0, -\frac{1}{2}}\right\rangle, \left|\boldsymbol{0, 2, -\frac{1}{2}}\right\rangle$), the same behavior is shown at $\boldsymbol{E_n = 21meV}$ since $\boldsymbol{\omega_y = 1.5\ \omega_x}$.

In Fig. 10(b), the presence of the external magnetic field totally removes the degeneracy of the states, so DOS gives one at each value of the energy spectra, with also increasing on the ground state due to increasing of the canonical momentum, equivalently kinetic energy, in the Hamiltonian, the larger separation between to two different spin states, due to large value of the bulk g factor of the InAs material.

The presence of the electric field as a source for the SOI significantly affects the DOS of the system, as shown in Fig. 10(c), even at zero magnetic fields. At the fixed electric field value $\boldsymbol{E = 3 * 10^5 V/cm}$ the RSOI dominates the Dresselhaus SOI, which shifts the states to lower energy eigenvalue, for example, the first peak of the red line in the figure (at $\boldsymbol{E_n = 4.7\ meV}$). On the other hand, the presence of SOI electric field partially removes the degeneracy of the higher states $\boldsymbol{n_x, n_y > 1}$.

Figure 10

DOS vs. Energy for isotropic and anisotropic quantum dot

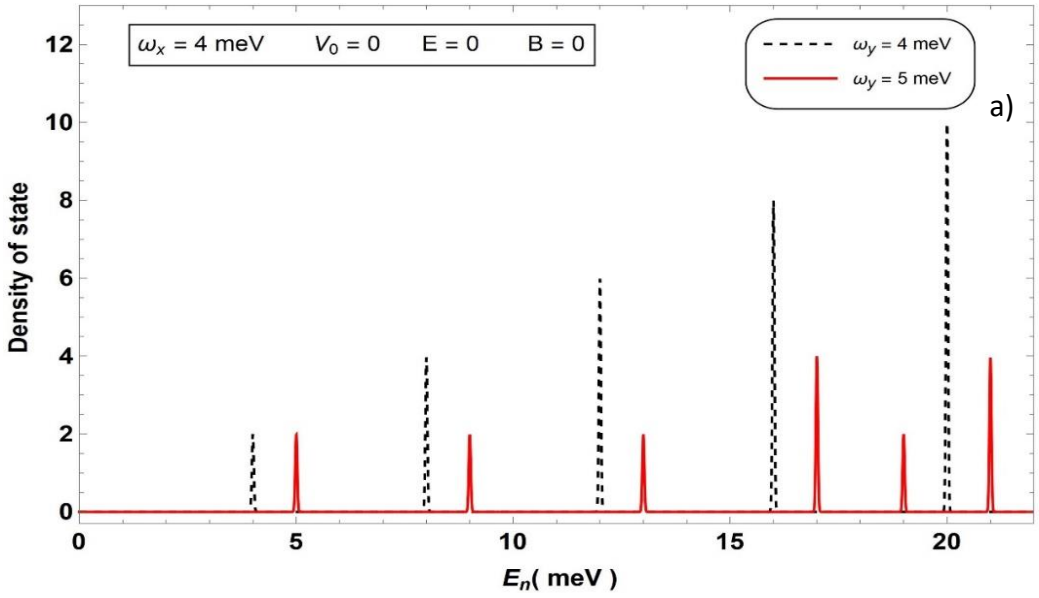

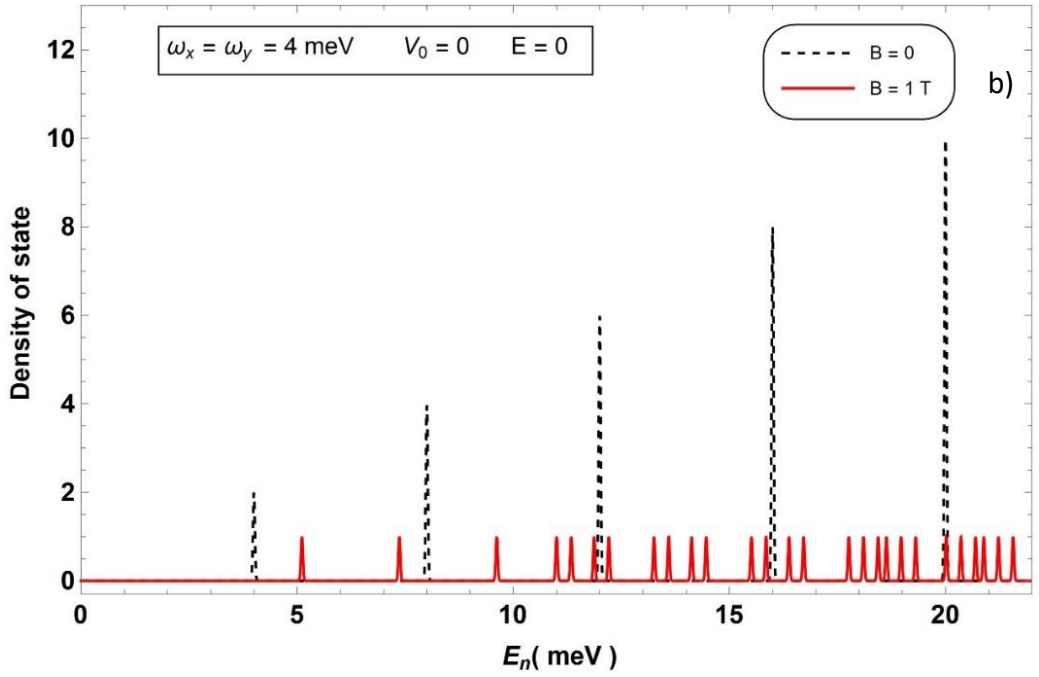

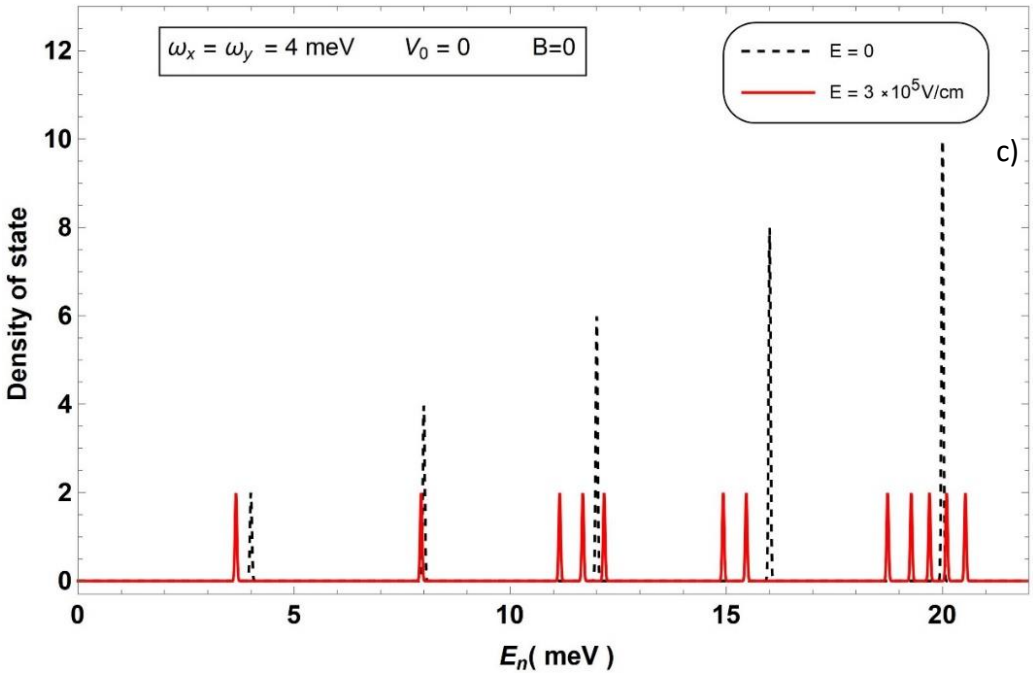
$\omega_x = \omega_y$ = 4 meV V_0 = 0 B=0
E = 0
E = 3 ×10^{5}V/cm
Density of state
E_n(meV)
c)

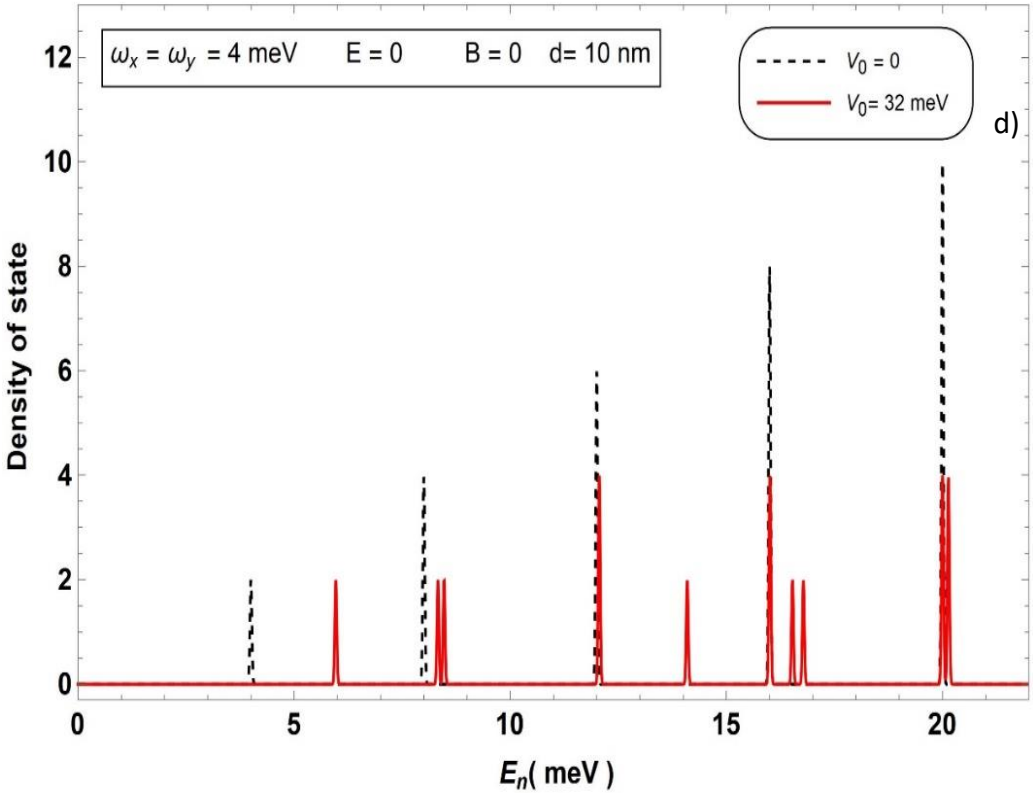
$\omega_x = \omega_y$ = 4 meV E = 0 B = 0 d= 10 nm
V_0 = 0
V_0= 32 meV
Density of state
E_n(meV)
d)

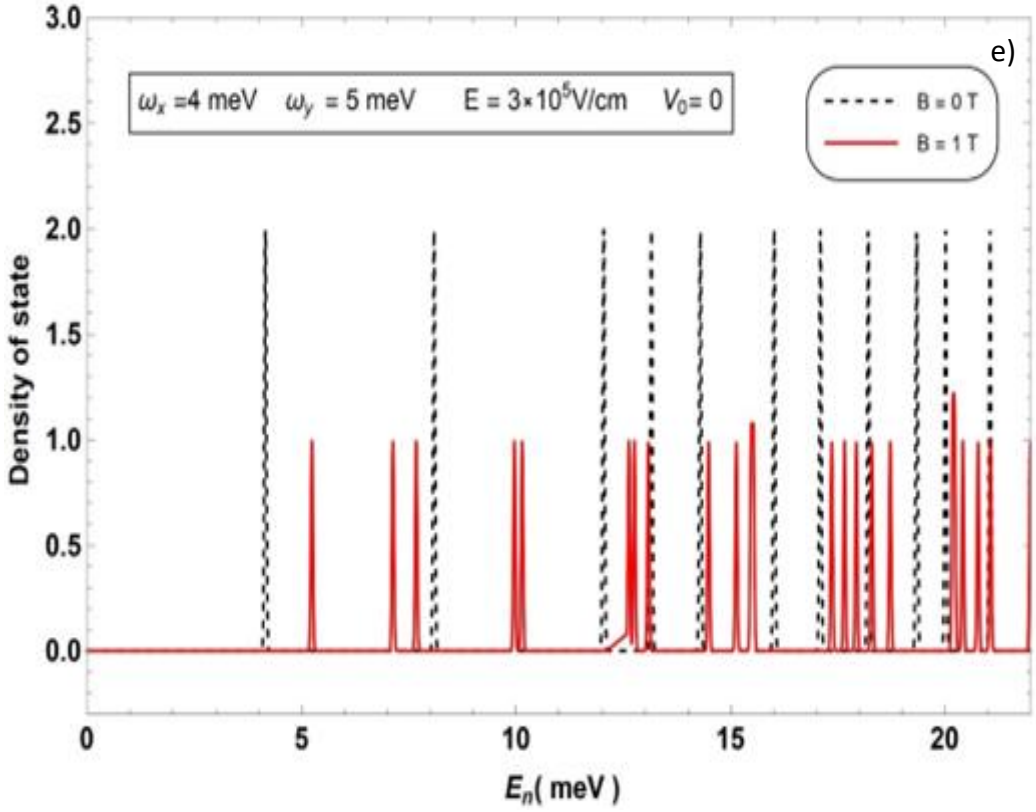
e)
ω_x =4 meV ω_y = 5 meV E = 3×10^{5}V/cm V_0= 0
B = 0 T
B = 1 T
Density of state
E_n(meV)

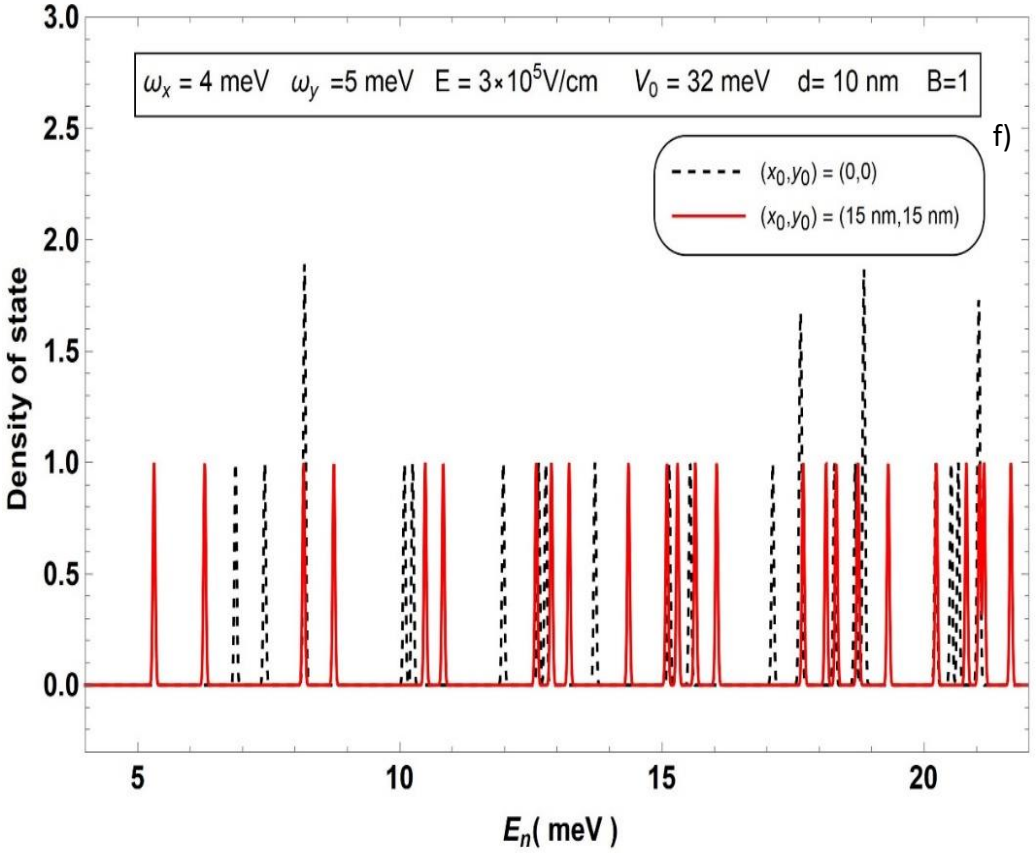
f)
ω_x = 4 meV ω_y =5 meV E = 3×10^{5}V/cm V_0 = 32 meV d= 10 nm B=1
(x_0,y_0) = (0,0)
(x_0,y_0) = (15 nm,15 nm)
Density of state
E_n(meV)

The presence of the acceptor impurity also affects the DOS plot, as shown in Fig. 10(d); at zero magnetic fields, the 2-spin fold degeneracy is still present, where the impurity split the states, in specific, the impurity added positive energy for each state unequally, with no significant effect at the states with odd quantum numbers (which have a node at the impurity location).
In Fig. 10(e), the DOS has been plotted versus the energy for $\boldsymbol{E = 3 \times 10^5\, V/cm}$, we notice from the figure that the anisotropy of the confinement potential partially removes the degeneracy of the states, whereas the spin degeneracy remains, as shown in the dashed black lines. In addition, as the magnetic field is turning on, the spin degeneracy is also lifted; this split is due to the Zeeman term in the Hamiltonian.

The combined effect of the impurity, SOI, and anisotropy of the quantum dot has been investigated in Fig. 10(f). There are accidentally degenerate states and a particular value of the energy for on-center impurity, while the presence of an off-center impurity totally removes the state's degeneracy.

In conclusion, the density of states (DOS) in a quantum system is influenced by various factors, including the Hamiltonian terms and parameters that govern the system's behavior. These factors interact in complex ways, leading to significant correlations with the DOS and affecting the system's physical properties.

The presence of a magnetic field is one such influential factor. In the case of an isotropic quantum dot, the magnetic field removes the spin degeneracy of the Fock-Darwin states, causing them to split. This spin splitting alters the DOS and introduces energy level spacings that depend on the strength of the magnetic field. Consequently, the DOS exhibits distinctive features related to the presence of the magnetic field.

The anisotropy of the parabolic confinement potential also has a substantial impact on the system's DOS. This anisotropy breaks the degeneracy associated with spatial quantum numbers, resulting in different energy levels for states with different spatial distributions. However, the spin degeneracy remains unaffected by the anisotropy of the confinement potential. Consequently, the DOS shows distinct variations due to changes in the spatial quantum numbers, while the spin degeneracy is preserved.

Furthermore, the introduction of impurities in the system can significantly manipulate the DOS. Impurities add or subtract energy unequally for each state, leading to a

modification of the DOS profile. The presence of impurities can create localized states within the energy spectrum, thereby altering the overall DOS distribution. The specific energy levels affected by the impurity depend on the impurity's characteristics and its interaction with the surrounding quantum system.

Additionally, the spin-orbit interaction (SOI) plays a crucial role in shaping the energy spectra and, consequently, the DOS. The SOI intertwines the spin and spatial quantum numbers, resulting in a mixing of these quantum degrees of freedom. This mixing modifies the energy levels and introduces additional splitting and shifts in the energy spectrum, further influencing the DOS distribution. The presence of SOI can give rise to phenomena such as spin-orbit splitting and spin textures that impact the DOS.

In summary, the combined effect of Hamiltonian terms and parameters strongly correlates with the density of states in a quantum system. The magnetic field removes spin degeneracy, the anisotropy of the confinement potential affects the spatial quantum numbers, impurities manipulate specific energy levels, and the spin-orbit interaction mixes the spin and spatial quantum numbers, all of which significantly modify the density of states. Understanding and controlling these effects are essential for comprehending the behavior of quantum systems and designing devices with desired electronic properties.

Chapter Four
Conclusions

In this work, the anisotropic quantum dot Hamiltonian has been solved using the diagonalization method in the presence of a perpendicular magnetic field and Gaussian impurity, considering both types of spin-orbit interaction: Rashba and Dresselhaus spin-orbit interaction.

The diagonalization process has been carried out using the one-dimensional harmonic oscillator basis to find the eigen solutions of the InAs QD for different cases. All the Hamiltonian matrix elements have been calculated in a closed analytical form.

In the computational process, the issue of convergence has been ensured, and the obtained numerical results have been tested. Using the closed analytical expression for the matrix elements significantly reduced the computational time and gave more accurate energy spectra.

The results of the energy spectra match the Landau level spectra in the case of the isotropic quantum dot, in the absence of the impurity and SOI, while as the quantum dot stretched in the y direction, the degeneracy of the landau level is partially removed.

The presence of the acceptor impurity significantly affects the eigen solution of the system, specifically causing an interesting crossing between the states and changing the ground state. Furthermore, the impurity's strength, position, and spatial stretch have been investigated.

As a second step, the obtained eigenenergies have been used to calculate the statistical average energy as a function of the system parameters and temperature.

The magnetic properties of the system (magnetization and magnetic susceptibility) of InAs QD have shown a diamagnetic-paramagnetic phase transition due to the impurity presence. This transition strongly correlates with the impurity profiles (strength, position, and influence domain), magnetic field, and temperature.

In applications, the magnetic phase transition (diamagnetic to paramagnetic transition) should be considered when estimating the applicability of material to be involved in future technologies such as switching devices and magnetic sensors.

In addition, the effective Lande g factor of the system has been studied. The result shows the strong dependence of g^* on the SOI interaction, the quantum dot confinement strength, and the isotropy of the quantum dot in addition to the magnetic field.

Finally, to physically describe each system parameter's effect on the energy spectra, we calculate the density of state of the system. The plots show the breaking of the harmonic oscillator symmetry as the magnetic field is tuning on, where the anisotropy of the confinement potential also breaks the symmetry.

List of Abbreviations

Abbreviation	Meaning
SOC	Spin-Orbit Coupling
QD	Quantum Dot
SOI	Spin-Orbit Interaction
DOS	Density of states
$2D$	Two-dimension
$1D$	One-dimensional
$0D$	Zero-dimension
k_z	Z -wave vector
g	Effective Lande g factor
EDM	Exact diagonalization method
M	Magnetization
χ	Magnetic susceptibility
n	Principal quantum number
ω_c	Cyclotron frequency
Ω	Effective frequency
m_l	Angular quantum number
A	Vector potential
B	Magnetic field
E	Electric field
ω_0	Isotropic radial confinement frequency
ω_x	x direction confinement frequency
ω_y	y direction confinement frequency
m^*	Effective mass
m_0	Free electron mass
$\hbar$	Reduced Plank constant
p	Momentum
e	Electron charge

Abbreviation	Meaning
V_0	Impurity strength
x_0, y_0	Impurity location
d	Impurity stretches
μ_B	Bohr magneton
α_R	Rashba coefficient
α_D	Dresselhaus coefficient
σ	Pauli matrices
δ	Kronic Delta
ψ	Wave function
Z	Partition function
Γ	Broadening factor
$E_{G.S}$	Ground state energy
$FWHM$	The full width of half maximum
M	Magnetization
χ	Magnetic susceptibility
$\langle E \rangle$	Average energy

References

[1] Ali, A. A., Shaer, A., & Elsaid, M. (2022). Simultaneous effects of Rashba, magnetic field and impurity on the magnetization and magnetic susceptibility of a GaAs-semiconductor quantum ring [Article]. *Journal of Magnetism and Magnetic Materials*, *556*, Article 169435. https://doi.org/10.1016/j.jmmm.2022.169435

[2] Ali, M., Elsaid, M., & Shaer, A. (2019). Magnetization and Magnetic Susceptibility of GaAs Quantum Dot with Gaussian Confinement in Applied Magnetic Field [Article]. *Jordan Journal of Physics*, *12*(3), 247-254. <Go to ISI>://WOS:000504056200007

[3] Alia, A. A., Elsaid, M. K., & Shaer, A. (2019). Magnetic properties of GaAs parabolic quantum dot in the presence of donor impurity under the influence of external tilted electric and magnetic fields [Article]. *Journal of Taibah University for Science*, *13*(1), 687-695. https://doi.org/10.1080/16583655.2019.1622242

[4] Ashoori, R. (1996). Electrons in artificial atoms. *Nature*, *379*(6564), 413-419.

[5] Avetisyan, S., Chakraborty, T., & Pietiläinen, P. (2016). Magnetization of interacting electrons in anisotropic quantum dots with Rashba spin–orbit interaction. *Physica E: Low-dimensional Systems Nanostructures*, *81*, 334-338.

[6] Avetisyan, S., Pietilainen, P., & Chakraborty, T. (2012). Strong enhancement of Rashba spin-orbit coupling with increasing anisotropy in the Fock-Darwin states of a quantum dot [Article]. *Physical Review B*, *85*(15), Article 153301. https://doi.org/10.1103/PhysRevB.85.153301

[7] Avetisyan, S., Pietiläinen, P., & Chakraborty, T. (2012). Strong enhancement of Rashba spin-orbit coupling with increasing anisotropy in the Fock-Darwin states of a quantum dot. *Physical Review B*, *85*(15), 153301.

[8] Bader, S., & Parkin, S. (2010). Spintronics. *Annu. Rev. Condens. Matter Phys.*, *1*(1), 71-88.

[9] Baghdasaryan, D., Hayrapetyan, D., Kazaryan, E., & Sarkisyan, H. (2018). Thermal and magnetic properties of electron gas in toroidal quantum dot. *Physica E: Low-dimensional Systems Nanostructures*, *101*, 1-4.

[10] Boda, A., & Chatterjee, A. (2016). Transition energies and magnetic properties of a neutral donor complex in a Gaussian GaAs quantum dot. *Superlattices Microstructures*, *97*, 268-276.

[11] Bzour, F., Shaer, A., & Elsaid, M. K. (2017). The effects of pressure and temperature on the exchange energy of a parabolic quantum dot under a magnetic field [Article]. *Journal of Taibah University for Science*, *11*(6), 1122-1134. https://doi.org/10.1016/j.jtusci.2017.02.004

[12] Camenzind, L. C., Svab, S., Stano, P., Yu, L., Zimmerman, J. D., Gossard, A. C., Loss, D., & Zumbühl, D. M. (2021). Isotropic and Anisotropic g-factor Corrections in GaAs Quantum Dots. *Physical Review Letters*, *127*(5), 057701.

[13] Castano-Yepes, J. D., Amor-Quiroz, D., Ramirez-Gutierrez, C., & Gómez, E. A. (2019). Impact of a topological defect and Rashba spin-orbit interaction on the thermo-magnetic and optical properties of a 2D semiconductor quantum dot with Gaussian confinement. *Physica E: Low-dimensional Systems Nanostructures*, *109*, 59-66.

[14] Chakraborty, T., & Pietiläinen, P. (2005). Optical signatures of spin-orbit interaction effects in a parabolic quantum dot. *Physical review letters*, *95*(13), 136603.

[15] Ciftja, O., & Faruk, M. G. (2005). Two-dimensional quantum-dot helium in a magnetic field: Variational theory. *Physical Review B*, *72*(20), 205334.

[16] Darwin, C. G. (1931). The diamagnetism of the free electron. Mathematical Proceedings of the Cambridge Philosophical Society,

[17] Datta, N. K., & Ghosh, M. (2011). Impurity strength and impurity domain modulated frequency-dependent linear and second non-linear response properties of doped quantum dots. *Physica Status Solidi*, *248*(8), 1941-1948.

[18] Datta, S. (2018). How we proposed the spin transistor. *J Nature Electronics*, *1*(11), 604-604.

[19] de Sousa, R., & Das Sarma, S. (2003). Gate control of spin dynamics in III-V semiconductor quantum dots [Article]. *Physical Review B*, *68*(15), Article 155330. https://doi.org/10.1103/PhysRevB.68.155330

[20] Dieny, B., Prejbeanu, I. L., Garello, K., Gambardella, P., Freitas, P., Lehndorff, R., Raberg, W., Ebels, U., Demokritov, S. O., & Akerman, J. (2020). Opportunities and challenges for spintronics in the microelectronics industry. *Nature Electronics*, *3*(8), 446-459.

[21] Dresselhaus, G. (1955). Spin-orbit coupling effects in zinc blende structures. *Physical Review*, *100*(2), 580.

[22] Elsaid, M., Ali, M., & Shaer, A. (2019). The magnetization and magnetic susceptibility of GaAs Gaussian quantum dot with donor impurity in a magnetic field [Article]. *Modern Physics Letters B*, *33*(34), Article 1950422. https://doi.org/10.1142/s0217984919504220

[23] Elsaid, M. K., Abu Alia, A., & Shaer, A. (2020). Rashba spin-orbit interaction effects on thermal and magnetic properties of parabolic GaAs quantum dot in the presence of donor impurity under external electric and magnetic fields [Article]. *Chinese Journal of Physics*, *66*, 335-348. https://doi.org/10.1016/j.cjph.2020.04.013

[24] Elsaid, M. K., Shaer, A., Hjaz, E., & Yahya, M. H. (2020). Impurity effects on the magnetization and magnetic susceptibility of an electron confined in a quantum ring under the presence of an external magnetic field [Article]. *Chinese Journal of Physics*, *64*, 9-17. https://doi.org/10.1016/j.cjph.2020.01.002

[25] Fock, V. (1928). Note to the Quantification of the harmonic Oscillator in a Magnetic Field. *Zeitschrift fur Physik*, *47*(5-6), 446-448.

[26] Grandshteyn, I., & Ryzhik, I. J. N. Y. A. P. (1980). Table of integrals, series, and products. *8*, 362.

[27] Gumber, S., Kumar, M., Gambhir, M., Mohan, M., & Jha, P. K. (2015). Thermal and magnetic properties of cylindrical quantum dot with asymmetric confinement. *Canadian Journal of Physics*, *93*(11), 1264-1268.

[28] Gumber, S., Kumar, M., Jha, P. K., & Mohan, M. (2016). Thermodynamic behaviour of Rashba quantum dot in the presence of magnetic field. *Chinese Physics B*, *25*(5), 056502.

[29] Hosseinpour, P. (2020). The role of Rashba spin-orbit interaction and external fields in the thermal properties of a doped quantum dot with Gaussian impurity. *Physica B: Condensed Matter*, *593*, 412259.

[30] Hosseinpour, P. J. J. o. I., Thin Films,, & systems, L. d. (2020). The control of nonlinear optical properties in a doped asymmetric quantum dot by the spin-orbit coupling and external electric field. *3*(2), 287-295.

[31] Hu, G., & Xiang, B. (2020). Recent Advances in Two-Dimensional Spintronics. *Nanoscale Research Letters*, *15*(1), 1-17.

[32] Jha, P. K., Kumar, M., Lahon, S., Gumber, S., & Mohan, M. (2014). Rashba spin orbit interaction effect on nonlinear optical properties of quantum dot with magnetic field. *Superlattices Microstructures*, *65*, 71-78.

[33] Kahraman, M., & Bulutay, C. (2021). Electron ground state g factor in embedded InGaAs quantum dots: An atomistic study [Article]. *Physical Review B, 103*(11), Article 115303. https://doi.org/10.1103/PhysRevB.103.115303

[34] Kandemir, B., & Cetin, A. (2005). Impurity magnetopolaron in a parabolic quantum dot: the squeezed-state variational approach. *Journal of Physics: Condensed Matter*, *17*(4), 667.

[35] Khordad, R. (2017). The effect of Rashba spin-orbit interaction on electronic and optical properties of a double ring-shaped quantum dot. *Superlattices Microstructures*, *110*, 146-154.

[36] Madhav, A., & Chakraborty, T. (1994). Electronic properties of anisotropic quantum dots in a magnetic field. *Physical Review B*, *49*(12), 8163.

[37] Prabhakar, S., Raynolds, J. E., & Melnik, R. (2011). Manipulation of the Lande g factor in InAs quantum dots through the application of anisotropic gate potentials: Exact diagonalization, numerical, and perturbation methods [Article]. *Physical Review B*, *84*(15), Article 155208. https://doi.org/10.1103/PhysRevB.84.155208

[38] Prabhakar, S., Raynolds, J. E., & Melnik, R. (2011). Manipulation of the Landé g factor in InAs quantum dots through the application of anisotropic gate potentials: Exact diagonalization, numerical, and perturbation methods. *Physical Review B*, *84*(15), 155208.

[39] Rashba, E. I. (1960). Properties of semiconductors with an extremum loop. I. Cyclotron and combinational resonance in a magnetic field perpendicular to the plane of the loop. *Soviet Physics, Solid State*, *2*, 1109-1122.

[40] Reimann, S. M., & Manninen, M. (2002). Electronic structure of quantum dots. *Reviews of modern physics*, *74*(4), 1283.

[41] Schliemann, J., Egues, J. C., & Loss, D. (2003). Nonballistic spin-field-effect transistor. *Physical Review Letters*, *90*(14), 146801.

[42] Shaer, A., Elsaid, M., & Elhasan, M. (2016). The magnetic properties of a quantum dot in a magnetic field. *Turkish Journal of Physics*, *40*(3), 209-218.

[43] Shaer, A., Hjaz, E., & Elsaid, M. (2019). The heat capacity of a semiconductor quantum dot in magnetic fields. *Nanosystems: Physics, Chemistry, Mathematics*, *10*(5), 530-535.

[44] Sharma, H. K., Boda, A., Boyacioglu, B., & Chatterjee, A. (2019). Electronic and magnetic properties of a two-electron Gaussian GaAs quantum dot with spin-Zeeman term:

A study by numerical diagonalization. *Journal of Magnetism Magnetic Materials*, *469*, 171-177.

[45] Stufler, S., Ester, P., Zrenner, A., & Bichler, M. (2005). Quantum optical properties of a single In x Ga 1− x As− Ga As quantum dot two-level system. *Physical Review B*, *72*(12), 121301.

[46] Takahashi, S., Deacon, R. S., Yoshida, K., Oiwa, A., Shibata, K., Hirakawa, K., Tokura, Y., & Tarucha, S. (2010). Large Anisotropy of the Spin-Orbit Interaction in a Single InAs Self-Assembled Quantum Dot [Article]. *Physical review letters*, *104*(24), Article 246801. https://doi.org/10.1103/PhysRevLett.104.246801

[47] Voskoboynikov, O., Bauga, O., Lee, C., & Tretyak, O. (2003). Magnetic properties of parabolic quantum dots in the presence of the spin–orbit interaction. *Journal of applied physics*, *94*(9), 5891-5895.

[48] Wolf, S., Awschalom, D., Buhrman, R., Daughton, J., von Molnár, v. S., Roukes, M., Chtchelkanova, A. Y., & Treger, D. (2001). Spintronics: a spin-based electronics vision for the future. *Science*, *294*(5546), 1488-1495.

[49] Yahyah, N. S., Elsaid, M. K., & Shaer, A. (2019). Heat capacity and entropy of Gaussian spherical quantum dot in the presence of donor impurity [Article]. *Journal of Theoretical and Applied Physics*, *13*(3), 277-288. https://doi.org/10.1007/s40094-019-0336-1

[50] Yakout, S. M. (2020). Spintronics: future technology for new data storage and communication devices. *Journal of Superconductivity Novel Magnetism*, *33*, 2557-2580.

[51] Yaseen, A., Shaer, A., & Elsaid, M. K. (2019). The magnetic properties of GaAs parabolic quantum dot in the presence of donor impurity, magnetic and electric fields. *Chinese journal of physics*, *60*, 598-611.

[52] Žutić, I., Fabian, J., & Sarma, S. D. (2004). Spintronics: Fundamentals and applications. *Reviews of Modern Physics*, *76*(2), 323.

Appendices

Appendix A

Figures

Figure A.11

Concept of spin transistor illustrating the analogy between photon polarization (top) and electron spin (bottom). (Datta, 2018)

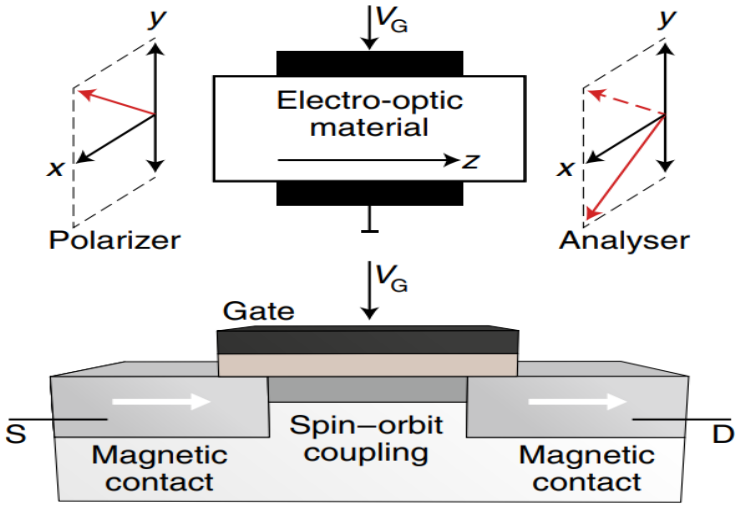

Figure A.12

Energy dispersion vs. wavevector for the one dimension, the solid line represents the spin-independent Hamiltonian while the red dashed (blue dashed) line denotes Zeeman (Rashba) splitting.

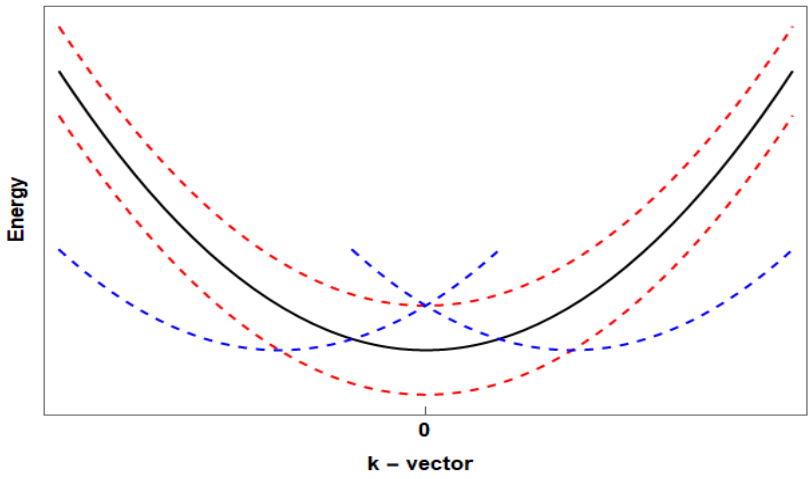

Figure A.13

The effect of the dimensionality on the density of states yields a different change in the system properties

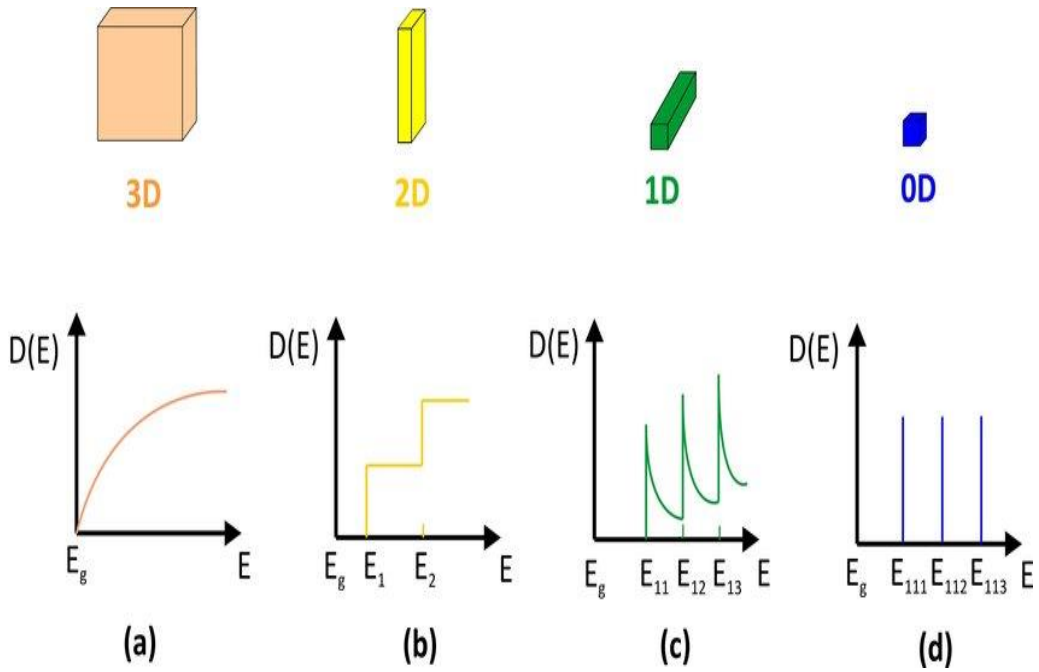

Figure A.14

Fock-Darwin energy levels (n, m_l) of an isotropic quantum dot as a function of the magnetic field B (in Tesla) with confinement of $\omega_0 = 4\ meV$.

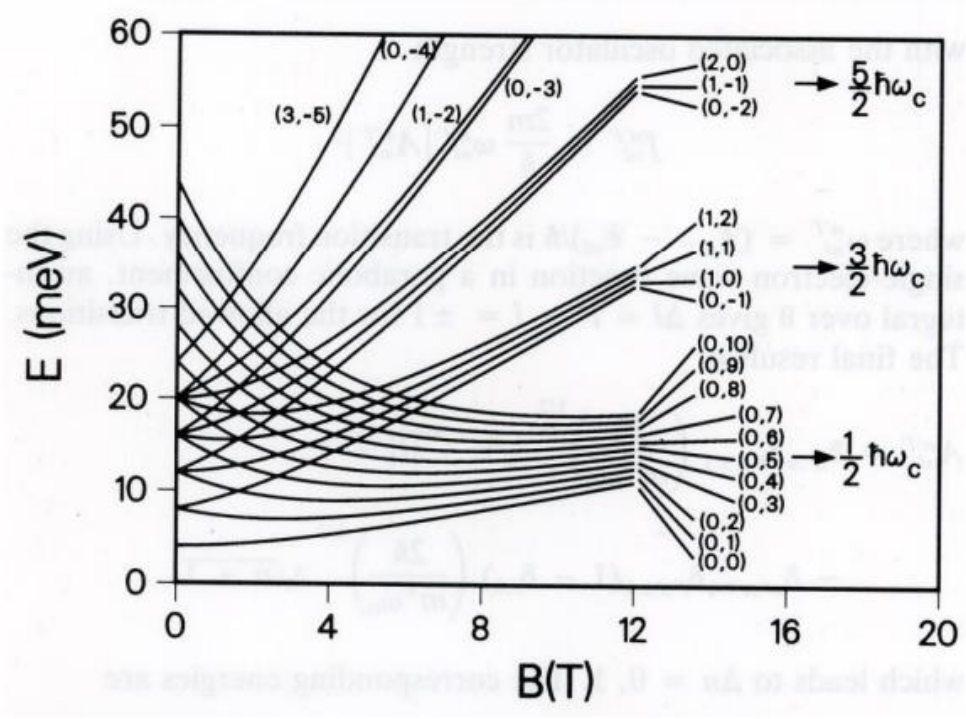

Figure A.15

Flowchart for the dissertation.

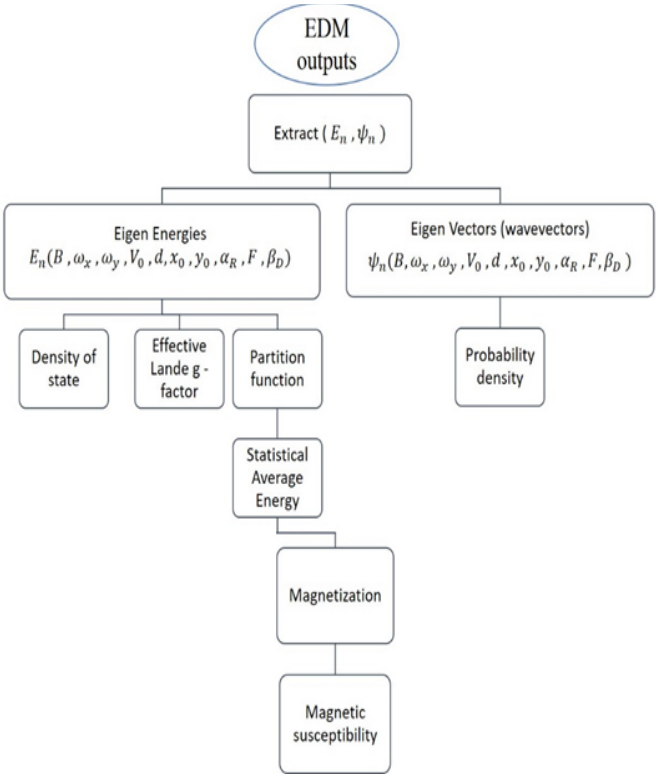

Figure A.16

Convergence tests for the spectra and partition function.

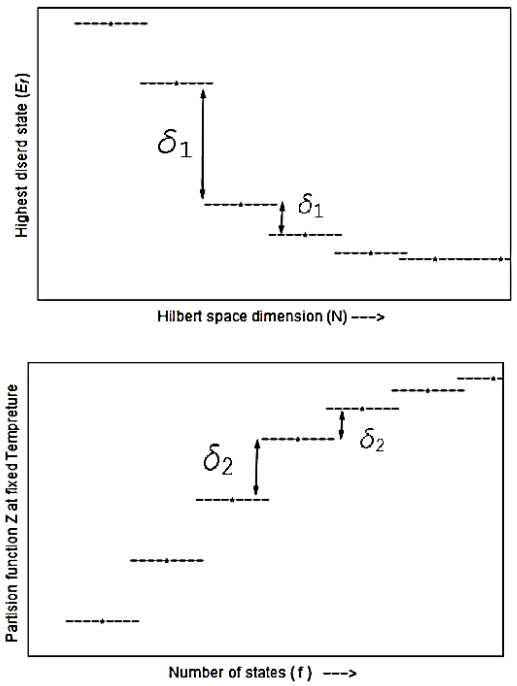

Figure A.17

Probability density $|\boldsymbol{\psi}|^{\mathbf{2}}$ *for the wavefunctions of the low-lying states* $|\mathbf{0},\mathbf{0}\rangle, |\mathbf{1},\mathbf{0}\rangle$, *and* $|\mathbf{0},\mathbf{1}\rangle$, *in the presence of on-center impurity with profiles (from up to down)* $(\boldsymbol{V_0}, \boldsymbol{d})$: $(\mathbf{0}, -), (\mathbf{24}, \mathbf{10}), (\mathbf{32}, \mathbf{10})$ *and* $(\mathbf{32}, \mathbf{20})$ *in meV and nm, respectively.*

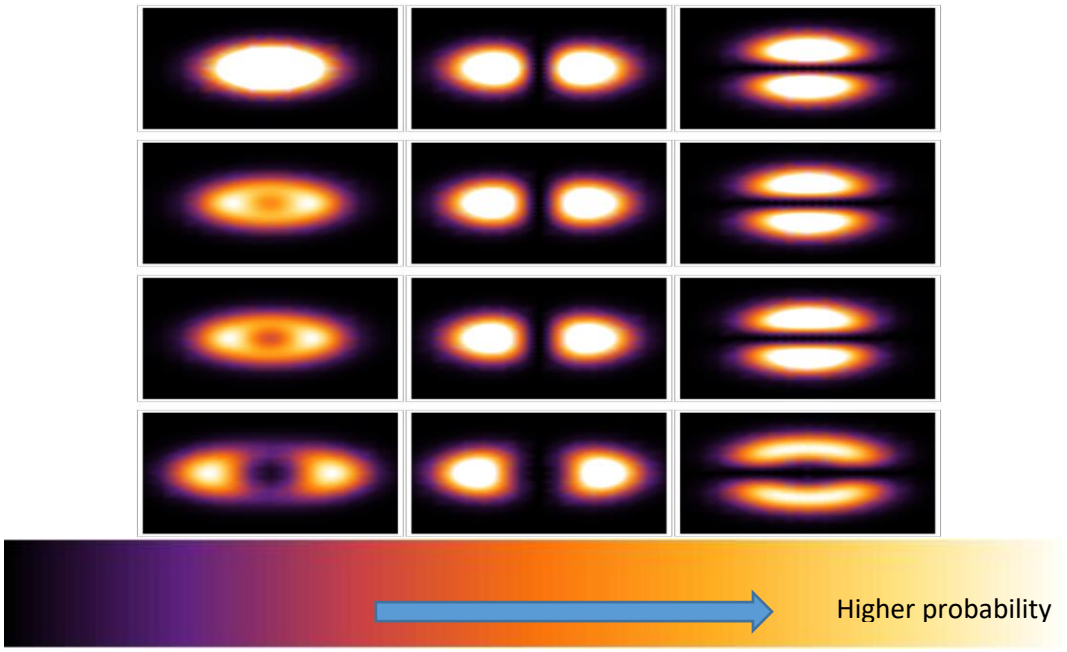

Figure A.18

Probability density $|\boldsymbol{\psi}|^{\mathbf{2}}$ *for the wavefunctions of the low-lying states, the top panel for* $\boldsymbol{V_0} = \mathbf{0}$ *and the other two panels in the presence of an off-center impurity with* $\boldsymbol{V_0} = \mathbf{32}\ \boldsymbol{meV}\ \boldsymbol{and}\ \boldsymbol{d} = \mathbf{10}\ \boldsymbol{nm}$, *located at* $(\boldsymbol{x_0}, \boldsymbol{y_0})$: $(\mathbf{22}, \mathbf{0}), (\mathbf{0}, \mathbf{22})$ *from up to down, respectively.*

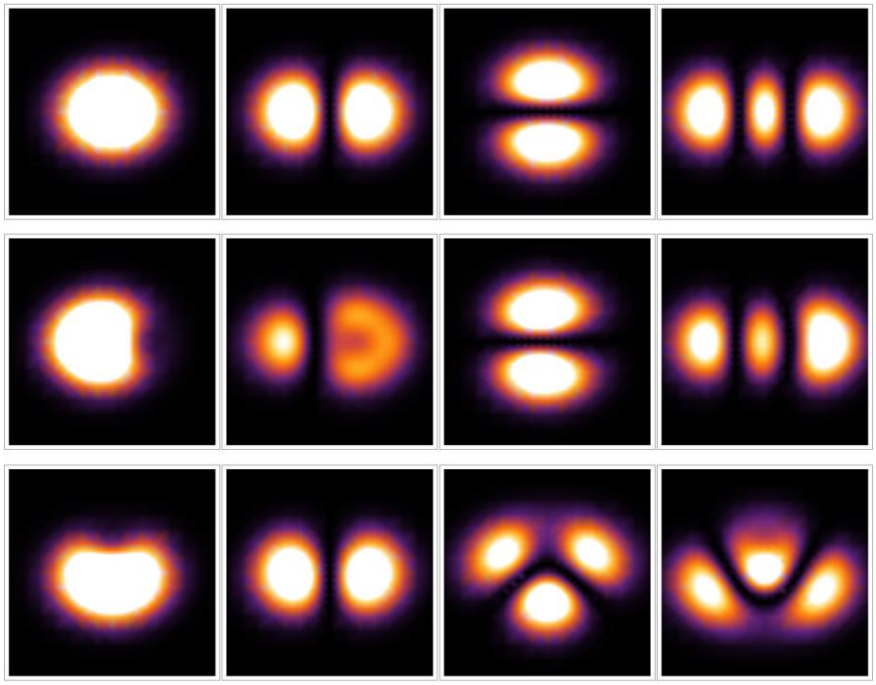

Figure A.19

a) ***M*** *vs. B and b)* χ *vs. B for different electric field strengths for lateral QD*

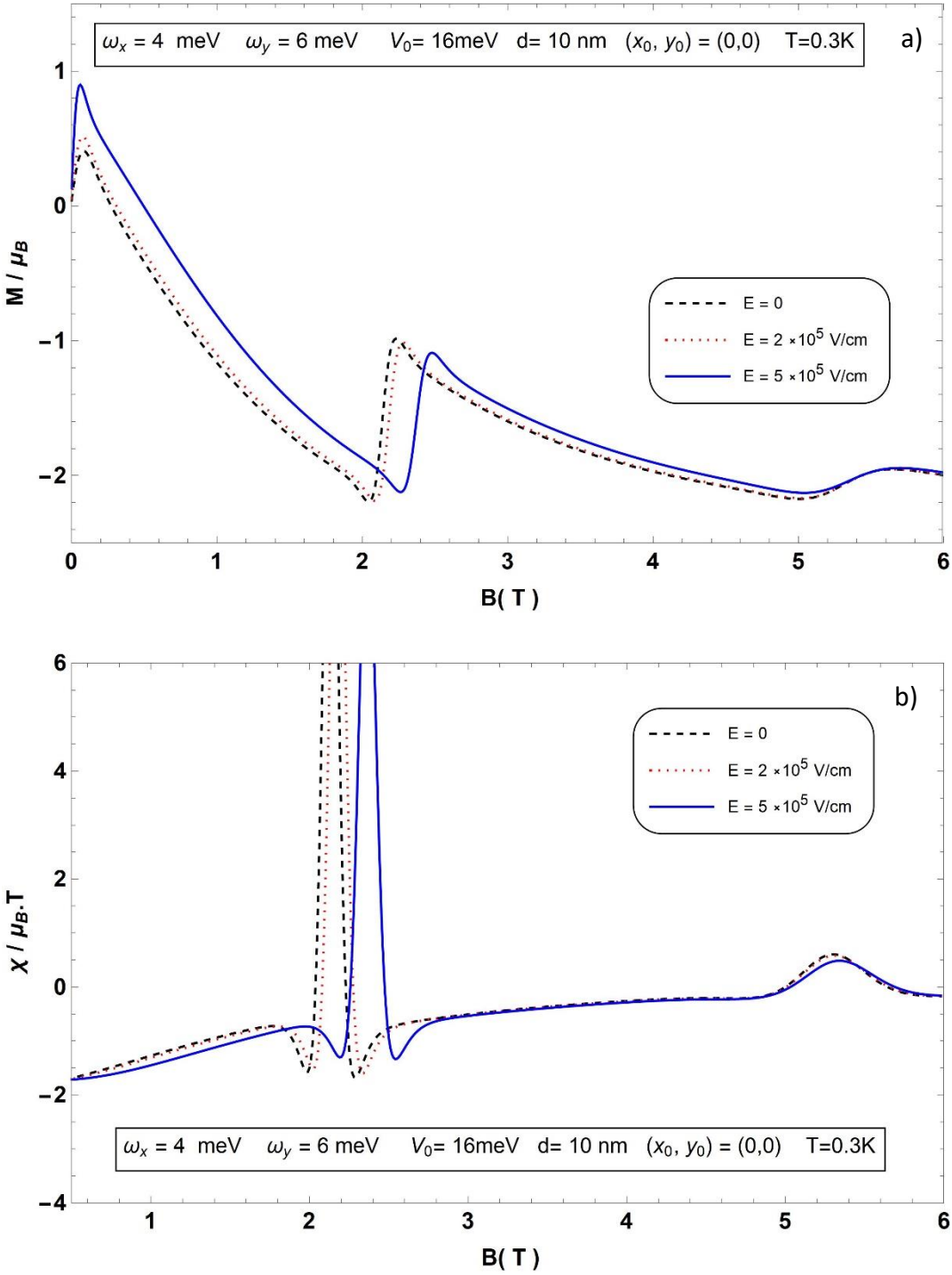

Appendix B

Certificate of acceptance of the research extracted from the dissertation

Research title: The Gaussian Impurity Effect on The Electronic and Magnetic Properties of an Electron Confined in a Lateral Quantum Dot

NANOSYSTEMS:
PHYSICS, CHEMISTRY, MATHEMATICS

Original article

Shaer A., Elsaid M.K. *Nanosystems: Phys. Chem. Math.*, 2022, **13** (3), 265–273.
http://nanojournal.ifmo.ru
DOI 10.17586/2220-8054-2022-13-3-265-273

The Gaussian impurity effect on the electronic and magnetic properties of an electron confined in a lateral quantum dot

Ayham Shaer, Mohammad K. Elsaid

Physics Department, An-Najah National University, Nablus, Palestine

Corresponding author: Ayham Shaer, ayham.shaer@najah.edu

ABSTRACT The Hamiltonian of a single electron trapped in a lateral quantum dot in the influence of an acceptor Gaussian impurity has been solved using a variational wavefunction as a superposition of a product of eigenfunctions of the harmonic oscillator in x and y coordinates. The effects of Gaussian impurity parameters on the system's spectra have been investigated as a function of the magnetic field. Furthermore, the electron probability has been displayed to investigate the impurity position effect on the energy levels. As a second step, the calculated energy spectra were utilized to compute and visualize the system's magnetic properties in the presence of the magnetic field and impurity. The obtained energy spectra show level crossings in the presence of acceptor impurity, which causes oscillations in the magnetic susceptibility and magnetization curves, resulting in an exciting diamagnetic–paramagnetic phase transition.

KEYWORDS lateral quantum dot, magnetic properties, Gaussian impurity, diamagnetic-paramagnetic transition

FOR CITATION Shaer A., Elsaid M.K. The Gaussian impurity effect on the electronic and magnetic properties of an electron confined in a lateral quantum dot. *Nanosystems: Phys. Chem. Math.*, 2022, **13** (3), 265–273.

جـامعـــة النجاح الوطنية

كليـــة الدراســـات العليـــا

الخواص المغناطيسية والإلكترونية لنقطة كمية مطعمة غير متماثلة من مادة زرنيخ الإنديوم (InAs) مع تأثير ارتباط الغزل والمدار : دراسة حسابية

إعداد

أيهم أنور أحمد شاعر

إشراف

أ. د. محمد خليل السعيد

قدمت هذه الرسالة استكمالا لمتطلبات الحصول على درجه الدكتوراة في الفيزياء، من كلية الدراسات العليا، في جامعة النجاح الوطنية، نابلس- فلسطين.

2023

الخواص المغناطيسية والإلكترونية لنقطة كمية مطعمة غير متماثلة من مادة زرنيخ الإنديوم (InAs) مع تأثير ارتباط الغزل والمدار: دراسة حسابية

اعداد

أيهم أنور أحمد شاعر

إشراف

أ. د. محمد خليل السعيد

الملخص

تم حل دالة هاملتون لنقطة كمية (quantum dot) غير متماثلة تحت تأثير مجال مغناطيسي معامد وبوجود شائبة غاوسية (Gaussian impurity) بطريقة قطرية المصفوفة (exact diagonalization method)، مع الأخذ بالاعتبار كلا النوعين من ارتباط الغزل والمدار: ارتباط رشبا (Rashba spin orbit interaction) وارتباط دريسيلهوس (Dresselhaus spin orbit interaction). تمت عملية الحساب باستخدام المتذبذب التوافقي احادي الأبعاد (harmonic oscillator) كاقتران بنائي.

تم استخدام المخرجات من عملية المصفوفة القطرية لحساب الكثافة الاحتمالية للإلكترون والطاقة الإحصائية والخصائص المغناطيسية وقيمة معامل لاندي (Lande g factor) وكثافة المستويات للنقطة الكمومية.

أظهرت النتائج أن وجود الشائبة الغاوسية يؤثر بشكل كبير على الحل المميز لدالة هاملتون، بحيث يؤدي الى تقاطع مستويات الطاقة بالتالي تغير ترتيب المدار الأرضي. بالإضافة تم دراسة تأثير متغيرات الشائبة (القوة ، الموقع، حيز التمدد)، و إستنتاج مدى أهمية الشوائب بتغيير والتحكم بخصائص النقطة الكمومية.

قمنا بدراسة الخصائص المغناطيسية (التمغنط، والنفاذية المغناطيسية) لهذه النقطة الكمومية، ولاحظنا وجود طور انتقالي للمادة من حالة الديامغناطيسية الى البارامغنطيسية عند درجات حرارة منخفضة بوجود الشائبة المستقبلة للالكترونات، ووجد أن ظروف الطور الانتقالي يعتمد بشكل كبير

على متغيرات الشائبة، حيث أن قيمة المجال المغناطيسي الذي حصل عنده الانتقال يقل بزيادة تركيز الشائبة.

بالإضافة الى ذلك، تم دراسة اعتمادية معامل لاندي بحالة وجود كلا النوعين من ارتباط الغزل والمدار على قوة المجال الكهربائي، وتبين ان زيادة قيمة المجال الكهربائي يعزز من القيمة المطلقة لمعامل لاندي نتيجة تأثير رشبا، ويقلل من القيمة المطلقة للمعامل نتيجة دريسيلهوس. ونظرا لسيطرة تأثير رشبا تم استنتاج ان زيادة المجال الكهربائي تعزز قيمة معامل لاندي للنقطة الكمومية.

من جهة أخرى، تبين أن معامل لاندي يأخذ قيمة عظمى عند قيمة محددة لجهد الحصر، وهذه القيمة تعتمد بشكل ملحوظ على مدى تماثل النقطة الكمومية.

واخيرا، تم حساب كثافة المستويات لتوضيح تأثير كل من المتغيرات في النظام على مدارات الطاقة، وأظهرت النتائج أن عدم التماثل في أبعاد النقطة الكمومية يؤدي إلى اختلال الانتظام المعروف في تماثل المتردد المتذبذب .

كلمات مفتاحية: نقطة كمومية، الخصائص المغناطيسية، ارتباط الغزل والمدار، معامل لاندي، فيزياء حاسوبية، كثافة المستويات، تأثير رشبا، تأثير دريسيلهوس.